SCANNING HALL PROBE MICROSCOPY (SHPM) USING QUARTZ CRYSTAL AFM FEEDBACK

A THESIS
SUBMITTED TO DEPARTMENT OF PHYSICS
AND THE INSTITUTE OF ENGINEERING AND SCIENCE
OF BILKENT UNIVERSITY
IN PARTIAL FULFILLMENT OF THE REQUIREMENTS
FOR THE DEGREE OF
MASTER OF SCIENCE

By
Koray Ürkmen
September, 2005

I certify that I have read this thesis and that in my opinion it is fully adequate, in scope and in quality, as a thesis for the degree of Master of Science.

_____

Assoc. Prof. Dr. Ahmet Oral (Supervisor)

I certify that I have read this thesis and that in my opinion it is fully adequate, in scope and in quality, as a thesis for the degree of Master of Science.

_____

Prof. Dr. Alexander Stanislaw Shumovsky

I certify that I have read this thesis and that in my opinion it is fully adequate, in scope and in quality, as a thesis for the degree of Master of Science.

_____

Dr. Tarık Reyhan

Approved for the Institute of Engineering and Science:

_____

Prof. Dr. Mehmet Baray

ABSTRACT

SCANNING HALL PROBE MICROSCOPY (SHPM) USING QUARTZ CRYSTAL AFM FEEDBACK

Koray Ürkmen

M.S. in Physics

Supervisor: Assoc. Prof. Dr. Ahmet Oral

September, 2005

Scanning Hall Probe Microscopy (SHPM) is a quantitative and non-invasive technique for imaging localized surface magnetic field fluctuations such as ferromagnetic domains with high spatial and magnetic field resolution of ~50nm & 7mG/√ Hz at room temperature. In the SHPM technique, Scanning Tunneling Microscope (STM) or Atomic Force Microscope (AFM) feedback is usually used for bringing the Hall sensor into close proximity of the sample. In the latter, the Hall probe has to be integrated with an AFM cantilever in a complicated microfabrication process. In this work, we have eliminated the difficult cantilever-Hall probe integration process; a Hall sensor is simply glued at the end of Quartz crystals, which are used as a force sensor. The sensor assembly is dithered at the resonance frequency and the quartz force sensor output is detected with a Lock-in and PLL system. SHPM electronics is modified to detect AFM topography and the phase, along with the magnetic field image. NIST MIRS (Magnetic Referance Sample) (Hard Disk) sample, 100 MB high capacity zip disk and Garnet sample are imaged with the Quartz Crystal AFM feedback and the performance is found to be comparable with the SHPM using STM feedback. Quartz Crystal AFM feedback offers a very simple sensor fabrication and operation in SHPM. This method eliminates the necessity of conducting samples for SHPM.

Keywords: Scanning Tunneling microscopy, Atomic Force Microscopy, Scanning Hall Probe Microscopy, Non-contact mode AFM, Quartz tuning forks.

ÖZET

KUARS KRİSTALİ KULLANILARAK AKM GERİ BESLEMELİ TARAMALI HALL AYGITI MİKROSKOPİSİ

Koray Ürkmen

Fizik Yüksek Lisans

Tez Yöneticisi: Doç. Dr. Ahmet Oral

Eylül, 2005

Taramalı Hall Aygıtı Mikroskopisi (THAM), ferromanyetik malzemelerdeki manyetik alanlar gibi lokalize yüzey manyetik alanlarını yüksek uzaysal çözünürlükle (~50nm) ve oda sıcaklığında bile 7mG/√ Hz manyetik alan çözünürlüğü ile etkileşimsiz ve nicel olarak ölçmek için kullanılan bir tekniktir. THAM tekniğinde, Hall aygıtını yüzeye yaklaştırmak için genellikle Taramalı Tünelleme Mikroskobu (TTM) veya Atomik Kuvvet Mikroskobu (AKM) geribeslemesi kullanılır. AKM geribeslemesi için Hall aygıtının karmaşık bir mikrofabrikasyon yöntemi kullanılarak AKM yayı ile entegre edilmesi gerekir. Bu çalışmada zor olan yay-Hall aygıtı entegrasyonunu gereksiz hale getirdik. Hall aygıtını kuvvet algılayıcısı olarak kullanılan bir kuvars kristali üzerine yapıştırdık. Algılayıcı rezonans frekansında titreştirildi, ve kuvars kristalinin çıktısı Lock in veya PLL sistemleri ile incelendi. THAM elektroniği AKM topografyasını ve faz değişimini manyetik alan bilgisiyle beraber alabilecek biçimde değiştirildi. NIST MIRS (Sabit Disk), 100 MB yüksek kapasiteli ZIP diski ve Demir-Garnet örnekleri Kuvars Kristali AKM geri beslemesi ile görüntülendi ve performansı TTM geri beslemesi kullanılan THAM ile karşılaştıralabilir bulundu. Kuvars Kristalli AKM geribeslemesi THAM için çok basit algılayıcı üretimini ve kullanımını vaad etmektedir. Bu metod THAM uygulaması için örneklerin iletken olması gereksinimini ortadan kaldırmaktadır.

Anahtar sözcükler: Taramalı Tünelleme Mikroskopisi, Atomik Kuvvet Mikroskopisi, Taramalı Hall Aygıtı Mikroskopisi, Temassız AKM, Kuvars Kristali Çatalları.

Acknowledgement

I would like to express my deep gratitude to my supervisor Assoc. Prof. Dr. Ahmet Oral, for his invaluable help and guidance.

I also want to thank to Mehrdad Atabak, Münir Dede, Muharrem Demir, Sevil Özer, Göksel Durkaya, Özgür Güngör, Ayşegul Erol, and especially Özge Girişen for their valuable help, useful remarks and for cheering me up. When I needed help, they were always there for me.

I dept special thanks to Assoc. Prof. Dr. Ceyhun Bulutay, Assoc. Prof. Dr. Lütfi Özyüzer for their friendly attitudes, remarkable help and motivation.

I also would like to express my special thanks to my parents Tacettin and Münevver Ürkmen, my second family Kutay, Bahar and Zeynep Ürkmen, all my brothers, my friends Emre Koçana, Tamer Başer, and Özlem Balkan enhancing my life. They never allowed me to become lonely in my life or during my work.

CONTENTS

1 Introduction ····· 1

1.1 Scanning Tunneling Microscopy (STM) ····· 2

1.2 Atomic Force Microscopy (AFM) ····· 5

1.3 Scanning Hall Probe Microscopy (SHPM) ····· 12

1.4 Scanning Probe Microscopy (SPM) scanning technique ····· 17

2 Experimental Set-up ····· 23

3 SHPM Probe Fabrication ····· 29

4 Scanning Hall Probe Microscopy (SHPM) experiments with STM feedback ····· 39

5 Quartz Tuning fork as a force sensor ····· 46

5.1 Force detection techniques ····· 49

5.1.1 Lock-in Amplifier ····· 51

5.1.2 PLL ····· 53

5.2 Historical background of the experimental set-up ····· 56

5.2.1 Preparation for High magnetic fields ····· 56

5.2.2 Different diameters for AFM tips ····· 58

5.2.3 Resonance frequency and Q factor change with temperature ····· 62

CONTENTS

5.2.4 Different dither voltages for AFM tips ····· 63

5.2.5 Images at different temperatures ····· 67

6 SHPM with AFM feed-back ····· 69

6.1 Lift-off mode SHPM imaging with AFM feed-back ····· 89

6.2 Tracking mode SHPM imaging with AFM feed-back ····· 93

7 Conclusion ····· 101

Bibliography ····· 103

List of Figures

Figure 1.1: Schematic view of a dimensional tunneling barrier····· 3
Figure 1.2: Schematic picture of the tunneling geometry. ····· 4
Figure 1.3: Interatomic force vs distance····· 6
Figure 1.4: The basic AFM set-up with beam deflection method. ····· 8
Figure 1.5: AFM cantilevers····· 8
Figure 1.6: A basic 4 quadrant photo detector for beam-deflected AFM set-up. ·· 9
Figure 1.7: Schematic SHPM scan mechanism ····· 13
Figure 1.8: Hall Probe with 50nm effective area ····· 13
Figure 1.9: Schematic description of Hall Effect····· 14
Figure 1.10: Schematic diagram of SPM····· 17
Figure 1.11. Schematic view of scanner tube ····· 20
Figure 1.12: Sharpness dependent resolution ····· 21
Figure 1.13: Electrochemical etch setup for AFM applications····· 21
Figure 1.14: SEM image of electrochemically etched W wire. The gray points on the tip are the carbon atoms which are deposited by the graphite electrode. (K.Urkmen and L.Ozyuzer, Izmir Institute of Technology, 2002)····· 22
Figure 1.15: STM image with 8μm x 8μm scan area on 6μm period grating sample at 4.2K, as an example of shadow effect of dual tip. ····· 22
Figure 2.1: Low Temperature Scanning Hall Probe Microscope. ····· 23
Figure 2.2: Low Temperature Scanning Hall Probe Microscope in details.····· 24
Figure 2.3: Slider part contents and the scanner head of LT-SHPM system. ····· 25
Figure 2.4: SPM control electronic.····· 26

LIST OF FIGURES

Figure 2.5: Available SPM probes: a) STM holder, b) Quartz Tuning Fork AFM probe, c) SHPM probe. ····· 27
Figure 2.6: Our homemade cryostat system which is directly inserted to the liquid nitrogen tank. ····· 28
Figure 3.1: Pseudomorphic High Electron Mobility Transistor P-HEMT wafer and its specifications that is used for Hall Probe fabrication ····· 29
Figure 3.2: Hall Probe with integrated STM tip ····· 30
Figure 3.3: Photolithography process ····· 31
Figure 3.4: Difference of negative and positive resists ····· 31
Figure 3.5: Etch process after photolithography ····· 32
Figure 3.6: Hall Probe definition with photoresist coating, after develop ····· 33
Figure 3.7: Hall Probe definition after RIE etch ····· 34
Figure 3.8: Mesa Etch by RIE ····· 35
Figure 3.9: Recess Etch by HCl ····· 35
Figure 3.10: Metallization development. ····· 37
Figure 3.11: Doped Au layer after RTP process on Hall Probe contacts ····· 37
Figure 3.12: Finished Hall Probe without STM Tip. ····· 38
Figure 3.13: B-H curves of Hall probes that are fabricated during this thesis work. ····· 38
Figure 4.1: Hall Probe with STM Tip. ····· 39
Figure 4.2: Alignment angle for SHPM operation. ····· 40
Figure 4.3: Schematic of alignment mechanism. ····· 41
Figure 4.4: Images of the hall probe and its reflection from the sample surface: a) from the first side after get parallel to the surface, b) from the second side after get parallel to the surface, c) after the tilt angle is given. ····· 41
Figure 4.5: Schematic SHPM scan mechanism ····· 42
Figure 4.6: Room temperature SHPM images of NIST magnetic reference sample over 40μm x 40μm area with 128 x 128 pixels resolution, 100 μm/sec scan speed, Lift Off Voltage=2.5V,Hall current= 3 μA, ····· 42

LIST OF FIGURES

Figure 4.7: Room temperature SHPM image of NIST magnetic reference sample over 40μm x 40μm area with 128 x 128 pixels resolution, 100 μm/sec scan speed, Lift Off Voltage=2.5V,Hall current= 3 μA, (Image shows unprocessed average of 10 fast scan SHPM images)····· 43

Figure 4.8: Low temperature (77K) SHPM image of Zip magnetic storage sample over ~17.6 μm x 17.6 μm area with 256 x 256 pixels resolution, 100 μm/sec scan speed, Lift Off Voltage=5V (0.43 μm), Hall current= 20 μA, (Image shows unprocessed average of 4 fast scan SHPM images ····· 44

Figure 4.9: Room Temperature tracking mode image of Iron-Garnet sample over 54μm x 54μm scan area, with 2 μm/sec scan speed, 2 μA Hall current and R_H = 0.1960 Ohm/Gauss Hall coefficient [16]····· 45

Figure 5.1: Resonance curve of 32 kHz Quartz Tuning Fork crystal in its own shield, calculated Q-factor is 102,710 ····· 47

Figure 5.2: 32 kHz Quartz tuning forks sizes, where each small interval is 1/100 inches. ····· 47

Figure 5.3: 100 kHz Quartz tuning fork sizes, where each small interval is 1/100 inches. ····· 48

Figure 5.4: 32 kHz Quartz tuning fork without original shield. ····· 48

Figure 5.5: Resonance and phase curve of a tip attached quartz tuning fork. ····· 50

Figure 5.6: Resonance and phase shift of quartz crystal with applied force.····· 50

Figure 5.7: The connection scheme of the lock-in and SPM electronic system ·· 52

Figure 5.8: AFM image of 6μm period grating at room temperature with lock-in amplifier, over 52 μm x 52 μm area with 1 μm/s speed····· 52

Figure 5.9: AFM image of 6μm period grating at low temperature with lock-in amplifier, over 8 μm x 8 μm area with 1 μm/s speed····· 52

Figure 5.10: Quartz AFM image of Morexalla bacteria over 2μm x 3μm area with 1μm/s speed, by using lock-in amplifier····· 53

Figure 5.11: The connection scheme of the PLL and SPM electronic system ···· 53

Figure 5.12:PLL circuit design····· 54

Figure 5.13:PLL connection schematic ····· 55

LIST OF FIGURES

Figure 5.14: The connections of the PLL card with feedback circuit and spare ADC circuit ····· 55
Figure 5.15: Old type of AFM probe with magnetic materials. ····· 56
Figure 5.16: New type of AFM probe with non-magnetic electrical connections57
Figure 5.17: AFM image of 6 μm period grating, taken at 10 K, under 3.5 Tesla magnetic field with the new type quartz tuning fork AFM probe by using lock-in system and Quantum Design's PPMS system. ····· 57
Figure 5.18: AFM image of 6 μm period grating, taken at 10 K, under 7 Tesla magnetic field with the new type quartz tuning fork AFM probe by using lock-in and Quantum Design's PPMS system. ····· 57
Figure 5.19: Old type of AFM probe with 125 μm thick etched Tungsten tip ···· 58
Figure 5.20: New type of AFM probe with 50 μm thick etched Tungsten tip····· 58
Figure 5.21: Old type of AFM probe with 0,125 mm tungsten tip, 0.5 V_{rms} dither voltage, 29,360 Hz Resonance Frequency and 326 Q-Factor ····· 59
Figure 5.22: New type of AFM probe with 0.5 V_{rms} dither voltage, 32,290 Hz Resonance Frequency and 6,458 Q-Factor ····· 59
Figure 5.23: Error signal (force gradient) image of 3μm period grating with 125μm diameter Tungsten wire obtained using PLL ····· 60
Figure 5.24: Phase shift signal image of 3μm period grating with 125μm diameter Tungsten wire obtained using PLL ····· 60
Figure 5.25: Feed-back signal image of 3μm period grating with 125μm diameter Tungsten wire obtained using PLL ····· 60
Figure 5.26: Cross section of feedback image of 3μm period grating with 125μm diameter Tungsten tip ····· 61
Figure 5.27: Error signal (force gradient) image of 6μm period grating with 50μm diameter Tungsten tip, by using PLL system ····· 61
Figure 5.28: Phase shift signal image of 6μm period grating with 50μm diameter Tungsten tip, by using PLL system ····· 61
Figure 5.29: Feed-back signal image of 6μm period grating with 50μm diameter Tungsten tip, by using PLL system ····· 61

LIST OF FIGURES

Figure 5.30: Cross section of feedback image of 6μm period grating with 50μm Tungsten tip ····· 62
Figure 5.31: Resonance frequency change with temperature ····· 63
Figure 5.32: Q-factor change with temperature ····· 63
Figure 5.33: AFM imaging with 40 mV RMS dither amplitude, 4μm/s scan speed, 100μs Lock-in time constant ····· 64
Figure 5.34: AFM imaging with 4 mV RMS dither amplitude, 3.5μm/s scan speed, 100μs Lock-in time constant, ····· 65
Figure 5.35: AFM imaging with 2 mV RMS dither amplitude, 3.5μm/s scan speed, 100μs Lock-in time constant, ····· 65
Figure 5.36: AFM imaging with 1 mV RMS dither amplitude, 3.5μm/s scan speed, 100μs Lock-in time constant, ····· 66
Figure 5.37: AFM imaging with 0.5 mV RMS dither amplitude, 3.5μm/s scan speed, 100μs Lock-in time constant ····· 66
Figure 5.38: AFM feedback data at 300K, over 21 μm x 21 μm area with 128 x 128 pixels resolution and 1 μm/sec speed. Image shows a 6 μm x 6 μm square periodic arrays with 4 μm squares and 2 μm spacing (Processed images) taken with Lock-in. ····· 67
Figure 5.39: AFM feedback data at 4.2K, over ~17.6 μm x 17.6 μm area with 256 x 256 pixels resolution and 0.15 μm/sec speed. Image shows a 6 μm x 6 μm square periodic arrays with 4 μm squares and 2 μm spacing (Processed images) taken with Lock-in. ····· 68
Figure 6.1: Microfabricated piezoresistive SHPM combined AFM cantilevers, [27, 28] ····· 70
Figure 6.2: Microfabricated piezoresistive SHPM combined AFM cantilevers, [27, 28] ····· 70
Figure 6.3: Fabrication process schematic SHPM integrated AFM cantilevers. [27, 28] ····· 71
Figure 6.4: Piezoelectric feedback mechanism for SHPM with two piezo plates [32] ····· 72

LIST OF FIGURES

Figure 6.5: Quartz Tuning Fork AFM guided Scanning Hall Probe ····· 72
Figure 6.6: Forward of 6μm period grating with the corner of a dummy Hall Probe chip ····· 73
Figure 6.7: Quartz Tuning Fork AFM guided Scanning Hall Probe ····· 74
Figure 6.8: Quartz Tuning Fork AFM guided Scanning Hall Probe with two free prongs ····· 75
Figure 6.9: Getting glued one of the prongs of the quartz tuning fork to avoid the broken symmetry problem.····· 75
Figure 6.10: Quartz tuning fork, prong and crystal sizes ····· 79
Figure 6.11: Measured resonance curve for a full Hall Probe attached 100 kHz quartz tuning fork between 5,000 Hz and 35,000 Hz ····· 80
Figure 6.12: Measured resonance curve for a full Hall Probe attached 100 kHz quartz tuning fork between 35,000 Hz and 70,000 Hz····· 80
Figure 6.13: Measured resonance curve for a full Hall Probe attached 100 kHz quartz tuning fork between 9,000 Hz and 13,000 Hz with fixed prong. ····· 81
Figure 6.14: Resonance curve of the quartz tuning fork with ¼ sized Hall probe. ····· 82
Figure 6.15: AFM topography by using the corner of the dummy chip····· 82
Figure 6.16: Photographs of Hall Probe definition and mesa corner of the used dummy Hall Probe for the feed-back tracking experiment ····· 83
Figure 6.17: Resonance tune between 5,000 and 100,000 Hz of 100 kHz Quartz crystal with dummy Hall Probe····· 84
Figure 6.18: Resonance and the phase curve of 100 kHz Quartz crystal with dummy Hall Probe that is used for experiment····· 84
Figure 6.19: Results of AFM topography imaging by using corner of Mesa (1) over 20μm x 20μm area with Δf =15 Hz, 1μm/s ····· 85
Figure 6.20: Results of AFM topography imaging by using corner of Mesa (2) over 15μm x 15μm area with Δf=8 Hz, 1μm/s ····· 86
Figure 6.21: Results of AFM topography imaging by using corner of Mesa (1) over 20μm x 20μm area with Δf=15 Hz, 1μm/s ····· 87

LIST OF FIGURES

Figure 6.22: Results of AFM topography imaging by using Mesa corner (3), over 20μm x 20μm area with Δf =25 Hz, 2μm/s ····· 88
Figure 6.23: Vacuuming pump for both insert shield and cryostat. ····· 89
Figure 6.24: SHPM image of the data tracks on the 100 MB ZIP media obtained in the lift-off mode ····· 90
Figure 6.25: Cross section of the data tracks ····· 90
Figure 6.26: SHPM image with Quartz AFM feedback, at 77K by using 5V lift-off voltage ····· 91
Figure 6.27: Cross section path on image and graph of cross section of the data tracks ····· 91
Figure 6.28: Cross section path on image and graph of cross section of the data tracks in Gauss scale ····· 93
Figure 6.29: Resonance curve of the Hall Probe attached quartz tuning fork, at 300K. ····· 94
Figure 6.30: Tracking mode SHPM image with Quartz AFM feedback, at 300K. ····· 94
Figure 6.31: Cross section path on image and graph of cross section of domains ····· 95
Figure 6.32: Resonance curve of the Hall Probe attached to quartz tuning fork, at 300K. ····· 95
Figure 6.33: Quartz AFM feedback tracking mode, force, phase and feedback data at 77K. ····· 96
Figure 6.34: Quartz AFM feedback tracking mode SHPM image at 77K. ····· 96
Figure 6.35: Cross section path on image and graph of cross section of domains ····· 96
Figure 6.36: Quartz AFM feedback tracking mode, force, and phase and feedback images at 77K. ····· 97
Figure 6.37: Tracking mode SHPM image with Q-AFM feedback, at 77K (2). · 97
Figure 6.38: Filtered and enhanced color tracking mode SHPM image with Q-AFM feedback, at 77K (2). ····· 98

LIST OF FIGURES

Figure 6.39: Cross section path on image and graph of cross section of the domains (2) ····· 98

Figure 6.40: Quartz AFM feedback tracking mode, force, phase and feedback data at 77K. ····· 99

Figure 6.41: Tracking mode SHPM image with Quartz AFM feedback, at 77K.(3) ····· 99

Figure 6.42: Cross section path on image and graph of cross section along the line (3)····· 100

List of Tables

Table 6-1: Sizes of one prong of 32 kHz quartz tuning fork and density of quartz ····· 76
Table 6-2: Sizes and density of Hall probe ····· 76
Table 6-3: Sizes of one prong of 100 kHz quartz tuning fork and density of quartz ····· 78
Table 6-4: Prong sizes, spring constants and calculated resonance frequencies of 32 kHz, 100 kHz and 153 kHz Quartz crystals ····· 79

Chapter 1

Introduction

Perhaps the most important ability of the humanity is developing tools and using them in the daily life. Although human beings are not strong enough to survive in nature, the tough we are one of the strongest creatures by using these tools. This ability can also be named as intelligence. Nowadays, the tools are still being developed to achieve a more comfortable and easier life for humanity. Nanotechnology and especially nanotechnology related tools are very important to achieve more functionality in gadgets for this purpose.

Humanity had to have a chance to investigate and understand a new world at atomic scales with the invention of the Scanning Tunneling Microscope (STM) by Gerd Bining and Heinrich Rohrer, at IBM laboratories, in 1981. This invention, which effectively started the nanotechnology, brought a Nobel Prize in physics to its inventors in 1986. With this invention, the researches focused on nanotechnology and new imaging techniques at nano-scale. In 1985, the invention of Atomic Force Microscopy (AFM) followed the STM. These new Scanning ProbeMicroscopy (SPM) techniques, as AFM, increased measurement ability and enlarge the knowledge at this nano-scale with wider range of sample types and surface properties. With increasing interest to these systems, it is succeed to made

atom manipulation and nano-lithography. These developments also allowed scientists to fabricate nano-scale mechanical and electronic devices. In their first applications, SPMs were used mainly for measuring 3D surface topography. Although 3D surface topography is still their primary application, they can now be used to measure many other surface properties as surface magnetic or electrical properties.

Magnetic imaging with Scanning Hall Probe Microscopy (SHPM) provides quantitative and non-invasive magnetic measurements at nanometer scale. SHPM technique is very important way of the understanding magnetic properties and magnetic behavior of magnetic and superconducting materials. In this thesis two of these tools AFM and SHPM are combined to a new, simple and cheaper solution to magnetic imaging of non-conducting materials. I will first describe the theory of STM. Then the thesis will continue with the theory of AFM and SHPM. Then a brief summary of superconductivity will be given. Experimental set-up and its history will be described. At the end with the results, conclusion and the future work will be summarized.

1.1 Scanning Tunneling Microscopy (STM)

One of the best known difference between classical and quantum mechanic is the quantum tunneling phenomena. In classical mechanics, if a ball is thrown into a wall, there is no doubt to be reflected back. But in quantum mechanics, there is a probability of tunneling of the ball, depending on the wall thickness and its kinetic energy. So according to the quantum mechanics an electron can penetrate through a potential barrier. In this forbidden region the wave function, ψ, of the electron decays exponentially. [1]

$$\psi(z) = \psi(0)\exp-\frac{\sqrt{2m(\phi - E)}z}{\hbar} \qquad (1.1)$$

Where m is the mass of the particle (electron) and $\hbar = 1.05 \times 10^{-34}$ Js.

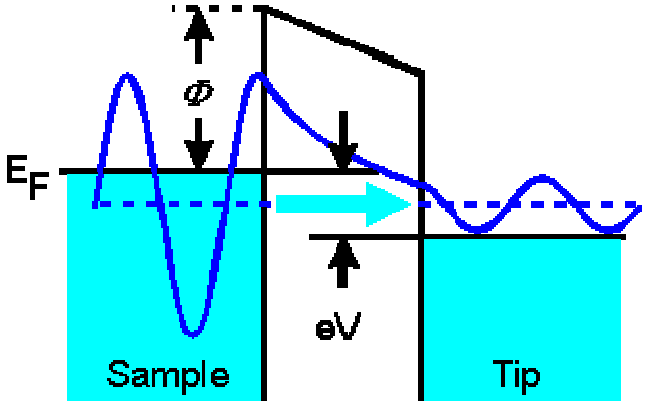

Figure 1.1: Schematic view of a dimensional tunneling barrier

This is a very simple theory to explain the tunneling phenomena. The most successful theory was developed by Tersoff and Hamann in 1983. Tersoff and Hamann modeled the tip as a spherical potential well, as illustrated in Figure 1.2 [2]. Here R is the local radius of curvature of the tip and d is the distance of the nearest approach to the surface.

By using the first order perturbation theory, the tunneling current can be written as,

$$I = (2\pi/\hbar)\sum_{\mu\nu} f(E_\mu)[1 - f(E_\nu + eV) \times \left|M_{\mu\nu}\right|^2 \delta(E_\mu - E_\nu) \qquad (1.2)$$

Here, f (E) is the Fermi function, V is the bias voltage, $M_{\mu\nu}$ is the tunneling matrix element between states ψ_μ of the probe and ψ_ν of the surface, and E_μ is the energy of state ψ_μ in the absence of tunneling. For the small voltages and temperatures, the equation takes the following form,

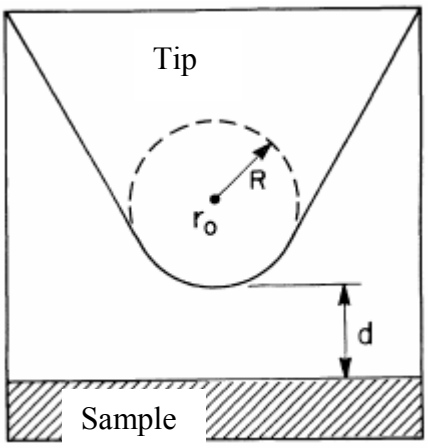

Figure 1.2: Schematic picture of the tunneling geometry.

$$I = (2\pi/\hbar)e^2 V \sum_{\mu\nu} \left| M_{\mu\nu} \right|^2 \delta(E_\nu - E_F)\delta(E_\mu - E_F) \tag{1.3}$$

where E_F is the Fermi level. Here the main problem is the calculation of the tunneling matrix. Bardeen [3] was found a solution for this as,

$$M_{\mu\nu} = (\hbar^2/2m)\int dS \cdot (\psi_\mu * \nabla\psi_\nu - \psi_\nu \nabla\psi_\mu *) \tag{1.4}$$

To evaluate the $M_{\mu\nu}$, Tersoff and Hamann expand the surface wave function ψ_μ and tip wave function ψ_ν into Bloch states. Finally, one can calculate the tunneling matrix with this method as;

$$M_{\mu\nu} = (\hbar^2/2m)4\pi k^{-1}\Omega_t^{-1/2} k\,\mathrm{Re}^{kR}\,\psi_\nu(\vec{r}_0) \tag{1.5}$$

where Ω_t is the probe volume, $k = \hbar^{-1}(2m\varphi)^{-1/2}$, φ is the work function and $\vec{r}_0$ is the center of curvature of the tip. So tunneling current can be expressed as,

$$I = 32\pi^3\hbar^{-1}e^2V\varphi^2D_t(E_F)R^2k^{-4}e^{2kR}\times\sum_{\nu}\left|\psi_\nu(\vec{r}_0)\right|^2\delta(E_\nu - E_F) \qquad (1.6)$$

where $D_t(E_F)$ is density of states at the Fermi level at the tip.

Finally the tunneling can be found as, [4]

$$\sigma_t \propto \rho(\vec{r}_0, E_F) \qquad (1.7)$$

where,

$$\rho(\vec{r}_0, E_F) = \sum_{\nu}\left|\Psi_\nu(\vec{r})\right|^2\delta(E_\nu - E\ ) \qquad (1.6)$$

is the local density of the states at position $\vec{r}$ and the energy E, for the surface.

Then it can be said that if the tip is not modified during the experiment and the distance is large enough, the STM data corresponds by charge density corrugation on the sample. The theory is only valid for the small s distances.

1.2 Atomic Force Microscopy (AFM)

In 1986, during the STM experiments it was seen that the barrier height between the tip and the surface dropped to zero at small separations. Coombs and Pethica [5] suggested that this small barrier height was caused by the repulsive force interaction between the tip and the sample. With this prediction the AFM was introduced by Binnig, Quate and Gerber. In this method, the force interaction between a sharp tip and the surface is measured with the help of a sensitive force detector, instead of tunneling current and utilized to scan the surface at a constant

height. Because this technique does not depend to the tunneling current during the experiment, it also provides the imaging of the non-conducting samples. This capability brings Scanning Probe Microscopy (SPM) technique to work in a wider sample range. This can be taken as the main advantage of the AFM.

The atomic forces near by the surface can be divided two parts as the long range van der Waals forces and short range chemical forces. Short range chemical forces arise from the overlap of electron wave functions and from the repulsion of the ion cores. Therefore, the range of these forces is comparable to the extension of the electron wave functions, less than one nanometer [1].

The short range forces can be modeled with the Morse potential. The Morse potential describes (1.7) a chemical bond with bonding energy E_{bond}, equilibrium distance σ, and a decay length κ. While the Morse potential can be used for a qualitative description of chemical forces, it lacks an important property of chemical bonds: anisotropy. Another model used widely is the Lennard-Jones potential (1.8). [6]

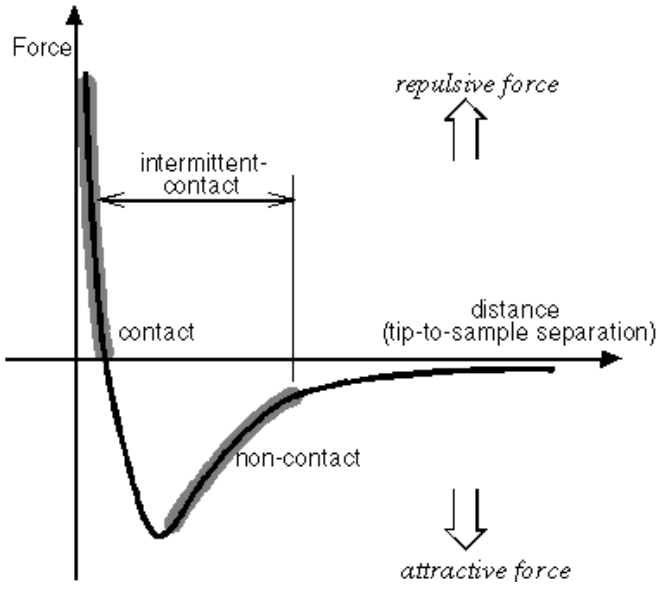

Figure 1.3: Interatomic force vs distance

$$V_{Morse} = -E_{bond}(2e^{-\kappa(z-\sigma)} - e^{-2\kappa(z-\sigma)}) \quad (1.7)$$

$$V_{Lennard-Jones} = -E_{bond}\left(2\frac{z^6}{\sigma^6} - \frac{z^{12}}{\sigma^{12}}\right) \quad (1.8)$$

On the other hand, van der Waals forces are dipole-dipole forces. They are caused by the fluctuations in the electric dipole moment of atoms and their mutual polarization. They always exist and they are always attractive. In short ranges van der Waals forces decays as $F \propto 1/r^7$, where as beyond r ≈ 5nm this power reduces to $F \propto 1/r^8$ [1]. There are two ways for calculating van der Waals forces. In first one the molecular forces are summed up for each geometry with assuming that they are pair wise additive. But the best way to calculate them is the Lifshitz theory. [1]

For the AFM experiments, force interaction between the surface and the tip can be measured by using tunneling detection, capacitance detection [7], beam deflection method [8] and piezoresistive measurement [9], piezoelectric [17] and interferometer [30].

In the first AFM, tunneling detection method is used to measure the cantilever deflection. STM tip is simply positioned behind the AFM cantilever and the change at the tunneling is measured between the STM tip and the back surface of the AFM cantilever. Although this method seems very sensitive for the force measurement, there are several problems as thermal drift and the surface roughness of the cantilever.

In the capacitive detection of the AFM, the back side of the cantilever is used simply as one of the electrode of a capacitor. An electrode is located at the back side of the cantilever as the second electrode of the capacitor. The air barrier between these two electrodes acts as dielectric. The capacitance change between

the AFM cantilever and the fixed electrode is observed to see the changes in applied force. With the capacitance change, feed-back circuit can track the force change easily.

The most common method for the force measurement in AFMs is the optical beam deflection method. In this method, the backside of the cantilever is used as a mirror for a laser beam (Figure 1.6). A laser beam is focused onto the cantilever and deflected beam is collected at a quadrant photo detector. The schematic of a 4 quadrant photo detector is given in Figure 1.7.

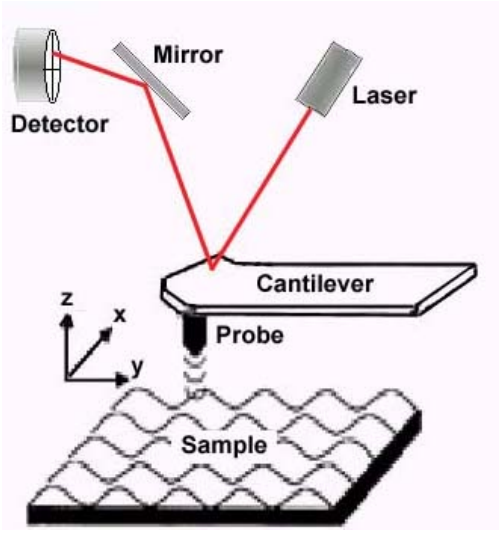

Figure 1.4: The basic AFM set-up with beam deflection method.

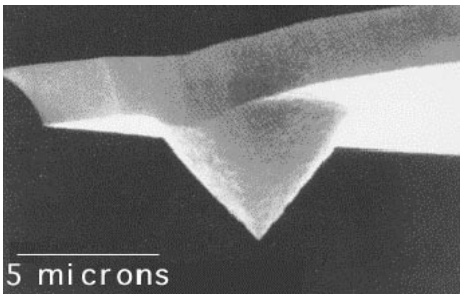

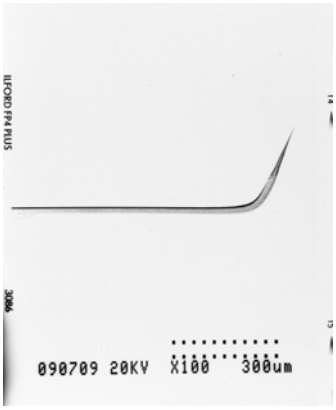

Figure 1.5: AFM cantilevers

With the help of a micro-positioner or piezo drivers the optical beam is located at the middle of the detector. The applied force causes the angle change at the deflection of the optical beam. With this angle change, the optical beam is shifted and of the optical power incident on the quadrants of the photo detector changes. The corresponded signal is measured by the photo detector. Using OPAMPs, this signal is used as an input for the feed-back loop. The feed-back loop works to recover the input signal to its beginning value by moving the sample up and down. The feed-back mechanism is also examined in the next part of this thesis. Almost all commercial room temperature ambient AFMs are based on this measurement technique. Although it is a very effective technique, limitations and practical design problems occurs for the special condition AFM microscopes as ultra high vacuum and low temperature conditions. The sensitivity of this technique can be as low as $2\times10^{-4}\,\text{Å}/\sqrt{Hz}$.

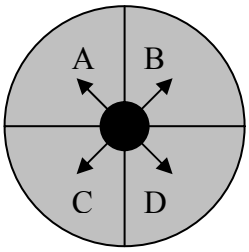

Figure 1.6: A basic 4 quadrant photo detector for beam-deflected AFM set-up.

Another method for force measurement is the piezoresistive measurement. In this method, the AFM cantilever is fabricated by using piezoresistive materials or the back side of the cantilever can be coated with the piezoresistive materials like Si or GaAlAs [10]. The resistance of the piezoresistive element changes with the applied force to the cantilever. One can measure the tip-sample force measuring the resistance change by using a Wheatstone bridge. This technique does not require optical alignment and extra elements, and therefore it is very effective for low temperature applications, where the working area is limited.

Piezoelectric cantilevers, such as quartz tuning forks, can also be used for force detection. In this method the cantilevers are dithered mechanically at the piezoelectric cantilevers resonance frequency with the help of a dither piezo. Piezoelectric cantilevers generate a voltage proportional to mechanical vibration amplitude. When a force is applied to the cantilever, the generated signal is changed. This change can be measured by comparing the shifted signal with initial resonance frequency. Then the changes are used as inputs for the feed-back mechanism.

AFM can be run basically in three modes: contact mode, non-contact mode and tapping (intermittent contact mode).

In contact mode, short range repulsive chemical forces play a role in measurement. In this mode, tip is gently touching to the surface. In this mode tip and the sample are damaged sligthly during the experiment. In contact mode harder materials are used for tip material as SiO_2 or SiN instead of Si tips. In contact mode, forces that are used to record data are grater than 10^{-9} N. Ferrante and Smith [11] have calculated the adhesive forces for several metals. According to these, the force of a single atom tip must be reduced to 10^{-10} N to avoid the deformation of the surface.

In non-contact mode, the cantilever is driven at its resonance frequency with an AC signal with the help of a dither piezo. And the resonance shift is measured by the system. So, in this method the force gradient $F' = -\partial F_z / \partial z$ is measured instead of force. In this mode, short range repulsive chemical forces loose their effect. Van der Waals forces, electrostatic forces and magnetic forces can be measured by this method. The effective spring constant of the cantilever in this method can be written as,

$$k_{eff} = k - F' \tag{1.9}$$

Here, k is the spring constant of the cantilever in the absence of tip-surface force interaction. So it can be seen that an attractive force interaction between tip and surface (positive F') soften the effective spring constant and the repulsive force interaction between tip and surface (negative F') strengthens the effective spring constant. The change in effective spring constant cause a frequency shift, w. This relationship can be explained as,

$$w = \left(\frac{k_{eff}}{m}\right)^{1/2} = \left(\frac{k - F'}{m}\right)^{1/2} = \left(\frac{k}{m}\right)^{1/2}\left(1 - \frac{F'}{k}\right)^{1/2} = w_0\left(1 - \frac{F'}{k}\right)^{1/2} \tag{1.10}$$

Where m is the effective mass and w_0 is the resonance frequency of the cantilever. If F' is small relative to k the equation can be re-written as,

$$w \approx w_0\left(1 - \frac{F'}{2k}\right) \tag{1.11}$$

and,

$$\frac{\Delta w}{w_0} \approx -\frac{F'}{2k} \tag{1.12}$$

So, the attractive force causes a decrease at the resonant frequency where the repulsive force cause increase at resonant frequency. On the other hand the relation between shift in the resonant frequency and the cantilever oscillation A can be written by using the perturbation theory as,

$$\frac{\Delta w}{w_0} kA = \int_0^{2\pi} \frac{d\varphi}{2\pi} F(\bar{z} + A\cos\varphi)\cos\varphi \qquad (1.13)$$

Where the integration is over the one oscillation cycle and $\bar{z}$ is the time averaged position of the tip. To achieve to good resolution in the non-contact force detection, we need a cantilever with soft spring constant, high resonance frequency and high quality factor. High quality factor increase the sensitivity measurement of the system and soft spring constant increase the deflection of the cantilever with force interaction. [12].

1.3 Scanning Hall Probe Microscopy (SHPM)

The surface examination of the materials is not limited only with the surface topography. The magnetic properties of the materials are very important. There are number tools for the magnetic measurement and imaging. Magnetic Force Microscopy (MFM) is the one of the best known magnetic imaging technique. It is a modified AFM technique. It measures magnetic force between magnetized tip and sample. The tip of the cantilever is coated with magnetic materials and magnetized. As the tip is scanned above the surface, magnetic forces acting to the tip deflect the cantilever. Although this is the best known and common magnetic imaging technique with a high spatial resolution, it is invasive and its magnetic field resolution is ill defined. Alternatively Superconducting Quantum Interference Devices' (SQUID's) can also be used for the magnetic measurement and magnetic imaging. SQUID's are known as the most sensitive magnetic flux sensors in the world. Their magnetic field resolutions can be up to 10^{-16} Tesla and they are also non-invasive measurement systems. But unfortunately their spatial resolution is limited to ~ 1μm and the noise increases while decreasing the effective area of the circuit to have a better spatial resolution. The Scanning Hall Probe Microscopy (SHPM) has a better spatial resolution than SQUID's and

better magnetic resolution then MFM and non-invasive. The SHPM technique uses the Hall Effect in semiconductors. In SHPM, the properties of Hall Probe material determine the magnetic field resolution where the size of the active area determines the spatial resolution. It is reported that the best achieved spatial resolution is the 50nm with a bismuth Hall probe with an active area of 50nm x 50nm as shown in Figure 1.9 [13].

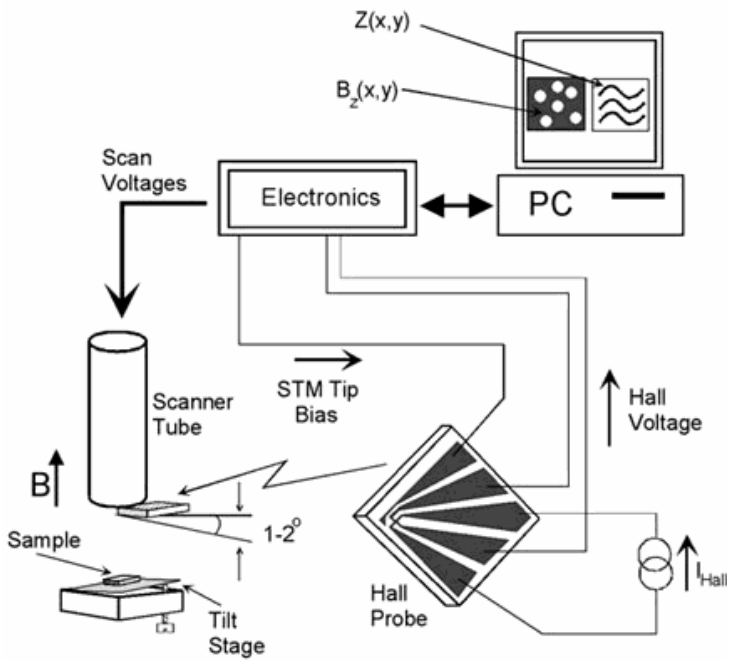

Figure 1.7: Schematic SHPM scan mechanism

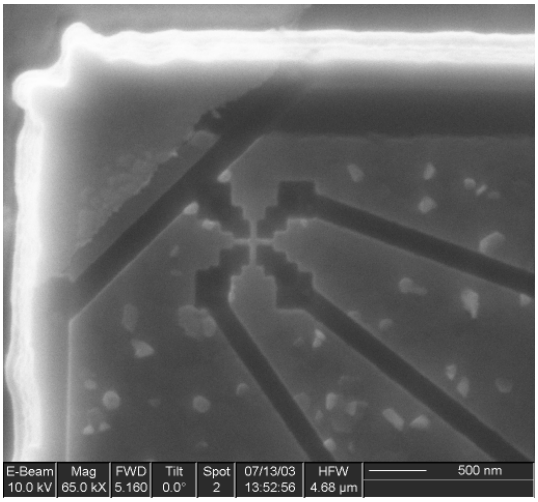

Figure 1.8: Hall Probe with 50nm effective area

The measurement only takes a place at the small square active area between the arms of the probe. A Hall current is passed between the opposite two arms, and the produced voltage, by the perpendicular magnetic field, is measured.

The Hall Effect is first observed by Edwin Herbert Hall in 1879. When a current flows along a conductor in a magnetic field perpendicular to the direction of the current, a Hall voltage is created across the conductor and perpendicular to the magnetic field and the current. Physically, the magnetic field causes the charge carriers to deviate from their original path and swerve towards the side. The Lorentz force (1.14) causes the deflection of the charge carriers.

$$\vec{F} = q\vec{\upsilon} \times \vec{B} \tag{1.14}$$

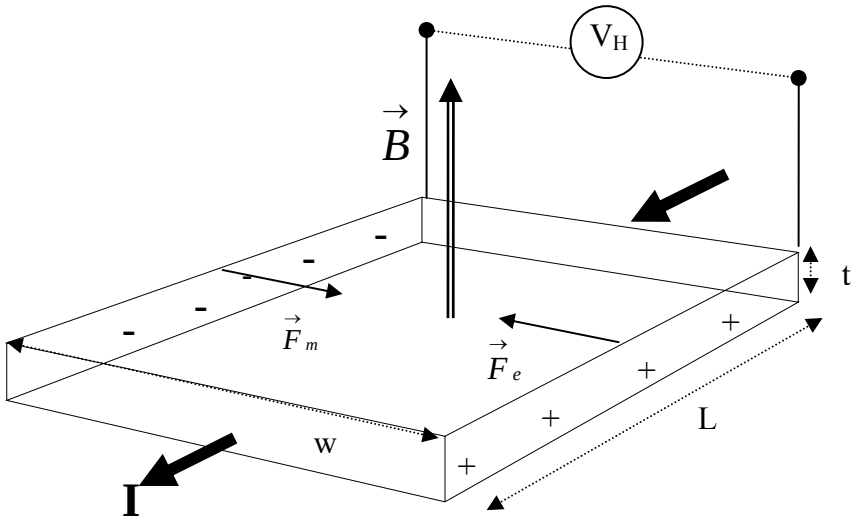

Figure 1.9: Schematic description of Hall Effect

If the carriers are electrons the forces directions will be as in the Figure 1.10. The Lorentz force $\vec{F}_m$ and the force $\vec{F}_e$ which caused by the accumulation of the electrons will cancel each other and an equilibrium is established.

$$\vec{F}_m = \vec{F}_e \tag{1.15}$$

$$-q(\vec{\upsilon}_d \times \vec{B}) = q\vec{E} \tag{1.16}$$

$$E = -\upsilon_d B \tag{1.17}$$

If we assume Q is the total moving charge with the drift velocity υ_d,

$$Q = nwtLq \tag{1.18}$$

Where n is the free carrier density. Then the transition time to pass through the way L is,

$$\tau = \frac{L}{\upsilon_d} \tag{1.19}$$

And the current that pass through the way L an be found as,

$$I = \frac{Q}{\tau} = \frac{twnLq}{L/\upsilon_d} = twnq\upsilon_d \tag{1.20}$$

If we now re-written the Equation 1.17,

$$E = -\frac{IB}{wtqn} = \frac{V_H}{w} \tag{1.21}$$

With this the V_H can be written as,

$$V_H = -\frac{IB}{tqn} \tag{1.22}$$

And the Hall constant can be found as,

$$R_H = -\frac{1}{qn} \tag{1.23}$$

So if we measure the Hall voltage generated for the applied magnetic fields, we can calculate the Hall coefficient R_H. Then, using this Hall coefficient it is possible to measure the unknown magnetic fields just above the surfaces. For a calculated R_H and known magnetic field one can easily calculate the free carrier density using Equation 1-23. Alternatively, if we know R_H, the applied magnetic field can be measured easily by using the measured Hall voltage by using relation 1.23.

$$V_H = I_H GBR_H \tag{1.24}$$

Where, *G* is the gain. Typically 10,010 for our measurement system.

1.4 Scanning Probe Microscopy (SPM) scanning technique

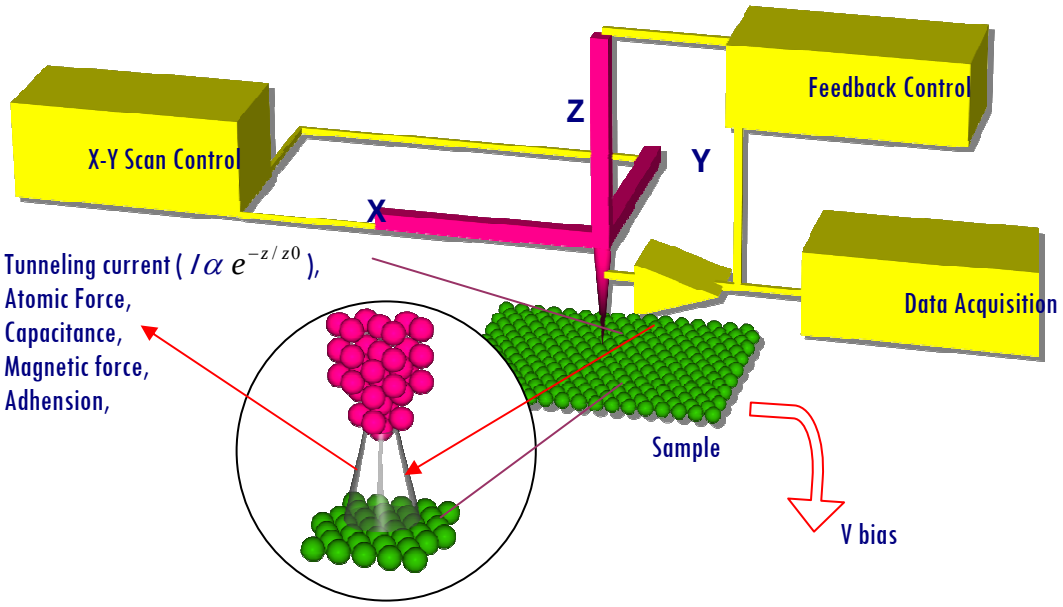

Figure 1.10: Schematic diagram of SPM

Scanning probe microscopy is the general name of the STM, AFM and similar techniques. The scanning mechanism of all the SPM techniques is similar each other. The sensor/tip is brought very close to the surface, using a coarse approach mechanism, and then it is scanned across the surface, acquiring data at each x-y point.

Because of the very fine movements are necessary for the SPM techniques, piezoelectric materials are used for scanners. The scanner range is typically between 1-100 μm in xy and 0.1-10 μm in z direction. In piezoelectric effect, an applied voltage between two electrodes of the material causes a change in stress and strain. By using this effect, a well controlled extension can be provided at the material. The reversible piezoelectric is also available. An applied stress or strain

causes an electric field to develop in the material. The extension that is caused by the applied electric field properties depends on the dimensions and geometry of the material. The resultant displacement coefficient for a PZT tube (2 inch long, 0.5 mm thick, 6.35 mm in diameter) is in a few thousands Å per volt in x-y directions. Therefore with a fine voltage source and with a good choice of piezoelectric material, extensions in Å scale is possible. These properties of piezoelectric materials are used for both coarse approach in z direction and fine scanning on x-y-z plane.

Although the piezoelectric material provides sub-Å scale movements, their maximum extension ranges are limited in μm scale. Therefore another, approach mechanism is needed for the coarse approach. A step motor can be used for this purpose. The important point here, the each step of the stepper should be less than scanner range in z. Otherwise the probe can be crashed to the surface. Generally an automatic approach procedure is established for the coarse approach process. This automatic approach routine first searches the probe-surface interaction is found or not by extending the z piezo. If the interaction (tunnel current, force, etc...) is not found, the sensor/tip is pulled back and a step is made with the coarse positioner. Because the steps of the coarse approach mechanism are smaller than the range of the fine approach there is no chance to crash the probe to the surface. Another example for the coarse approach mechanism is the slip-stick mechanism which is also used in our experimental setup. A metal slider puck is fixed on quartz tube, which is glued to a piezo tube, with the help of a leaf spring. When the quartz tube moves forward slowly and then pulled back suddenly, the slider puck can not overcome its inertia and slides with respect to the quartz tube.

After the coarse approach, the second most important part in SPM is the scanning mechanism. The probe is moved on the surface on a controlled manner with the help of piezoelectric materials which controls the movement in x-y plane. For each x-y-z direction coordinate, the data is recorded during the scan and

stored in a matrix. So the images are 3D in SPM techniques where there is a surface properties measurement data for each x-y coordinate. This surface property data can be height data for STM and AFM techniques or can be a magnetic field strength for SHPM technique. Generally we can talk about two methods for the scanning process. The first one is known as constant height mode. In this mode, the z position of the probe does not change during the scan. Only the change in the interaction (force, tunneling current, magnetic field etc…) is recorded. This technique is simpler and the more dangerous one. If there is a point on the surface, which is higher than the distance between the probe and the surface, the probe can be crashed onto the surface. On the other hand the probe can be too far from the surface, and then the interaction will be lost. To avoid these disadvantages, constant current/interaction mode, can be used. In this mode, the distance between the probe and surface is kept constant with the help of the feedback loop driving piezoelectric scanner. In STM the tunneling current, in AFM the force is kept constant for this purpose. A simple feed-back loop is utilized to achieve this. Feed-back loop moves the sensor towards the sample when the probe current/force is decreased and moves the sensor away if the interaction is increased. So the distance between the probe and surface is kept constant during the scan process. The voltage applied to the z-piezo, is logged as the data for the surface topography. Because the voltage change at piezo is mostly linear with the distance change between the surface and probe, the feedback data is smoother and more reliable from the direct measurement data especially for the STM operation. On the other hand, the scan is done slowly, line by line. Typically, the data are taken for two times, one for forward movement and another one reverse movement. This also provides a verifying mechanism for the reliability of the measurement.

A 4 quadrant scanner piezoelectric tube is usually used for scans in x-y plane and fine movement in z direction. The working mechanism can be explained below.

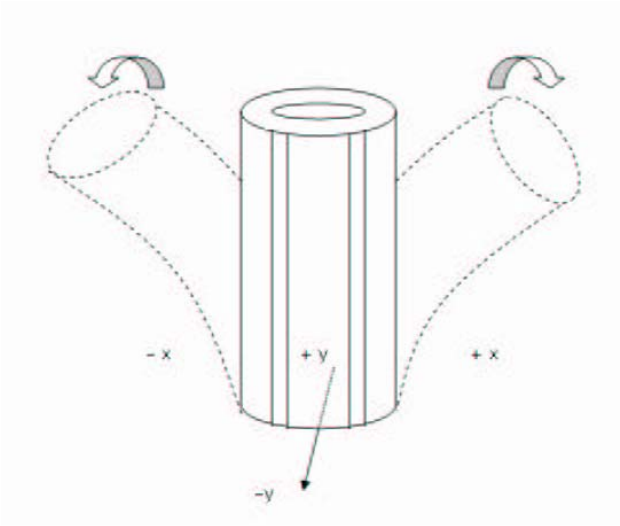

Figure 1.11. Schematic view of scanner tube

Here, with applying different voltages to the different quadrants of the scanner tube cause different extensions at each quadrant. By using this mechanism the scan process can be supplied as in Figure 1.11. Movement in x-y plane is limited with 56 μm where the length of the scanner piezo is 2 inch. So we can ignore the angle that cased by crimping. If we apply to all quadrants the scanner tube extends or retracts.

It is also possible to extend or retract the tube in the z direction at the same time when scanning it to x and y directions with applying voltages with different values. The z-voltage is simply added to the 4 quadrants using high voltage amplifiers.

Other important parameter for the SPM techniques is the quality. This depends on probe quality and responsible from the resolution in x-y plane. This resolution is named as “spatial” resolution. To increase the spatial resolution the sharpness of the tip for STM and AFM processes and the active area of the probe for SHPM probe are important (Figure 1.12). The common way to get sharper tips to increase the spatial resolution can be given as the electrochemical etching

process. A tungsten wire can be etched with the typical values of 7 V and with a typical 2M NaOH or KOH solution for the AFM tips (Figure 1.13). Because the tungsten wire gets oxidized quickly, the Pt-Ir tips are commonly preferred for the STM operations. The Pt-Ir tips can be also etched electrochemically in NaCl or can be cut for the STM [14,15]. For the micro fabricated device probes as SHPM probes, the size of the effective active area determines the resolution.

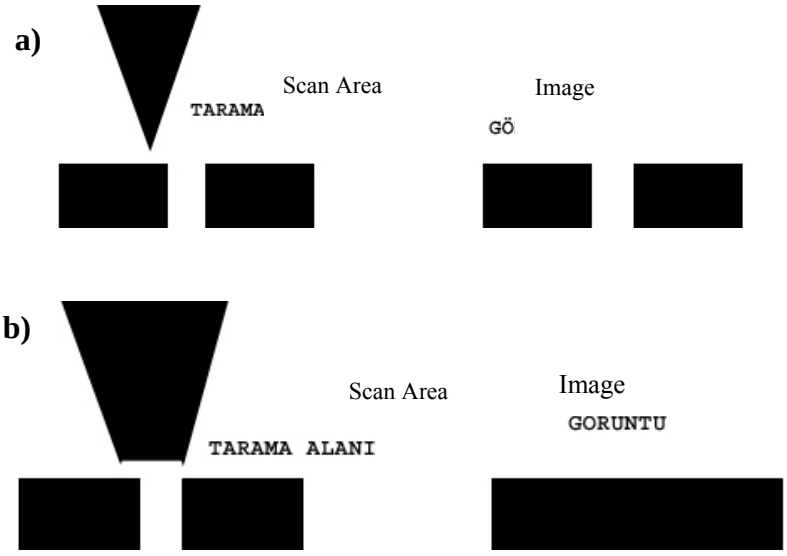

Figure 1.12: Sharpness dependent resolution

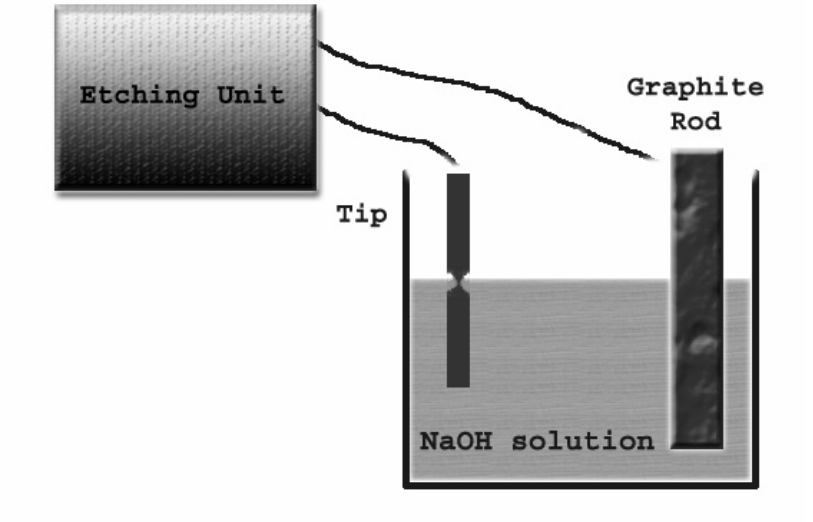

Figure 1.13: Electrochemical etch setup for AFM applications

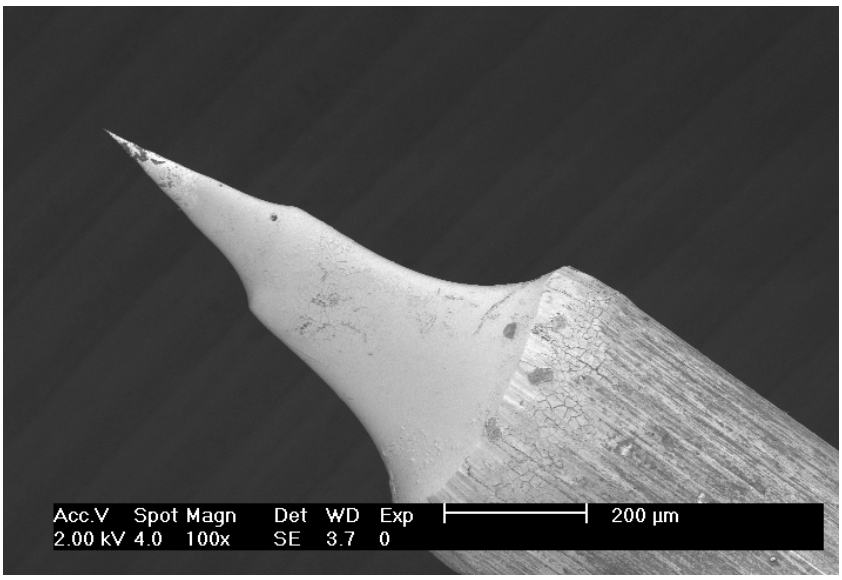

Figure 1.14: SEM image of electrochemically etched W wire. The gray points on the tip are the carbon atoms which are deposited by the graphite electrode. (K.Urkmen and L.Ozyuzer, Izmir Institute of Technology, 2002)

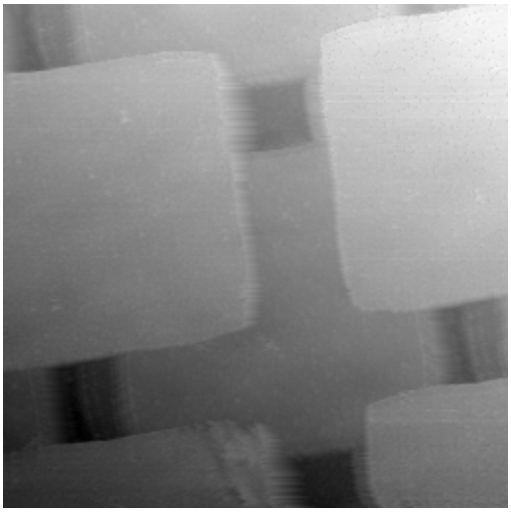

Figure 1.15: STM image with 8µm x 8µm scan area on 6µm period grating sample at 4.2K, as an example of shadow effect of dual tip.

Chapter 2

Experimental Set-up

As a main part of our experimental setup we used Nanomagnetics Instruments' commercial Low Temperature Scanning Hall Probe Microscope (LT-SHPM) system [31]. This LT-SHPM system includes mainly two parts as microscope (Figure 2.1 and 2.2) and SPM control electronics.

Figure 2.1: Low Temperature Scanning Hall Probe Microscope.

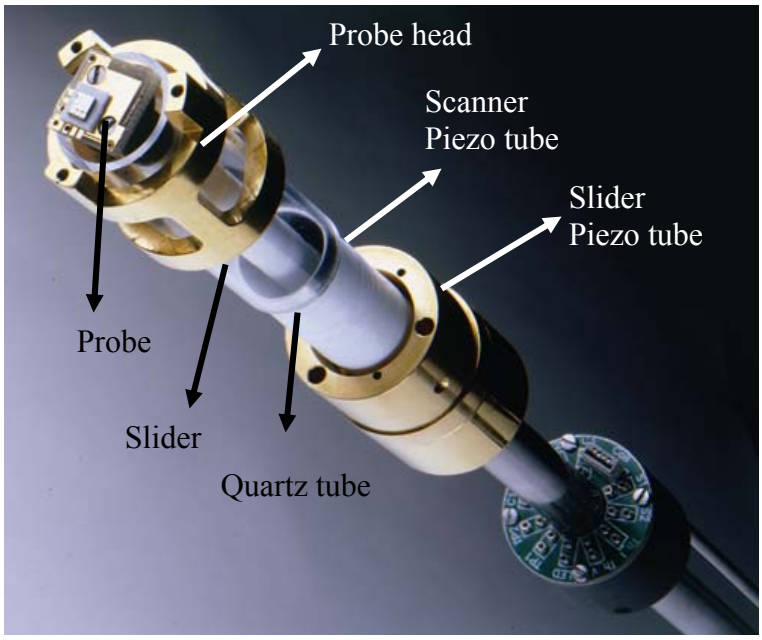

Figure 2.2: Low Temperature Scanning Hall Probe Microscope in details.

The microscope is composed of the scanner piezo, slider piezo, slider, sample holder and electrical connections. Scanner piezo is used for the scan with resolution in Å scale and fine approach. Probe head fixes the probe with the help of 2 screws and provides the electrical connections of the Hall probe and STM tip. Slider piezo is used for the coarse approach and coarse x-y movement. The scan range of the scanner piezo tube of our system is ~ 56μm x 56μm on the x-y plane and the extension range is ~ 4.8 μm at room temperature. The piezo constants change with the temperature. Piezo constants decrease by factor of 3.8 when the system is cooled from room temperature to 77K.

In LT-SHPM system, the probe is simply screwed to the probe head which is just located on the scanner piezo (Figure 2.3). The sample is fixed to the sample holder with silver paint to carry bias voltage to the sample. Front and back sides of the sample holders are screwed to each other. Screw does not fix the sample holder to the slider. A spring is located on screws to fix the sample holder to the slider part. This provides coarse moving of sample on the slider puck. High

voltage pulses applied to the appropriate electrodes of slider piezo to extend it on x-y directions to provide this coarse movement of sample holder. The quartz balls that are located between the sample holder parts and slider puck make this x-y movement with less friction. The slider puck can be fixed to the main part of the slider with using spacers for normal AFM and STM operations. In AFM and STM operations, angle between the probe and the sample is not critical. For SHPM operations the angle between the probe and sample plays an important role. Because of this, slider puck is fixed with alignment springs as shown in Figure 2.3.

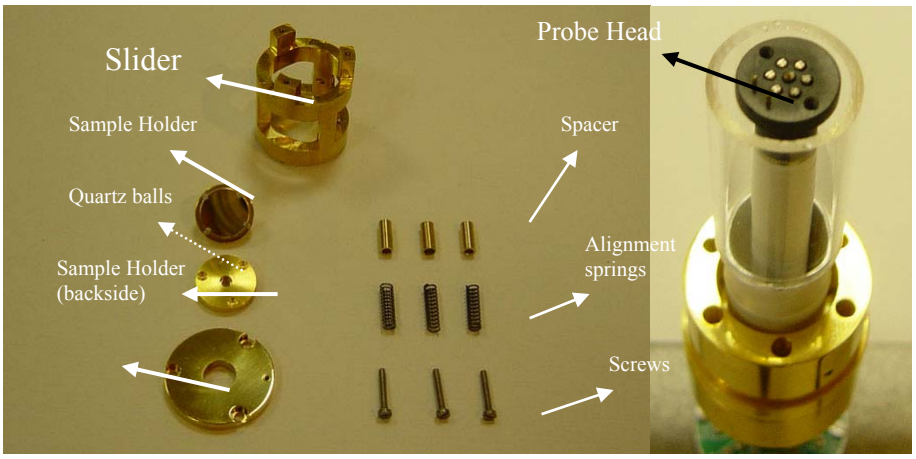

Figure 2.3: Slider part contents and the scanner head of LT-SHPM system.

After the slider part get ready, the slider is fixed on the quartz tube of the microscope with the help of a leaf spring. It can move with a powerful pulse with using stick-slip movement. The bias voltage cable is connected to the related part of the slider. The movement of the slider part is controlled firstly by hand and then by sending high voltage pulses to the slider piezo. After all, the shield is located around the microscope head to avoid noise and to safe guard the microscope.

The operation is controlled by the SPM Control Electronics (Figure 2.4). The software and computer are also used as user interface for inputs and outputs. The software also collects data, converts it to image, processes and saves images. All

other features, as feed-back control, are controlled by the SPM Control Electronics. For our experimental set-up, the electronic cards that we need, are listed below,

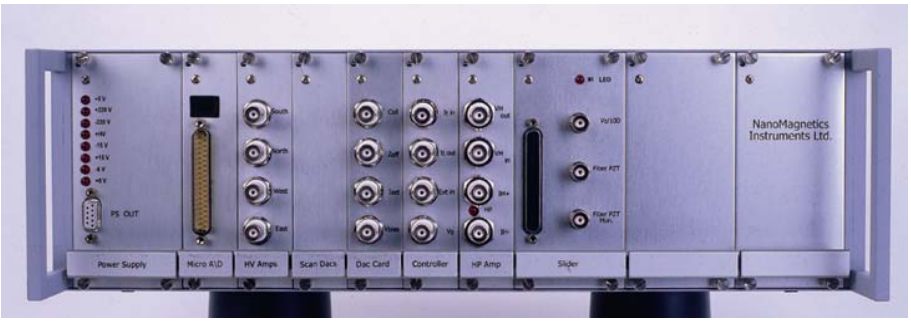

Figure 2.4: SPM control electronic.

Power Supply Card: Supplies the power to pre-amplifier, electronics and the microscope. The pre-amplifier of the microscope is connected to this card by using a D9 connector.

Micro A/D Card: Establishes the connection between the SPM Control Electronic and the computer. It uses serial and parallel interfaces for computer connection. It also includes a microprocessor inside to run the time critical function

High Voltage Card: Provides the high voltage for the scanner piezo. If there is no separated dither part of the scanner piezo, dither voltage should be entered this card externally to dither the scanner piezo for the AFM experiments. Each electrodes of the 4 quadrant scanner tube are connected the output channels of this card by using BNC connectors.

Controller Card: is responsible from the feed-back. It also collects the data from both tunneling input and external input channels. Tunneling input contains a logarithmic amplifier. It can run feed-back mechanism by using tunneling input or external input according to the users' choice.

Slider Card: Provides the exponential high voltage pulses to the slider piezo for the coarse movements. It also provides LED signal for an IR-LED which is

located at the slider part of the microscope to excite the carriers of the Hall Probe in low temperatures.

HP Card: Provides the Hall current between -1mA and 1mA to the Hall Probe, amplifies and measures the Hall voltage.

PLL Card: Provides the AC signal with 4 mHz resolution and with amplitude up to 20 V_{pp}. The main job of this card is to set the system into oscillation and measure resonance frequency shifts signal of the AFM sensor. This card also has a second feed-back loop inside for the measurement of the dissipation energy changes.

Scan DAC Card: Controls the scan process during the scanning.

DAC Card: Supplies various voltages for various purposes using 4 off 16 bit DACs.

Our experimental setup also can work in three modes with three different SPM probes: STM, AFM and SHPM. (Figure 2-5)

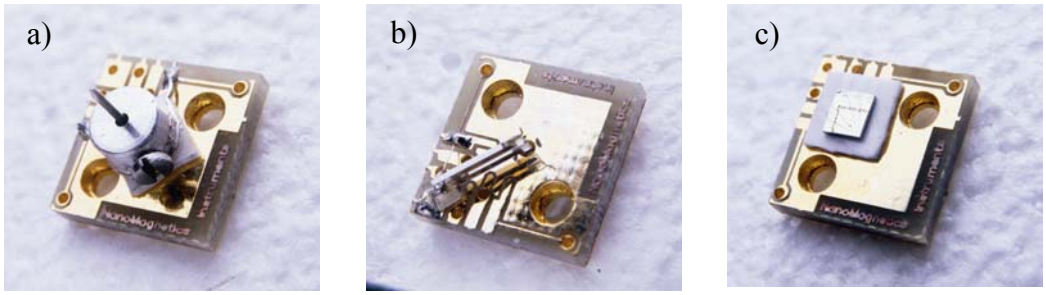

Figure 2.5: Available SPM probes: a) STM holder, b) Quartz Tuning Fork AFM probe, c) SHPM probe.

Another part of our experimental setup is a homemade cryostat system that was build by our under-grad student Duygu Can (Figure 2.6). This cryostat system is used for the controlled cooling down and warming up processes. Temperature changing rate is very critical for the LT-SHPM system because of the piezoelectric materials and quartz tube. The cooling rate should be smaller

than 2K/minute. It is also possible to fix the temperature at specific point and fix the temperature change rate with the help of the Oxford Research System's ITC 601 controller. This controller is programmed by Objectbench software.

Figure 2.6: Our homemade cryostat system which is directly inserted to the liquid nitrogen tank.

Chapter 3

SHPM Probe Fabrication

The Hall Probes are micro fabricated devices. As it is discussed in Chapter 1, they are based on Hall Effect on a cross effective area which is limited with the 4 arms of the probe. To observe a Hall Effect on the material, the material should be conductive. The high carrier concentration decreases the Hall coefficient and the sensitivity of the probe. The high mobility enables one to pass current without heating the sensor. Then for an optimum measurement, semiconductors are used to fabricate the Hall Probes. Thin semiconductor films on insulating wafer or 2DEG wafers can be used. Other advantages of using thin films or 2DEG wafers are limiting the measurement area on the z direction. Otherwise the measurement takes the average of the magnetic field that penetrates to the probe. In this thesis work, a P-HEMT wafer was used for probe fabrication. The structure and the specifications of this wafer are given in Figures 3.1 and 3.2.

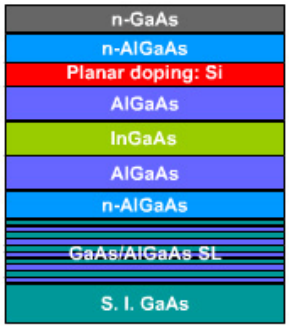

9 Å AlAs
1000 Å N_+ ($10^{13}cm^{-2}$)
9 Å Undoped AlAs
230 Å Undoped AlGaAs
Si Pulse (4.4 10^{12})
20 Å Undoped AlGaAs
20 Å Undoped InlGaAs
4500 Å SLB
Pseudomorphic layer
Substrate with Low DX centers

Figure 3.1: Pseudomorphic High Electron Mobility Transistor P-HEMT wafer and its specifications that is used for Hall Probe fabrication

Photolithography and e –beam lithography are commonly used for fabrication of Hall Probes. These techniques are based on masking the samples and etching or making metallization using lift-off process after this.

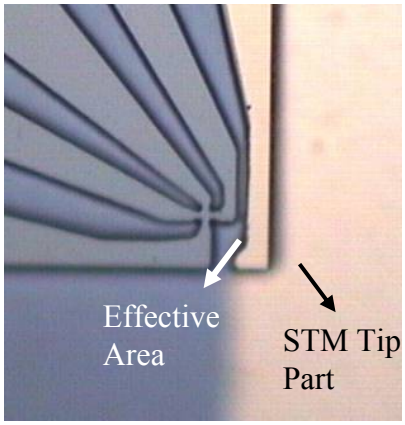

Figure 3.2: Hall Probe with integrated STM tip

Photolithography is the process of "writing" on a surface using light. The process is extremely simple and consists of only a few steps. The initial step in photolithography is to cover a substrate with a polymer photoresist that changes its properties upon exposure to certain wavelength of light. First, the resist is dissolved in a liquid solvent. Second, the resist is placed drop wise onto the substrate surface and spun at speeds between 1,000-10,000 rpm. This process, called spin coating, allows for control of resist thickness of the substrate by varying the rotation speed. The higher the rotation rate the thinner the resist layer. Third, the substrate is baked on a hot plate to force off the solvent leaving behind a resist layer. This resist layer is adsorbed to the surface by a weak interaction arising from Van der Waals forces. This weakness is advantageous for a couple reasons: one, using a polymer that would chemically bond to the substrate surface could change or damage desired surface features; two, it is advantageous for the process to be easily reversible, allowing for a complete stripping of the resist from the substrate by a solvent wash called a developer.

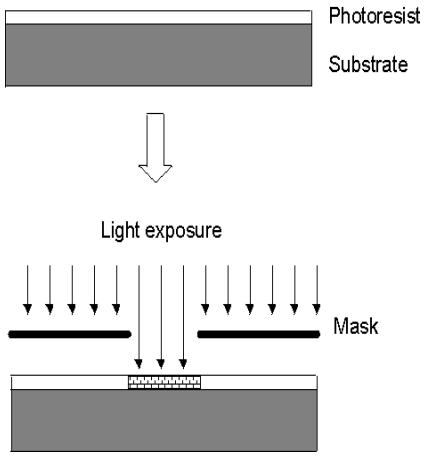

Figure 3.3: Photolithography process

The resist layer is then irradiated through a pattern mask that is either in contact with the resist layer or held at a significant height above the surface. The photoresist exposed to radiation undergoes a structural change, and its solubility changes as a result. If the exposed resist becomes soluble to the developer, it is referred to as the positive resist; if it becomes less soluble, it is called the negative resist.

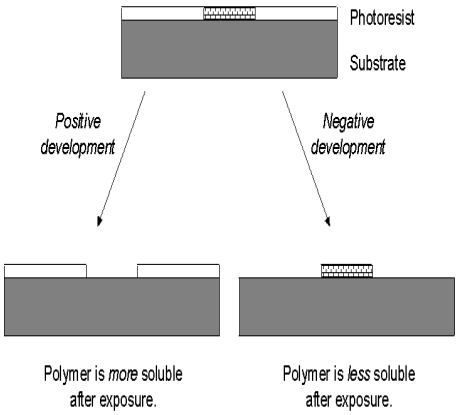

Figure 3.4: Difference of negative and positive resists

After exposure to radiation, a pattern is left on the resist layer consisting of the altered polymers. The entire resist layer is then treated with a developer that

removes either the exposed or unexposed resist material depending upon the solubility of the resist used. The substrate below the resist layer is thus exposed.

The exposed substrate material is then treated with some processes such as etching, metal deposition, or ion implantation that does not interact with the resist material. Finally, the resist material is completely stripped away with another solvent wash, typically acetone. This process can be repeated several times to build layers of features onto the substrate surface.

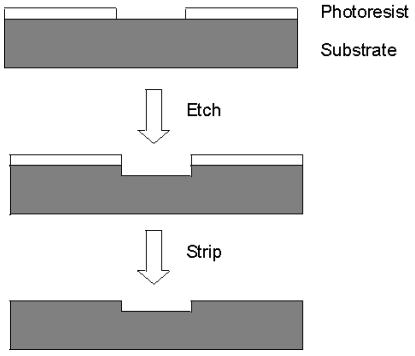

Figure 3.5: Etch process after photolithography

There are various ways of etching the wafer by different methods. Most preferred method is a physical etching, which is done by reactive ion bombardment of the surface called reactive ion etching (RIE). This technique gives possibility to etch the wafer from the surface to inside very uniformly and precisely to a desired value. The high energy ion bombardment can cause etching on the undesired regions of the wafer, moreover it consumes various enchant gases. Therefore we do the etching process by means of chemical etch using an acidic solution that is called wet etching technique. In this technique, the chemicals etch the surface. Although the chemical etch is simpler, the side etch problem occurs during the etching, because of the etching through the crystallographic directions. During etching process, the pattern, that we do not want to etch are protected by the photoresist material.

In our case, the first step is the Hall Probe definition with using these two techniques. For this purpose, first our wafer is cut into (5mm x 5mm) pieces with the help of a diamond scriber. To avoid the damage the surface of our wafer, the wafer can be coated with a thick layer of photoresist before this process. After the wafer is cut; the pieces, that will be used, are washed first with acetone and then with propanol-2. Then the wafer is dried with dry N_2 gas without giving permission to propanol-2 dry naturally. This drying process avoids the defects that can be caused by the residues of the chemicals. After the cleaning process the wafer is coated with photoresist (AZ5214) by spinning at 10,000 rpm. Then it is baked at 110 ºC for 50 seconds by using a hotplate, which is known as soft bake. In the next step the wafer is placed under the mask at the mask aligner (Karl Suss, MJB 3). After a good alignment with the mask aligner, the powerful UV light with 5mW is exposed to the surface for about 35 or 40 seconds. Then the wafer is developed by watching the color changes at the surface. When the fast color change is finished the wafer is washed in a fresh de-ionized water to remove the developer chemical on it. The development process takes about 15 second for the given photoresist thickness and exposure time.

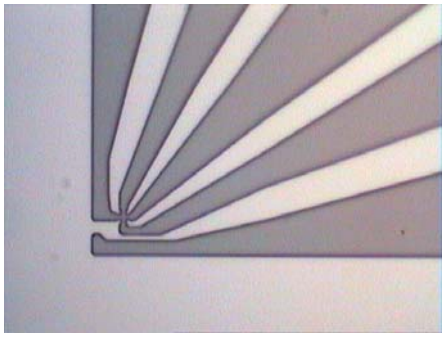

Figure 3.6: Hall Probe definition with photoresist coating, after develop

The Hall Probe definition that coated with photoresist is examined under a powerful optical microscope. If developed pattern is satisfactory, the etching chemicals or the RIE is getting prepared. For the chemical wet etching, the

usual chemicals for the Hall Probe definition are H_2SO_4, H_2O_2 and H_2O. The mixture is prepared by using these chemicals with the ratio 1:8:320, respectively. But in this thesis work, a problem is occurred during wet etching process which is what we think caused by the wafer quality. Then for a second choice, we used Reactive Ion Etching (RIE) system for the Hall Probe definition with 20 sccm CCl_2F_2. The parameters can be given as 30 second for gas condition time and 74 W in $4x10^{-3}$ mbar pressure. To measure the etch rate, an unused part of the sample is used. The etch rate is determined as 15.7Å/sec. Then our developed wafers are etched for 2 min and 10 second (~200 nm) to pass the 2DEG layer which is located about 180 nm down from the wafer surface.

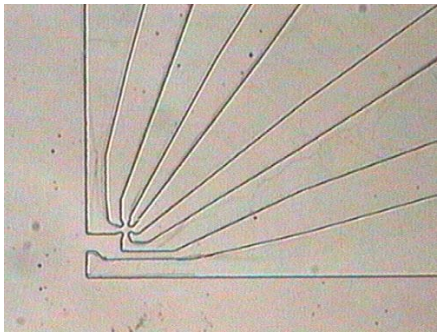

Figure 3.7: Hall Probe definition after RIE etch

As the second step in Hall Probe fabrication the mesa etch is done with using same procedure. By this step, we separate the Hall Probes on the wafer with sharp edges. This is also important for this thesis work where the corner of the mesa is used as the sharp tip for the AFM feed-back. In this time, parameters are changed as 6,000 rpm for the spin, and 20 minutes for the mesa etch time with RIE for 1.8μm. A very important point for this step is the alignment. The mesa mask should be located precisely aligned with respect to the Hall Probe definition. The mesa mask hides the Hall probe definitions to protect from the light, and then a real challenge is occurred at this step. For this reason the turns of the micrometer screws of the mask aligner is recorded carefully for the

alignment in x and y directions and then alignment is done blindly just with these records.

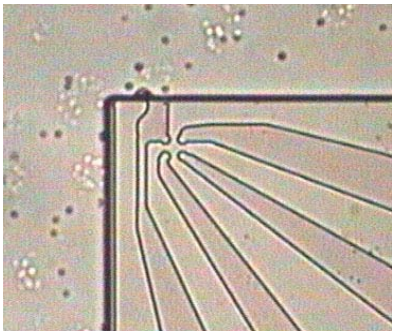

Figure 3.8: Mesa Etch by RIE

For the third step of Hall probe fabrication the recess etch is done similarly. This step is done to avoid the shorting of the sample and the Hall Probe's electrical connections during the SHPM experiment. So the edges close to the sides of the Hall probes is etched about 50-60 μm deep in this step. For the lithography part the wafer is spun at 6,000 RPM again, and exposed for 60 seconds. To avoid the undercut etch, a mask is used with gear tooth like edges. The sides of the mask are aligned carefully to locate the Hall Probes at the centre of the light protective area. After development the sides of the wafer is cleaned by acetone with help of a Q-tip and an extra photoresist drop is applied on the centre of the wafer over the thick photoresist layer that left after development. Because the etch depth is so high, the HCl is used with ratio 4 HCl, 10 Hydrogen peroxide, 55 DI water for 1 hour period.

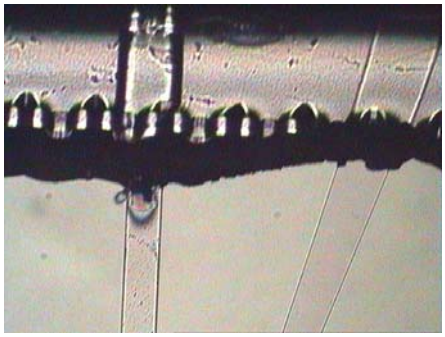

Figure 3.9: Recess Etch by HCl

The last step in Hall Probe fabrication for this thesis work is the metallization. In order to have an ohmic contact behavior of the contact of metal and GaAs, the metal should be defused or alloyed into the GaAs wafer. Ohmic behavior means linear dependence of the current passing through the contact on the voltage applied across the contact. A good ohmic contact possesses low resistance, long endurance in time and high stability against temperature. The common technique used for the ohmic contact is to coat metal film through exposed and developed sample the photolitogrpahed sample, lift-off photo resist and unwanted metals and alloy the metal into GaAs by Rapid Thermal Processing (RTP).

For this purpose the wafer is again coated with AZ 5214 resist by spinning at 10,000 RPM. The metallization mask is carefully aligned as in mesa step. In this step, Hall Probe part and the ways between the connection paths are protected by the mask. Then the photoresist is removed only from the connection paths after development. After these preparations are finished, we metallize the whole wafer by using the box-coater (Leybold, LE 560). Box-coater thermally evaporates the material in the high vacuum and deposits its vapor into the wafer surface. The used vacuum condition is about 10^{-6} mbar and the wafer is hold about 20 cm above the metal boats. Our process involves multilayered metal deposition with Ge dopant included in between layers. Ge will play the role for obtaining ohmic behavior of the contact after the layers are alloyed into GaAs. Ni and thin Au layers are deposited to help Ge penetrating into GaAs. 1,500A^0 Au layer is deposited for increasing the conductivity for and easy bonding. For next step after the metallization of Ti, Au and Ge layers, photoresist is lifted-off with the metals on it. Metallized wafer is put into acetone to dissolve PR (photoresisit). Since PR is dissolved in the acetone the metal parts on PR become free and float in the acetone where the metal parts of the bare wafer stay. This procedure is called the lift off. At the end, the desired patterns are obtained on the surface of GaAs wafer. Ohmic contact formation

after photolitography as mentioned before a cleaning process is essential before passing the next step which is RTP. Cleaning is performed by the previously described washing with acetone and propanol-2 method. RTP is generally named annealing or rapid thermal annealing RTP. This is thermal process in which the wafer can be annealed by blackbody radiation of a filament.

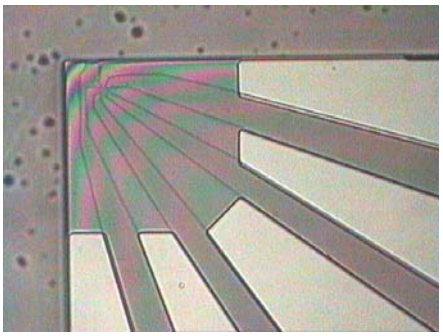

Figure 3.10: Metallization development.

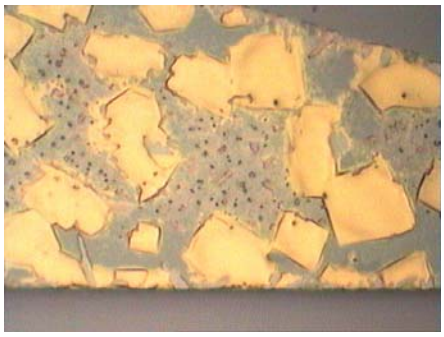

Figure 3.11: Doped Au layer after RTP process on Hall Probe contacts

For the STM feed-back SHPM Hall Probes, the tip metallization can be done before the final cutting step. But for this thesis we ignore this step. The finished Hall probe's photograph is given in Figure 3.12 and B-H curves are given in Figure 3.13.

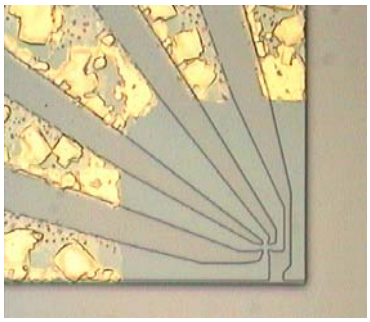

Figure 3.12: Finished Hall Probe without STM Tip.

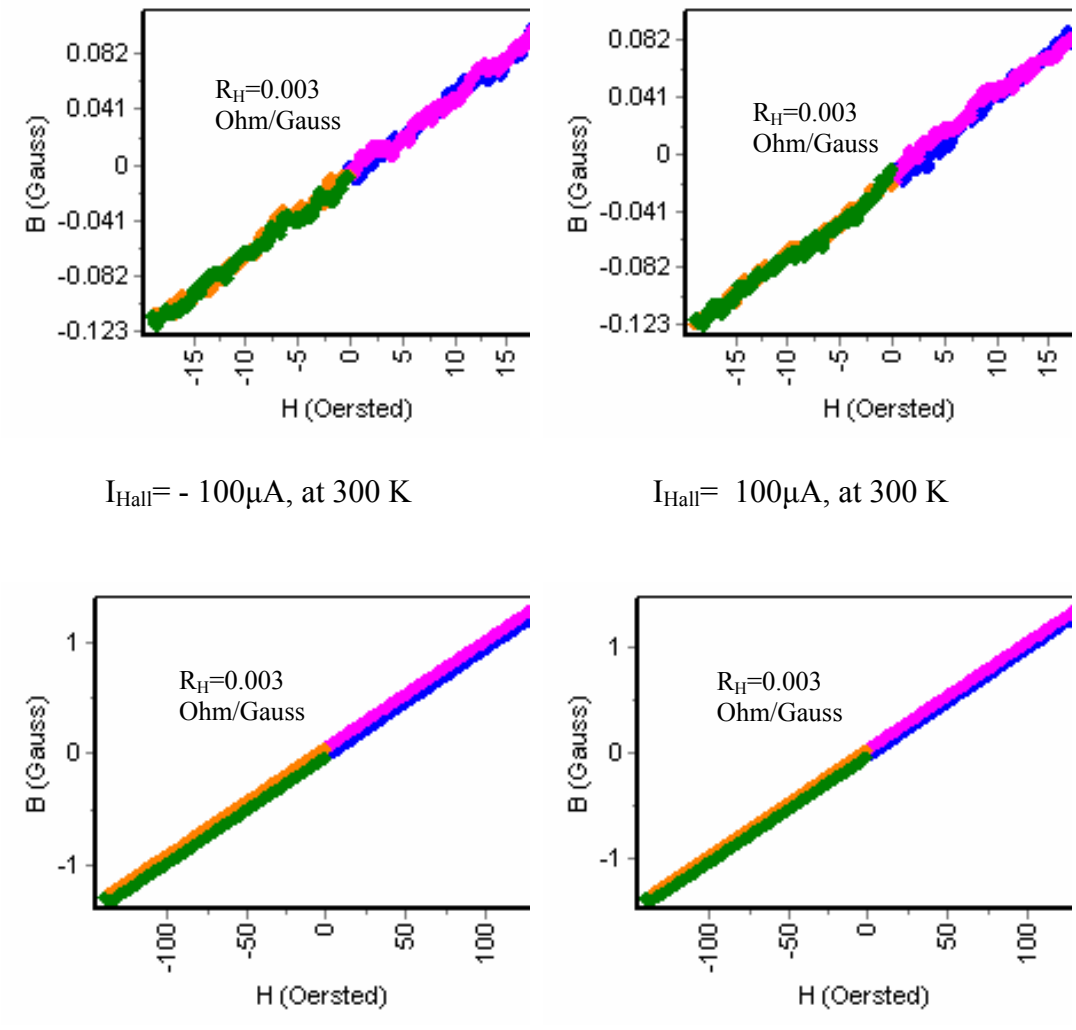

I_{Hall}= - 100µA, at 300 K

I_{Hall}= 100µA, at 300 K

I_{Hall}= - 100µA, at 77 K

I_{Hall}= - 100µA, at 77 K

Figure 3.13: B-H curves of Hall probes that are fabricated during this thesis work.

Chapter 4

Scanning Hall Probe Microscopy (SHPM) experiments with STM feedback

In SHPM, a micro-fabricated Hall sensor is positioned very close to the surface for measuring very small magnetic field data. It is known that the magnetic field strength is decreasing with $1/r^3$, where r is the distance between the probe and the surface. So the distance between the surface and the probe is very important for not losing the field strength.

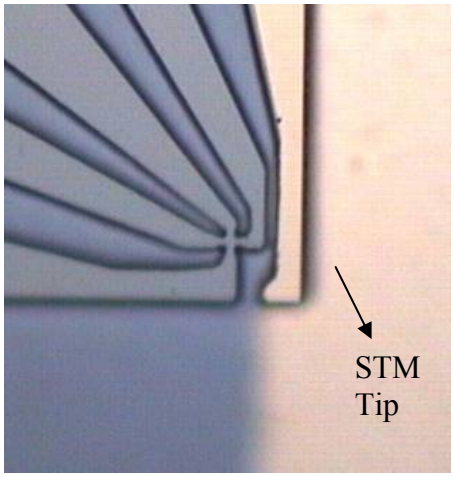

Figure 4.1: Hall Probe with STM Tip.

Therefore SHPM technique should be combined with other SPM techniques as STM or AFM. The STM tracking mechanism is the simpler one for this purpose. A STM tip or in other words a gold coated mesa corner for tunneling can be located near the SHPM probe as given in Figure 4.1. Because this gold coated mesa corner is used for STM feedback mechanism in our system, the sample should be given an angle about 1.25º to make the STM tip closest to the surface than anything else (Figure 4.2). The sample must be conductive STM tracking SHPM. For the non-conductive samples, 10 or 20 nm thick Au layer can be coated on the sample surface.

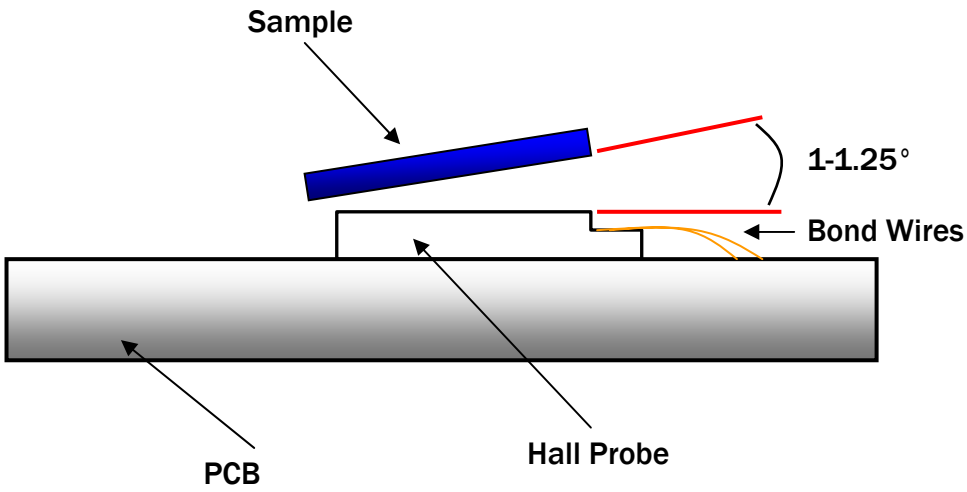

Figure 4.2: Alignment angle for SHPM operation.

To give the correct angle between the probe and the surface, a careful alignment procedure is employed. The sample is fixed to the slider puck with three springs for this purpose. One of these springs is located to the end corner of the SHPM probe just to align the angle as shown in Figure 4.2. First of all, using the three screws, the probe is made parallel to the surface. Then using the screw at the bottom is loosened to give desired tilt angle.

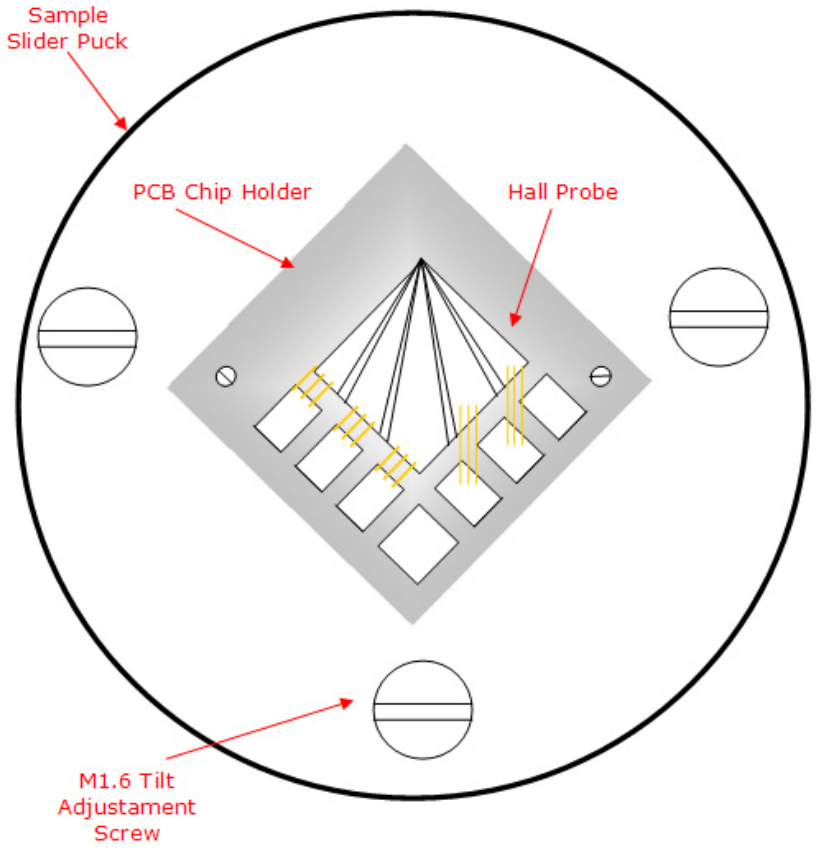

Figure 4.3: Schematic of alignment mechanism.

Figure 4.4: Images of the hall probe and its reflection from the sample surface: a) from the first side after get parallel to the surface, b) from the second side after get parallel to the surface, c) after the tilt angle is given.

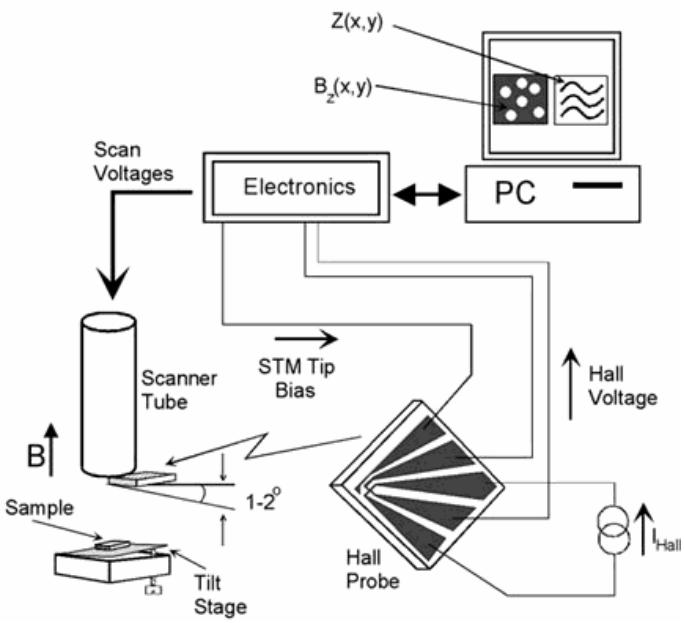

Figure 4.5: Schematic SHPM scan mechanism

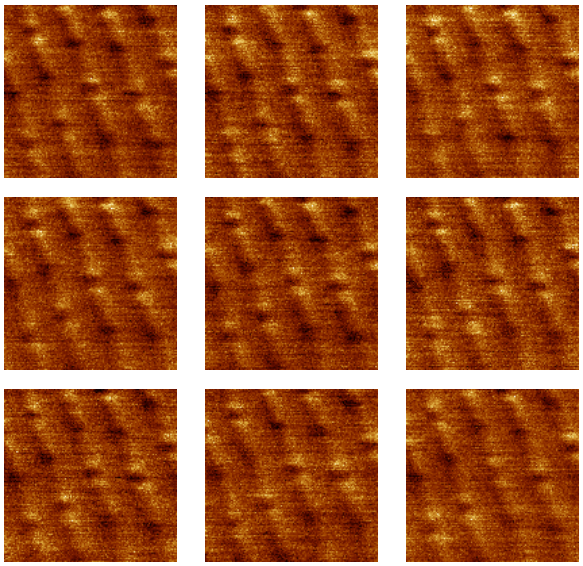

Figure 4.6: Room temperature SHPM images of NIST magnetic reference sample over 40µm x 40µm area with 128 x 128 pixels resolution, 100 µm/sec scan speed, Lift Off Voltage=2.5V,Hall current= 3 µA,

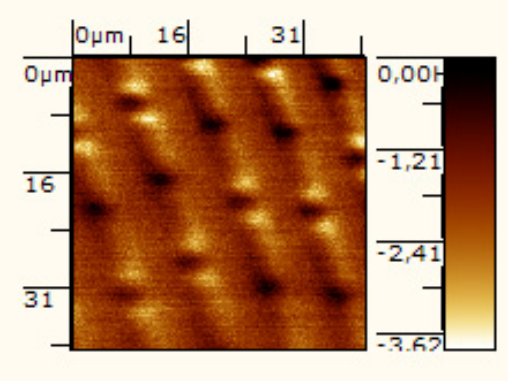

Figure 4.7: Room temperature SHPM image of NIST magnetic reference sample over 40µm x 40µm area with 128 x 128 pixels resolution, 100 µm/sec scan speed, Lift Off Voltage=2.5V,Hall current= 3 µA, (Image shows unprocessed average of 10 fast scan SHPM images)

In SHPM, two methods can be used for the scanning. The most common one is the lift off mode. In this mode, after the alignment step Hall Probe is approached to the surface by using automatic approaching at x=28 µm, y=28 µm coordinates which is the closest position of the scanning tube to the surface. After the tunneling current is found between the tip and surface the probe is lifted off to a fixed desired height, losing the tunneling contact. Then the probe is moved to all other corners of the scan area by a speed ~2µm/s and the change in tunneling current is watched. Any increase in tunneling current means that there is a point on the surface higher than the upper right corner. Corner check process is cancelled in this case and probe is retracted. The sample can be checked again with the higher lift off at the same place or the probe position on the sample can be changed with using x-y sliders. At a scan area which gives no tunneling current during the corner checks, the probe is moved to x=-28 µm, y=-28 µm coordinates to begin the scan. After the scan parameters are entered, the scan mode is selected. There are three scan modes for our system. The first one is the normal scan mode which uses the feed-back mechanism for during the scan. The feed-back loop makes the scan safer but the speed must be slower (1-2 µm/sec). The second one is the fast scan mode which does not turn the feed-back loop off but simply scans

faster (up to 100 μm/sec). The third and last one is the real time scanning mode which does not care about feed-back any more and scan very fast up to one image at one second. It is also important that to scan the surface as fast as possible to decrease the 1/f noise. Usually N images are taken at one scan for SHPM experiment to average them to reduce the noise. Averaging N images decreases the noise by a factor of $\sqrt{N}$.

In the STM tracking SHPM, the probe is at the tunneling distance during the whole scan. In this case the probe is approached to the surface at the x=-28 μm, y=-28 μm coordinates. Only normal scan mode can be used to protect the probe and the surface. In this case the Hall probe is closest to the surface and measured magnetic field strength is powerful but speed of the scan is very slow because of the feedback tracking. At the same with the SHPM scanning, the 3D topography of the surface can be imaged by this mode (figure 4.6) simultaneously with the magnetic image.

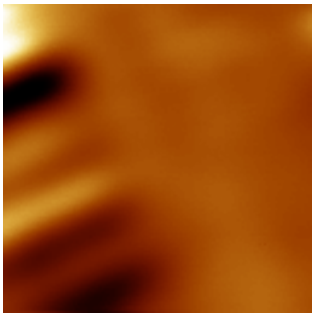

Hall Voltage (forward)

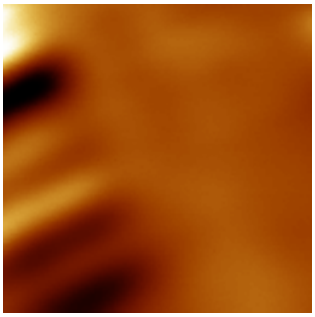

Hall Voltage (reverse)

Figure 4.8: Low temperature (77K) SHPM image of Zip magnetic storage sample over ~17.6 μm x 17.6 μm area with 256 x 256 pixels resolution, 100 μm/sec scan speed, Lift Off Voltage=5V (0.43 μm), Hall current= 20 μA, (Image shows unprocessed average of 4 fast scan SHPM images

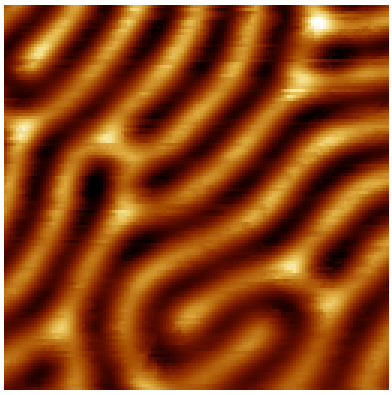

Hall Voltage

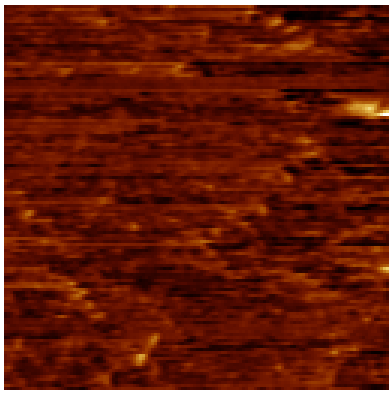

Tunneling Current (error signal)

Figure 4.9: Room Temperature tracking mode image of Iron-Garnet sample over 54µm x 54µm scan area, with 2 µm/sec scan speed, 2 µA Hall current and R_H = 0.1960 Ohm/Gauss Hall coefficient [16]

Chapter 5

Quartz Tuning fork as a force sensor

Quartz tuning fork is one of the best mechanical oscillators. The piezoelectric properties of quartz allow exciting and detecting the oscillation of the tuning fork fully electrically. With high quality factors and resonance frequency, the quartz tuning forks can be used for gyroscopes, micro balances, and gas sensors [17]. In 1995 the quartz tuning fork is introduced in to scanning probe microscopy for distance-sample control in near field scanning probe microscopy [18]. Then atomic steps observation were in 1999 [19], and atomic resolution in 2000 with quartz tuning fork feed-back were reported [20]. Other applications in SPM can be given as also Magnetic Force Microscopy [21] and force microscopy in liquid environment [22]. The quartz tuning forks are very stiff (1,800 - 100,000 N/m) respect to the Si cantilevers (1 – 40 N/m). Since two electric contacts are enough to take data for self sensing quartz tuning fork, it is suitable for the low temperature systems where the experiment area is limited. Other advantage of the quartz tuning fork can be given as working without light for semiconductors where photoelectric effect of semiconductors limits the beam deflected AFM techniques.

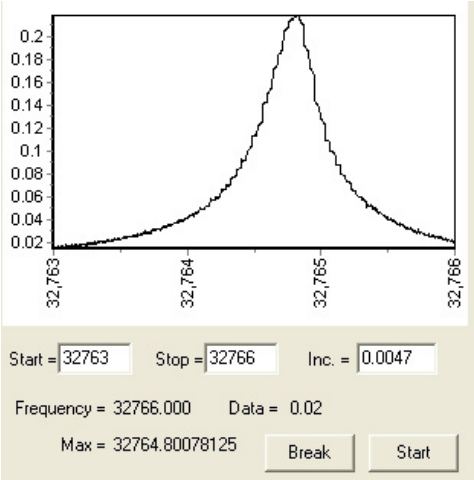

Figure 5.1: Resonance curve of 32 kHz Quartz Tuning Fork crystal in its own shield, calculated Q-factor is 102,710

However, the high stiffness is also a disadvantage for detection of the small forces, and is a danger for the tip to be crashed since the force is not limited by a soft spring.

In our experimental setup, we mainly use two types of quartz tuning fork, one with 32,768 Hz and 100,000 Hz resonance frequency. The quartz crystals that are used in watch industry are 32,768 Hz. The resonance curve is given in Figure 5.1. The Q factor is calculated as 102,710 for the quartz in its own shield. We used 100 kHz quartz tuning forks to increase resonance frequency for Hall probe attached experiments which will be explained in detail in next chapters.

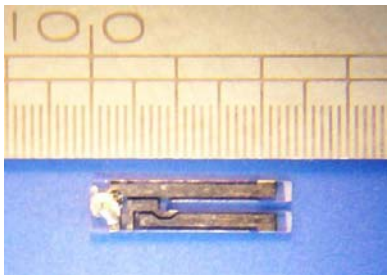

Figure 5.2: 32 kHz Quartz tuning forks sizes, where each small interval is 1/100 inches.

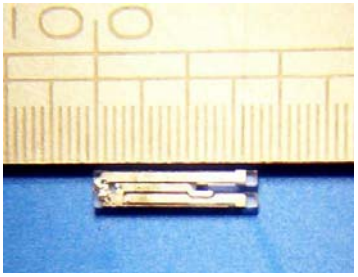

Figure 5.3: 100 kHz Quartz tuning fork sizes, where each small interval is 1/100 inches.

We cut the shield of the quartz crystal and take it out to put our tip or other kind of probes on it. During this process we break the vacuum environment inside the original shield and we damage the quartz a little bit. The resonance curve of the quartz tuning fork which was taken out from its original shield is given in Figure5.4. The calculated Q factor for this case is around 10,000.

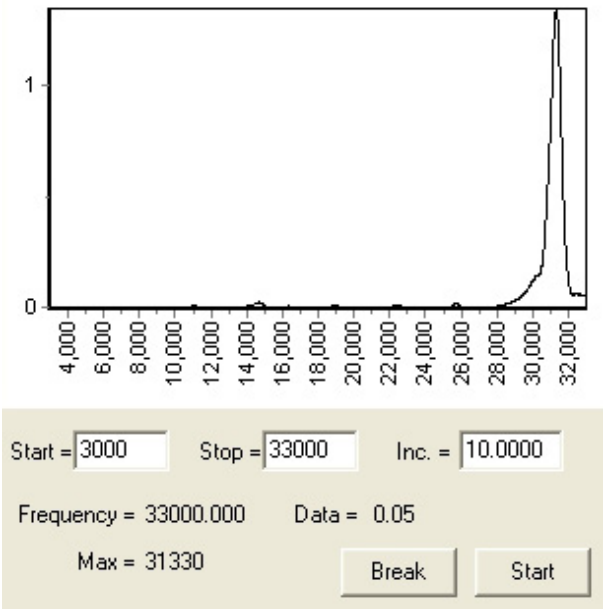

Figure 5.4: 32 kHz Quartz tuning fork without original shield.

5.1 Force detection techniques

Because of the piezoelectric properties of quartz tuning fork, it generates an AC voltage when it is vibrated by an external AC dither voltage with the help of a dither piezo. This generated voltage's amplitude becomes maximum, and the phase difference between the prongs is minimum at the resonance frequency (Figure 5.5). The movements of the prongs are similar to the scissors at the resonance frequency. When a force is applied to one of these prongs, the movement symmetry is broken and the resonance frequency shifts (Figure 5.6). One can measure the applied force by measuring the resonance shift. So the basic principle of the force measurement with the quartz tuning fork is just locking in to the resonance frequency and measuring the shifts at amplitude and phase. For this purpose, a lock-in amplifier system or a phase locked loop (PLL) can be used. In this point the quality factor (Q-factor) which gives the sharpness of the resonance curve plays an important role. (Figure 5.5). Because our measurement techniques are limited at detecting changes at voltage or phase, there will be at least a frequency change that can change the voltage or phase in the measurement range. Sharper resonance peak or higher Q-factor gives bigger changes at small frequency intervals.

The quality factor can be calculated simply after measure f_{res}, f_1 and f_2 that are shown in Figure 5.6, with using the formula that is given below.

$$Q = \frac{f_{res}}{f_2 - f_1} \tag{5.1}$$

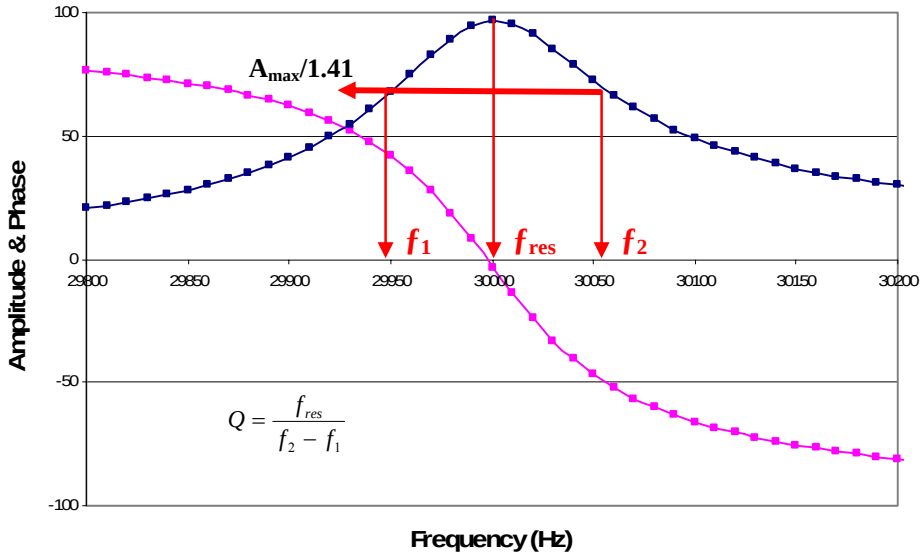

Figure 5.5: Resonance and phase curve of a tip attached quartz tuning fork.

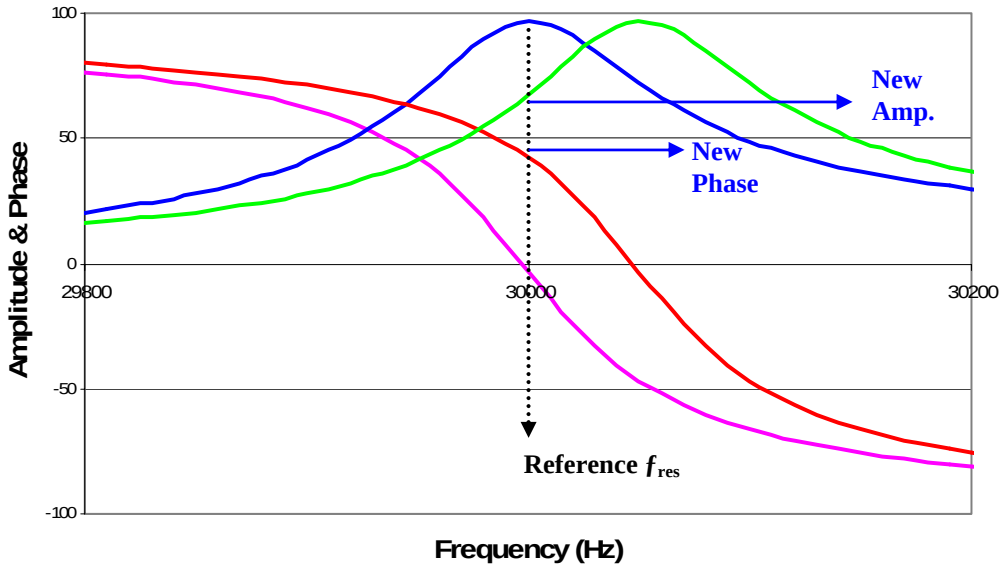

Figure 5.6: Resonance and phase shift of quartz crystal with applied force.

In this figure blue curve is the resonance frequency curve, pink one is the phase curve, the green one is the shifted resonance frequency curve and the red one is the shifted phase curve.

5.1.1 Lock-in Amplifier

Lock-in amplifier is basically a system designed for locking to a distinct frequency, and measuring the amplitude change at that frequency. When an attractive van der Waals force is applied to the quartz, the resonance frequency of the quartz decreases [23]. Then the amplitude, at the initial resonance frequency, decreases. We can use lock-in amplifier to measure this change at the amplitude and use the feed-back loop to fix the amplitude change during the scan. The connection scheme of the lock-in and SPM electronic system connection is given in Figure 5.6. In this technique an AC dither signal is sent to dither piezo to vibrate quartz mechanically. This dither signal is connected to reference input and lock-in is locked to this signal. When quartz crystal is mechanically dithered, it generates a voltage because of its piezoelectric property. The voltage that is generated from the quartz is connected to the input of the lock-in system. The dither signals frequency is changed around the expected value of the resonance frequency and the amplitude changes are monitored by lock-in. The dither voltage frequency is fixed at the highest amplitude and off-set mode of the lock-in selected. A value about 1/5 times of the maximum voltage is set for the feed-back loop and automatic approach is started. The channel 1 is signal amplitude and channel 2 is phase output of the lock-in system. These two channels are collected as signal inputs by SPM electronics. Amplitude output is used for the feedback loop and phase output is collected as an extra data. With this technique feedback loop works for keeping amplitude shift, constant. Several examples for lock-in used force measurements are given below. Figure 5.7 is the 6 μm period grating image at room temperature, Figure 5.8 is the 6 μm period grating image at low temperature (77K) with the given scan parameters. Figure 5.9 is AFM image of collapsed Morexalla bacteria in ambient conditions. This biological work is done with the collaboration of Prof. Dr. Kamruddin Ahmed, Biology Department, Bilkent University.

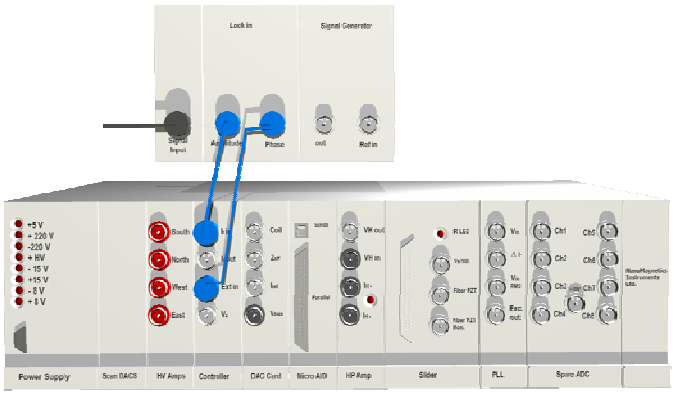

Figure 5.7: The connection scheme of the lock-in and SPM electronic system

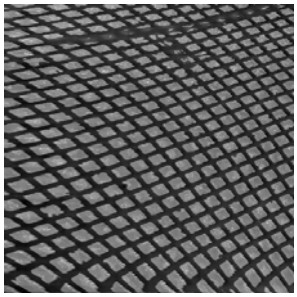

Quartz-AFM feedback data

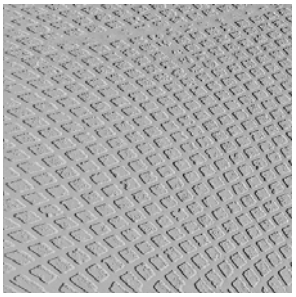

Quartz-AFM phase data

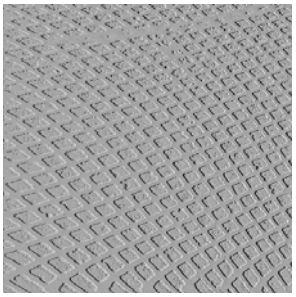

Quartz-AFM force gradient

Figure 5.8: AFM image of 6µm period grating at room temperature with lock-in amplifier, over 52 µm x 52 µm area with 1 µm/s speed

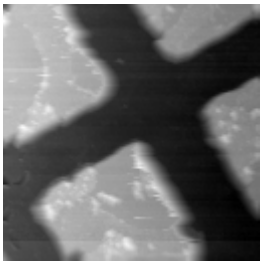

Quartz AFM feedback data

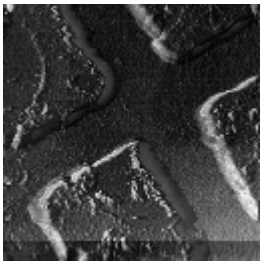

Quartz AFM phase data

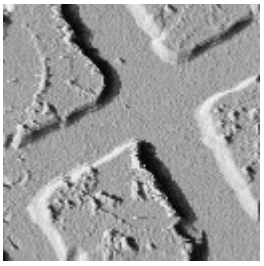

Quartz AFM force gradient

Figure 5.9: AFM image of 6µm period grating at low temperature with lock-in amplifier, over 8 µm x 8 µm area with 1 µm/s speed

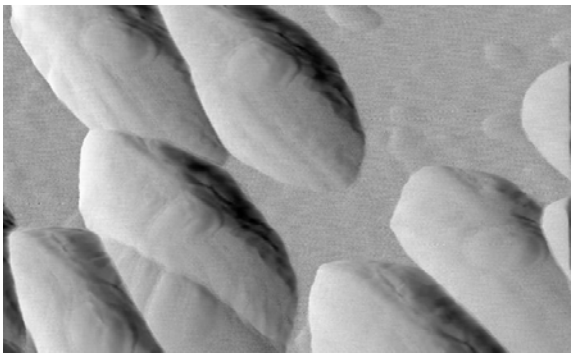

Figure 5.10: Quartz AFM image of Morexalla bacteria over 2µm x 3µm area with 1µm/s speed, by using lock-in amplifier

5.1.2 PLL

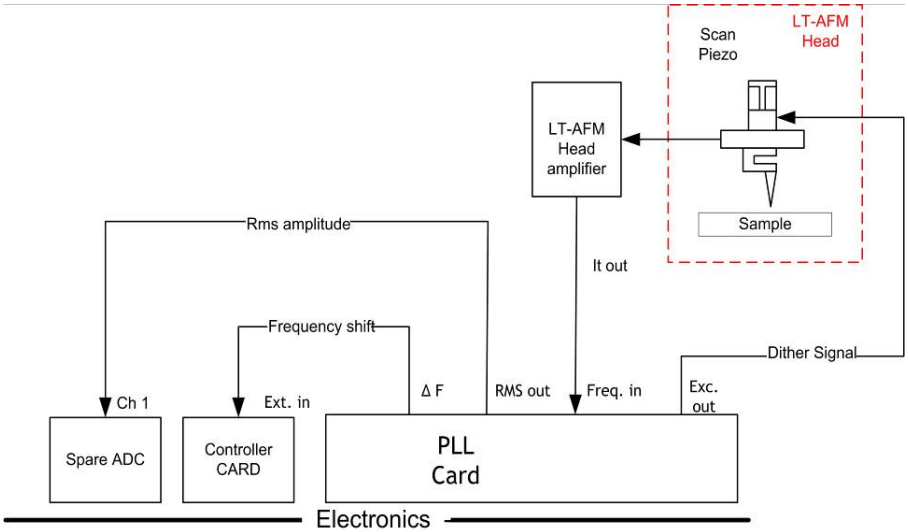

Figure 5.11: The connection scheme of the PLL and SPM electronic system

Although lock-in amplifier method is a very simple system for the force measurement by using quartz crystal, it is very slow. So, we began to use Phase Locked Loop (PLL) system. This new system is faster and more sensitive. PLL system drives an AC voltage to dither piezo to oscillate the quartz mechanically and sets the system into oscillation by measuring the signal generated by quartz. It also measures the frequency shifts, Δf output in to the front panel gives 1V for every 15 Hz shift in resonance frequency. The schematic of PLL circuit is given

in Figure 5.12. The generated voltage from the quartz crystal is first amplified by a low noise amplifier. After the amplification, signal is compared with the driven AC signal generated by the digitally controlled oscillator by a Phase Detector. Then signal passes through the Loop Filter and ADC. Finally the signal arrives to microcontroller. In this design DDS (1) is used to oscillate the circuit. ADC, microcontroller and DDS (1) operate as a digital controlled oscillator (DCO) and they are used to close PLL loop. With help of this microcontroller data is processed and sent to the SPM software. Microcontroller also sends a command to DDS (2) to give a phase shift to the system to not damp the quartz tuning fork. DDS (2) works at the same frequency with DDS (1) and only gives a phase difference. Connection scheme of PLL is also given in Figure 5.13.

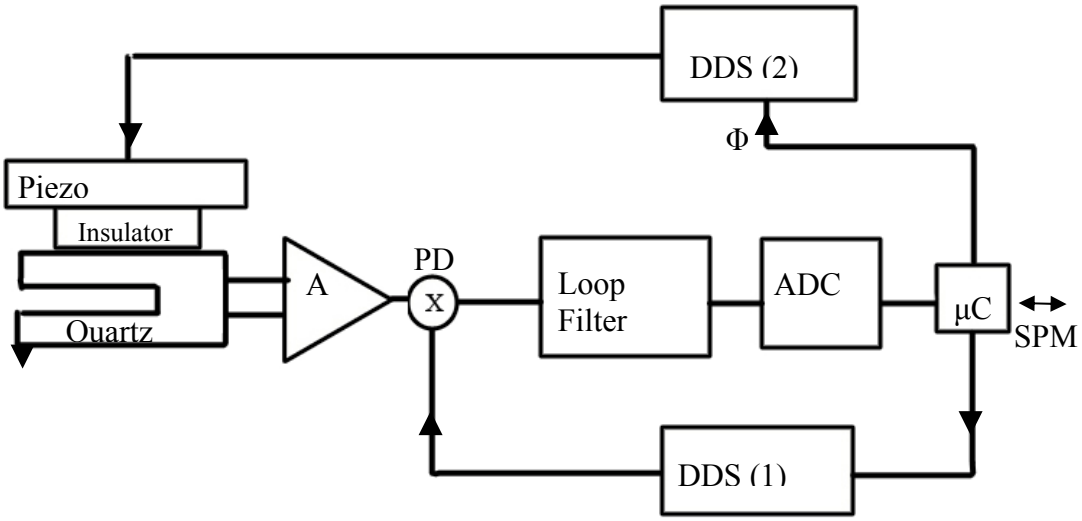

Figure 5.12:PLL circuit design

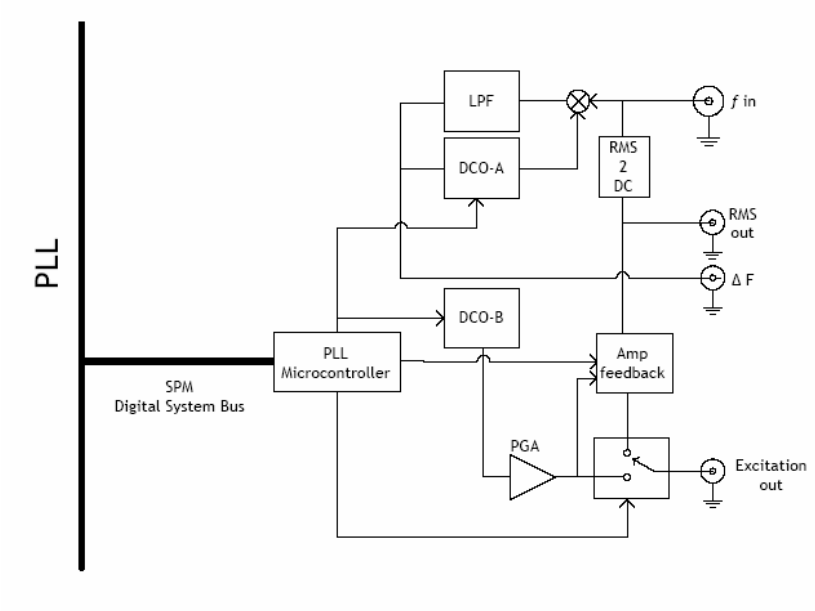

Figure 5.13:PLL connection schematic

PLL system is faster and more reliable respect to the lock-in amplifier. The amplitude change of the input signal is also monitored at the same time. In our system, if chosen, there is a second feed-back loop inside the PLL design which tries to keep the amplitude fixed by changing the amplitude of the dither voltage during the scan. This second loop allows us to measure the dissipation energy change at the quartz during the scan, in the constant amplitude operation of PLL.

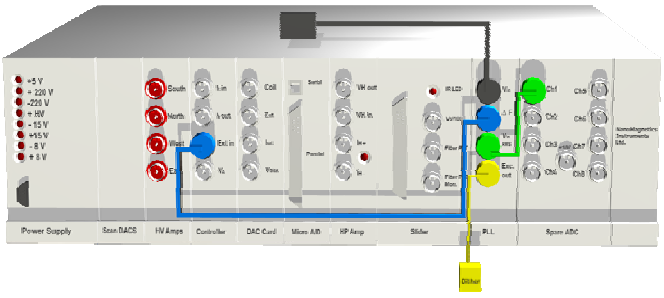

Figure 5.14: The connections of the PLL card with feedback circuit and spare ADC circuit

5.2 Historical background of the experimental set-up

In this part of this thesis the historical developments and improvements are summarized below.

5.2.1 Preparation for High magnetic fields

One of the advantages of quartz tuning forks is ability to be used in high magnetic fields as a force sensor [24, 25]. In the first applications of our system, only the original shield of the quartz was removed and the original electrical connections were kept to use. But it is observed that the original electrical connections of the quartz are magnetic then the resonance frequency is shifted in magnetic fields. Probably the sensor position is changed because of the magnetic force. So, simply the electrical connections of the quartz are changed with non-magnetic connections. The new connections are tried in high magnetic fields up to 7 Tesla. Only an unexpected, big resonance shift is observed around 400 Gauss. Except this, it is observed that there is no interaction between the electrical connections and the magnetic fields.

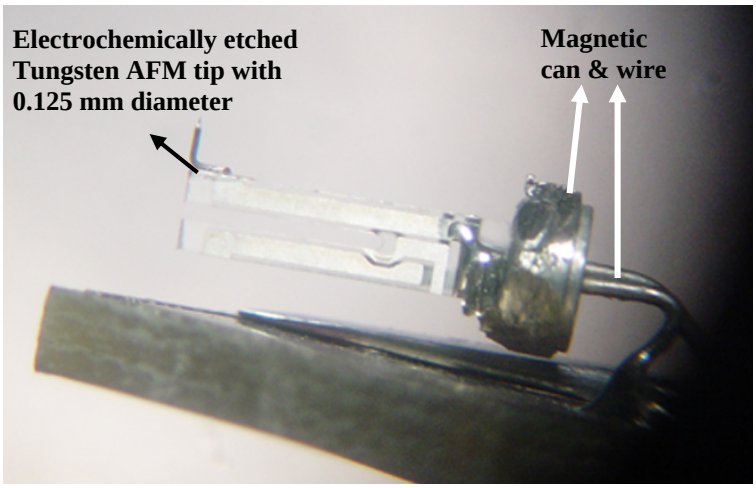

Figure 5.15: Old type of AFM probe with magnetic materials.

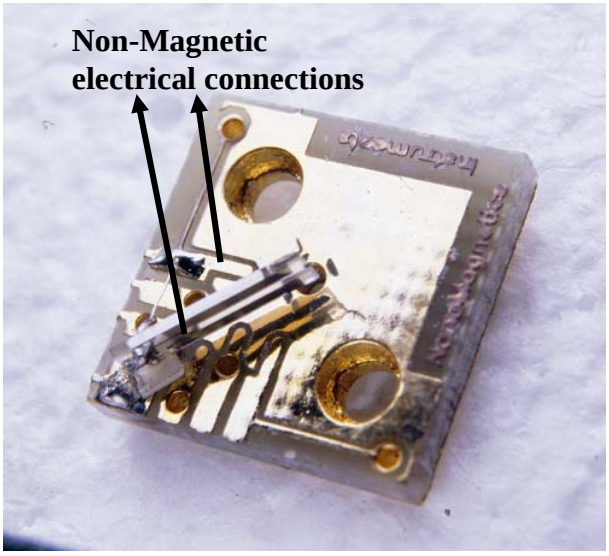

Figure 5.16: New type of AFM probe with non-magnetic electrical connections

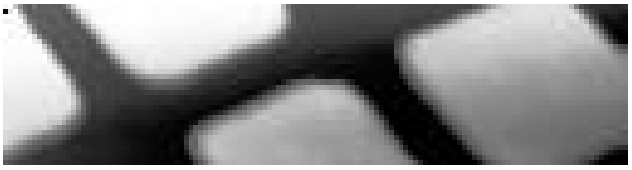

Figure 5.17: AFM image of 6 μm period grating, taken at 10 K, under 3.5 Tesla magnetic field with the new type quartz tuning fork AFM probe by using lock-in system and Quantum Design's PPMS system.

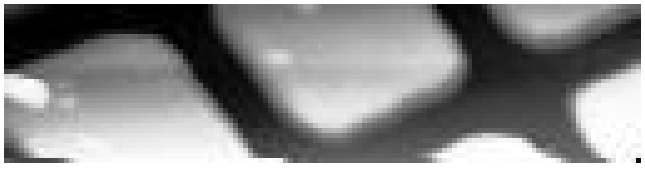

Figure 5.18: AFM image of 6 μm period grating, taken at 10 K, under 7 Tesla magnetic field with the new type quartz tuning fork AFM probe by using lock-in and Quantum Design's PPMS system.

5.2.2 Different diameters for AFM tips

The weight of the AFM tip decreases the resonance frequency and Q factor of the quartz. The decrease in resonance frequency and Q factor also decreases the resolution of quartz crystal as a force sensor. To avoid this, different diameters of AFM tips were attached to quartz tuning fork. The changes at the resonance frequency, quality factor and the resolution of the quartz tuning forks were examined.

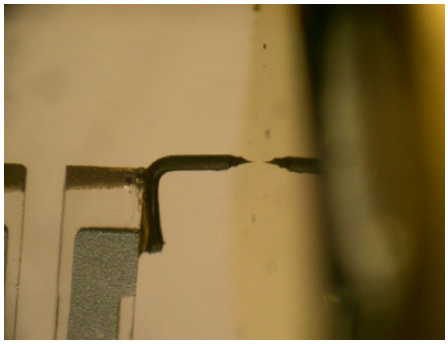

Figure 5.19: Old type of AFM probe with 125 μm thick etched Tungsten tip

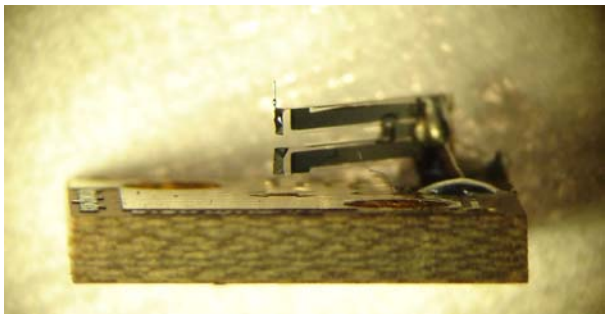

Figure 5.20: New type of AFM probe with 50 μm thick etched Tungsten tip

We observed that the experimental results are satisfied this theoretical approach. We prepared two kinds of AFM probes, one uses an etched tungsten wire with diameter 125μm and another with 50μm diameter. The lengths of the etched tips are nearly same. The resonance, Q factors can be given as,

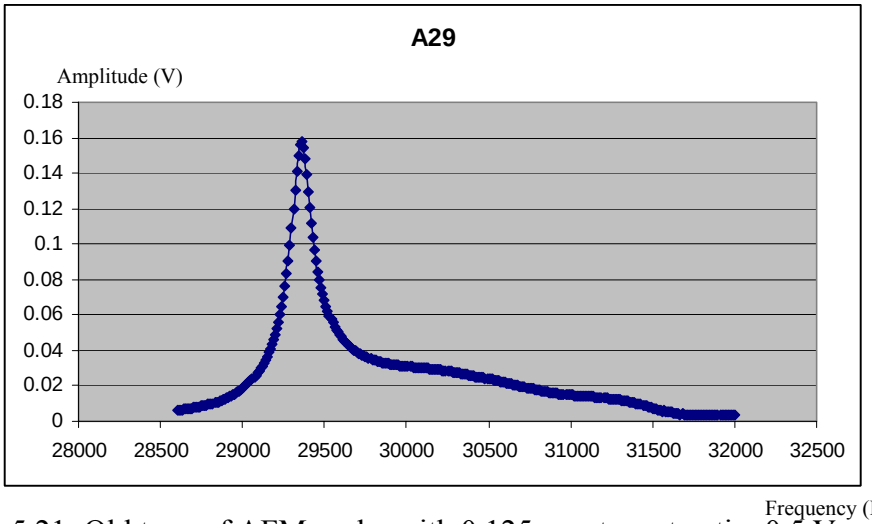

Figure 5.21: Old type of AFM probe with 0,125 mm tungsten tip, 0.5 V_{rms} dither voltage, 29,360 Hz Resonance Frequency and 326 Q-Factor

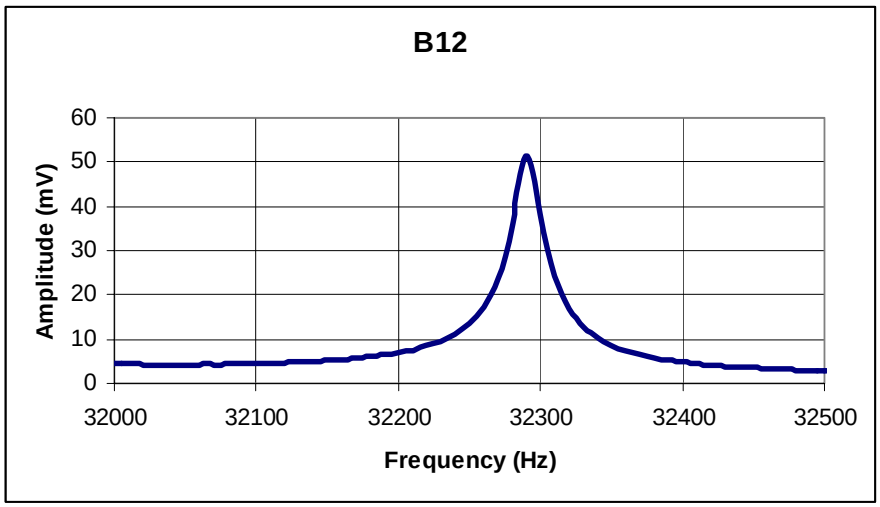

Figure 5.22: New type of AFM probe with 0.5 V_{rms} dither voltage, 32,290 Hz Resonance Frequency and 6,458 Q-Factor

We reached up to around 6,000 for the Q factors using 50 µm diameter tungsten wires. Q-factors that we were using before, were changing between 100 and 1,000. The taken images are compared with the cross sections as below. It can be seen that the details of the thinner tips, at the z direction better then the thick ones. First image is taken over 20 µm x 20 µm area with 1 µm/s at 300K by using

PLL system. Where the second results are taken over 8 µm x 8 µm area with 1 µm/s at 300K by using PLL system.

Figure 5.23: Error signal (force gradient) image of 3µm period grating with 125µm diameter Tungsten wire obtained using PLL

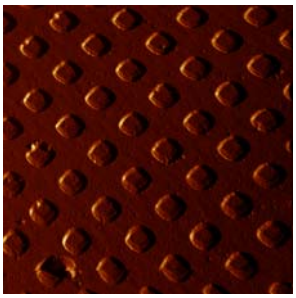

Figure 5.24: Phase shift signal image of 3µm period grating with 125µm diameter Tungsten wire obtained using PLL

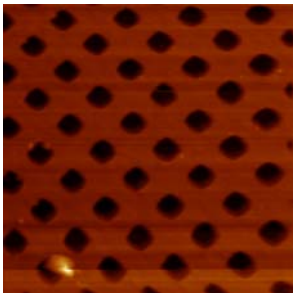

Figure 5.25: Feed-back signal image of 3µm period grating with 125µm diameter Tungsten wire obtained using PLL

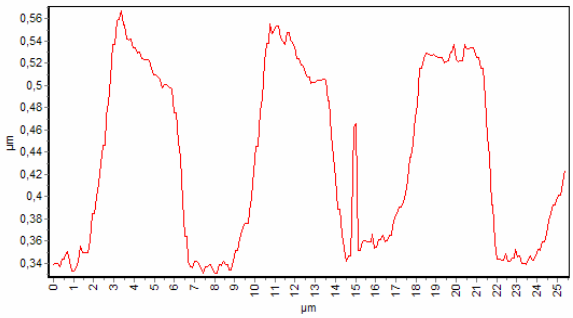

Figure 5.26: Cross section of feedback image of 3µm period grating with 125µm diameter Tungsten tip

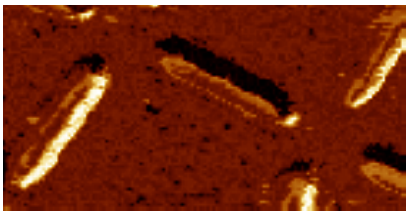

Figure 5.27: Error signal (force gradient) image of 6µm period grating with 50µm diameter Tungsten tip, by using PLL system

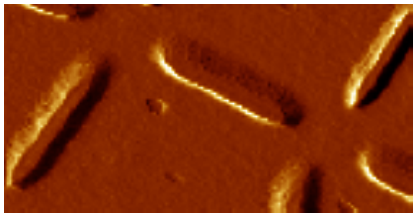

Figure 5.28: Phase shift signal image of 6µm period grating with 50µm diameter Tungsten tip, by using PLL system

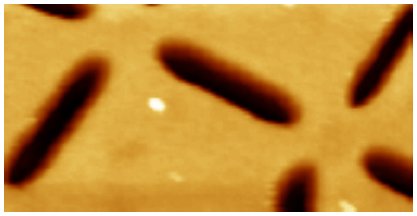

Figure 5.29: Feed-back signal image of 6µm period grating with 50µm diameter Tungsten tip, by using PLL system

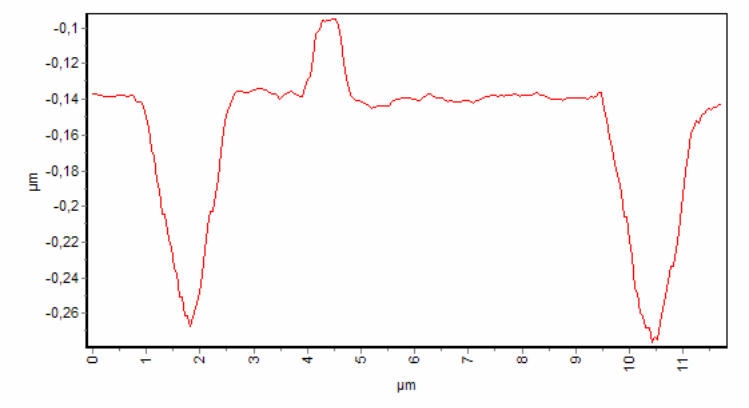

Figure 5.30: Cross section of feedback image of 6µm period grating with 50µm Tungsten tip

5.2.3 Resonance frequency and Q factor change with temperature

Quartz tuning forks electrical properties change with the temperature because of its piezoelectric properties. The resonance frequency and the Q factor dependence of the quartz tuning forks were also studied. For this purpose, a quartz tuning fork which is prepared for force detection is used without any tip on it. Resonance frequency curves are plotted at every 10 K between 300K and 77K. Using these resonance curves, the corresponding Q factors are calculated for each temperature. It is observed that the resonance frequency is first increasing a little, and then decreasing, where there is no meaningful change at Q factor. About 185 K another unexpected little increasing observed at the resonance frequency. The responding curves can be found below as,

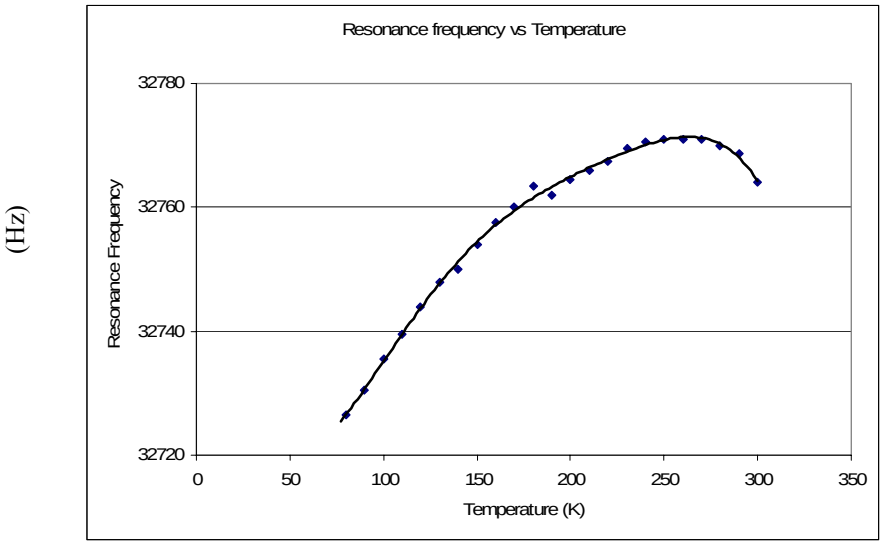

Figure 5.31: Resonance frequency change with temperature

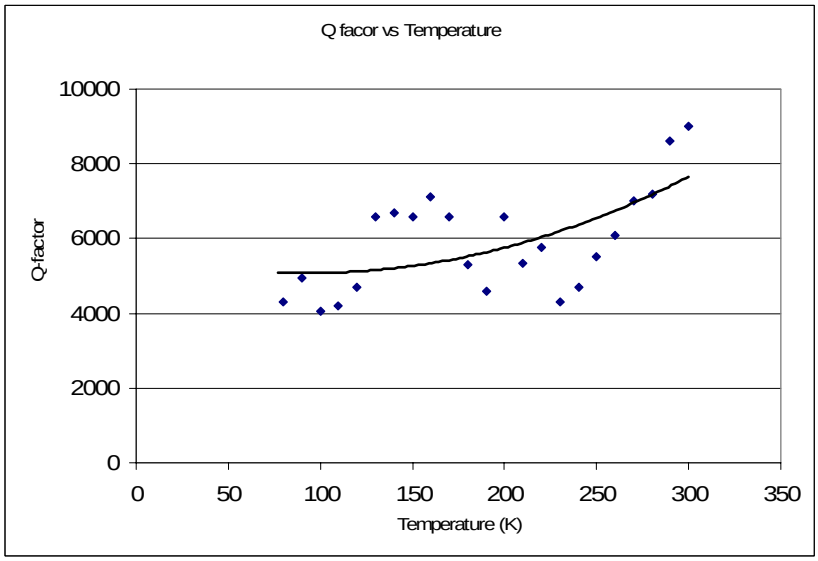

Figure 5.32: Q-factor change with temperature

5.2.4 Different dither voltages for AFM tips

One of the important parameters in non-contact mode AFM imaging is the mechanical amplitude of the AFM cantilever. The lower mechanical amplitude decreases the risk of disturbing the sample and probe. But, on the other hand, for very small amplitudes system noise can be dominant. Therfore, to find the optimal

dither amplitude for the cantilever, we performed AFM experiments in different excitation voltages. Unfortunately, because we damage the quartz tuning forks when removing the shields, the optimum dither voltages can be change for every quartz tuning forks. But we also used this study as a general reference work which can be applied to quartz crystals proportional to their generated voltages. The resonance frequency was 32.05 kHz, and the Q-factor was 801, with the 125 μm diameter tip attached to quartz tuning fork that used for this study. This study was performed using lock-in amplifier for the force measurement. The time constants and the noise filtering constants are also given below. The error signal of the results corresponds to directly amplitude change at the resonance frequency then to the force gradient. The phase images correspond to phase change at the resonance frequency during the scan and the feed-back images corresponds to voltage change of the feed-back mechanism. The applied dither voltages and the responding results can be listed as,

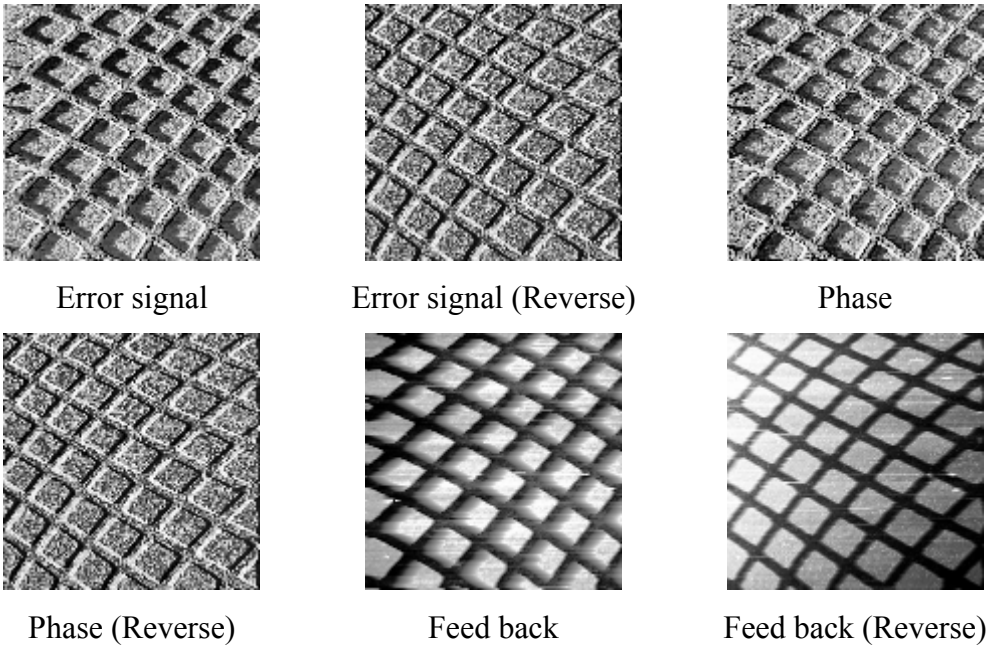

Figure 5.33: AFM imaging with 40 mV RMS dither amplitude, 4μm/s scan speed, 100μs Lock-in time constant

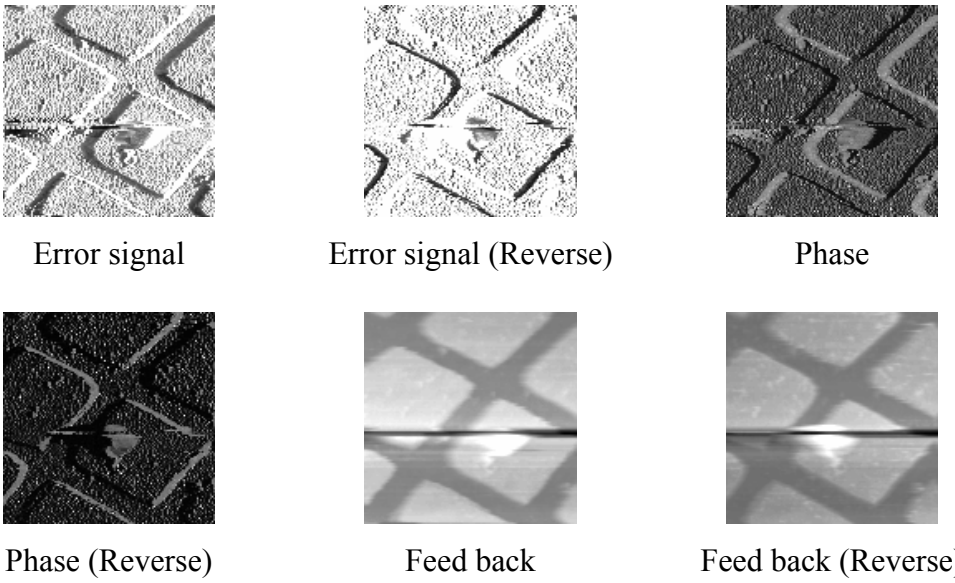

Figure 5.34: AFM imaging with 4 mV RMS dither amplitude, 3.5µm/s scan speed, 100µs Lock-in time constant,

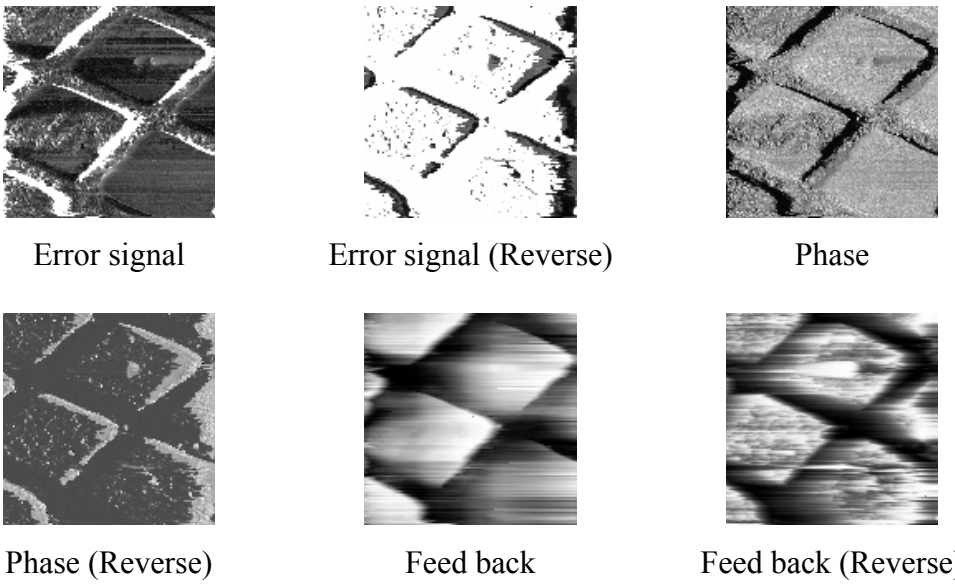

Figure 5.35: AFM imaging with 2 mV RMS dither amplitude, 3.5µm/s scan speed, 100µs Lock-in time constant,

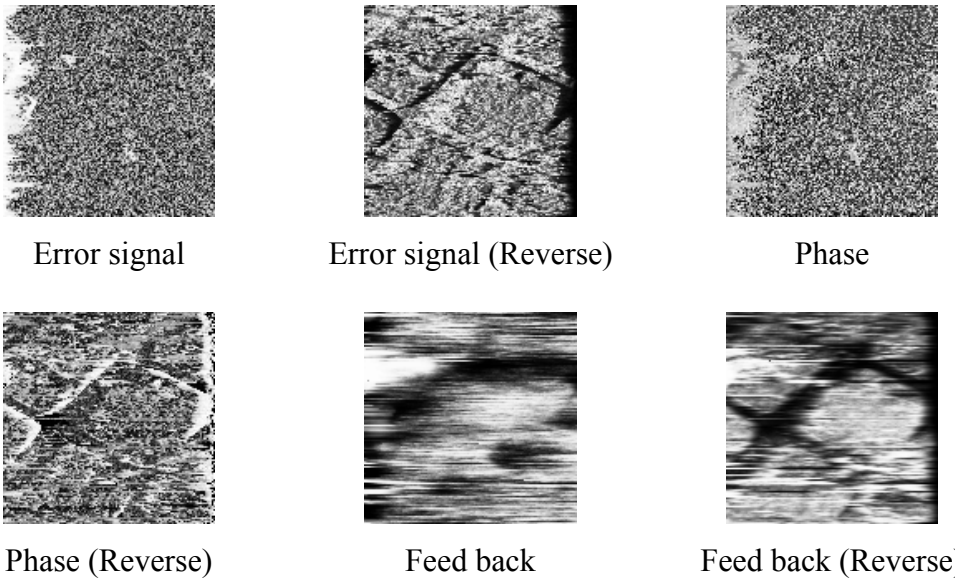

Figure 5.36: AFM imaging with 1 mV RMS dither amplitude, 3.5µm/s scan speed, 100µs Lock-in time constant,

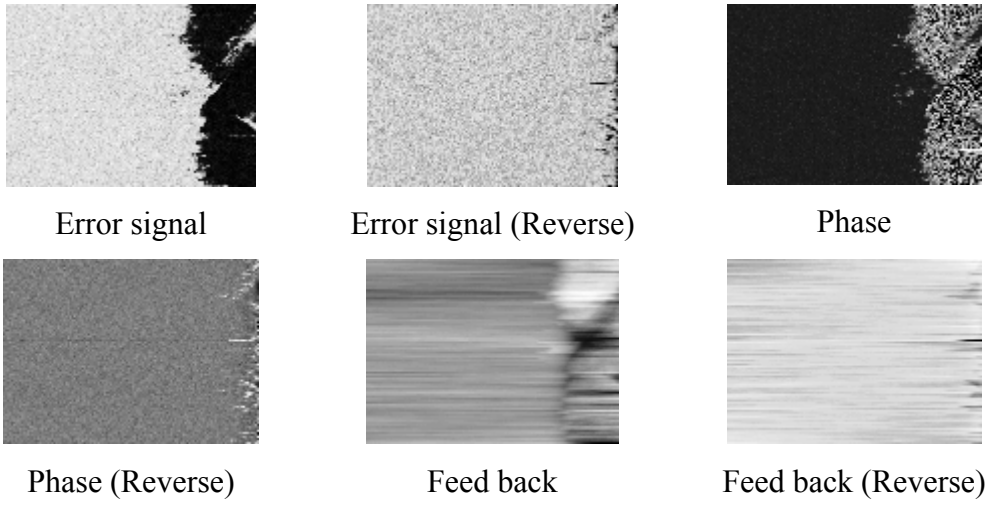

Figure 5.37: AFM imaging with 0.5 mV RMS dither amplitude, 3.5µm/s scan speed, 100µs Lock-in time constant

5.2.5 Images at different temperatures

Perhaps the biggest advantage of the using piezoelectric AFM cantilevers can be given as their reliability at the low temperatures. Quartz tuning fork can be operated down the to the mK temperatures [26]. In this thesis work we also choose the quartz tuning fork as a force detector because of this reason. The different grating images at different temperatures can be found at below.

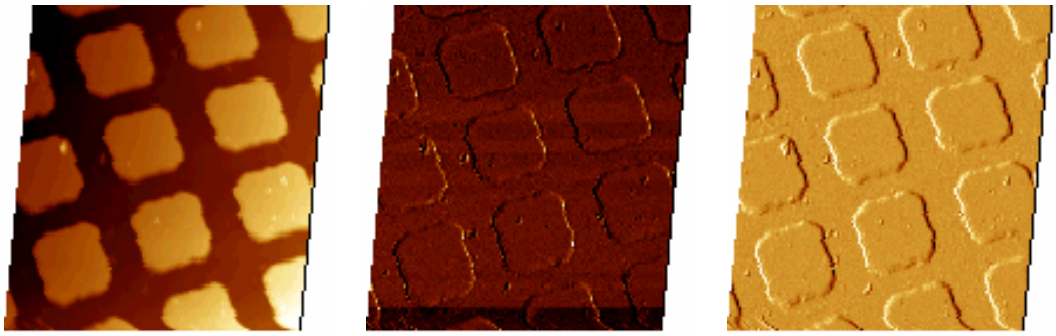

Quartz Tuning Fork-AFM feedback data

Quartz Tuning Fork-AFM phase data

Quartz Tuning Fork-AFM Amplitude change data

Figure 5.38: AFM feedback data at 300K, over 21 µm x 21 µm area with 128 x 128 pixels resolution and 1 µm/sec speed. Image shows a 6 µm x 6 µm square periodic arrays with 4 µm squares and 2 µm spacing (Processed images) taken with Lock-in.

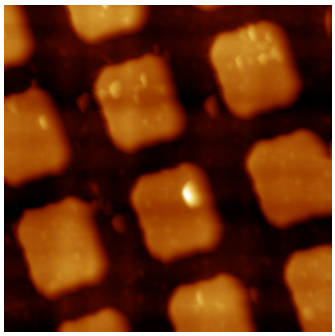

Quartz Tuning Fork-
AFM feedback data

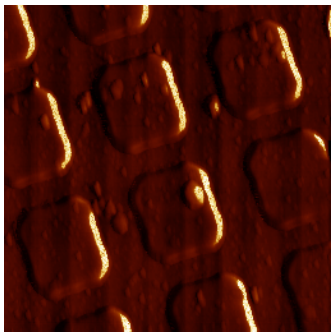

Quartz Tuning Fork-
AFM phase data

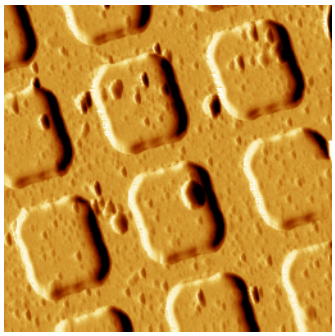

Quartz Tuning Fork-
AFM Amplitude change

Figure 5.39: AFM feedback data at 4.2K, over ~17.6 µm x 17.6 µm area with 256 x 256 pixels resolution and 0.15 µm/sec speed. Image shows a 6 µm x 6 µm square periodic arrays with 4 µm squares and 2 µm spacing (Processed images) taken with Lock-in.

Chapter 6

SHPM with AFM feed-back

The STM feedback for Scanning Hall Probe Microscopy is working very well as discussed in the Chapter 4. But the STM feedback limits the approach process only with the conducting samples. The non-conducting samples can be coated with a thin layer of gold to make them conductive. But in practical applications the gold coating can cause some problems. At least, the Au coating causes an extra distance between the probe and magnetic media. Because magnetic field strength is decreasing with the distance, this extra distance also causes a loss in data. In some cases the gold coating can damage the sample by creating short circuits or during the middle of the manufactory process the user may not prefer to coat the specimen for a hard-disk. So, AFM feedback can be preferred for this purpose. The micro fabricated piezoelectric cantilevers were reported in the literature [27, 28]. Basically the Hall probe is fabricated to the edge of the piezoresistive cantilever (Figure 6.1 and 6.2). Applied force causes resistance change at the cantilever. This resistance change is taken as the signal input for the feedback. In this method there is no need to any optical apertures, and then these cantilevers can work at low temperature environment where the area is limited. But fabricating these cantilevers is expensive, very difficult and takes long time. Two sided alignment is needed for this purpose. At this point, as the main aim of this thesis work, we only glued a micro fabricated Hall Probes on a quartz tuning fork to provide an AFM feedback. This technique is quite easy and cheaper with respect to the other technique.

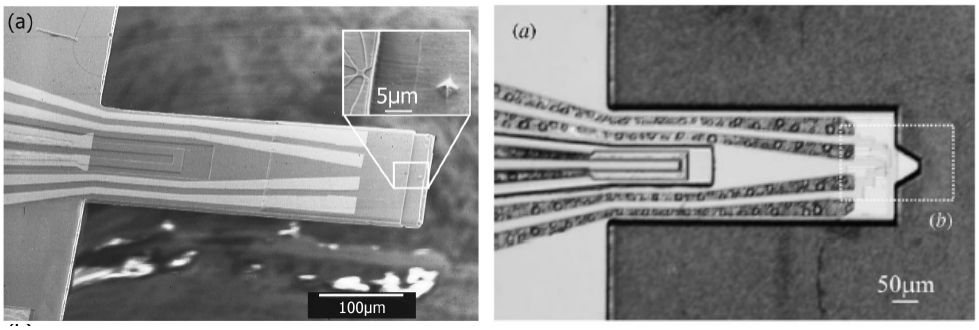

Figure 6.1: Microfabricated piezoresistive SHPM combined AFM cantilevers, [27, 28]

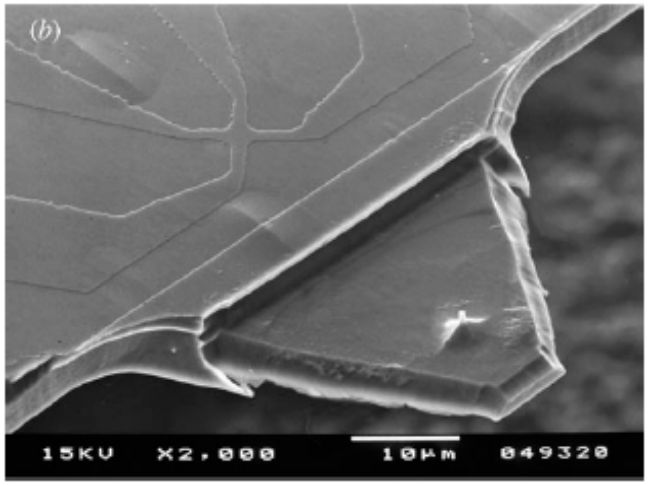

Figure 6.2: Microfabricated piezoresistive SHPM combined AFM cantilevers, [27, 28]

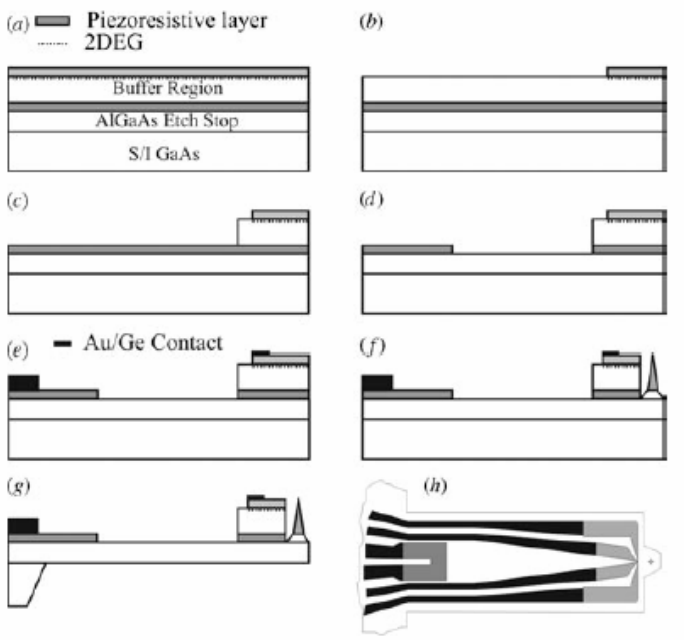

Figure 6.3: Fabrication process schematic SHPM integrated AFM cantilevers. [27, 28]

A similar work with our technique is studied by Weiss *et al* [32]. In this study a narrow GaAs chip (~ 0.4 mm, 0.5mm, 0.4mm in size) is sandwiched between two piezo plates as a cantilever. A micro-fabricated Hall Probe is glued to the edge of GaAs chip as shown in Figure 6.4. They used one of the piezoelectric plates to drive the system at resonance frequency. The other piezoelectric plate generated a corresponding AC voltage to this mechanical vibration. They measured the amplitude shift of the second piezoelectric plate which is caused by applied shear forces on cantilever. A successful experiment is run at air conditions and magnetic image is taken of a HDD with AFM topography. In our technique we used commercial cheap quartz tuning forks as piezoelectric cantilevers with the same aim. In our work, we measured the perpendicular forces to the surface. With using quartz tuning forks for perpendicular force measurement, we keep the mechanical amplitude smaller and perpendicular to the surface. Although, our technique does not need any special cantilever preparation, we could not manage

to have a good AFM topography data during our experiments. However our technique can be found more practical for commercial applications because of cheaper and easier fabrication process.

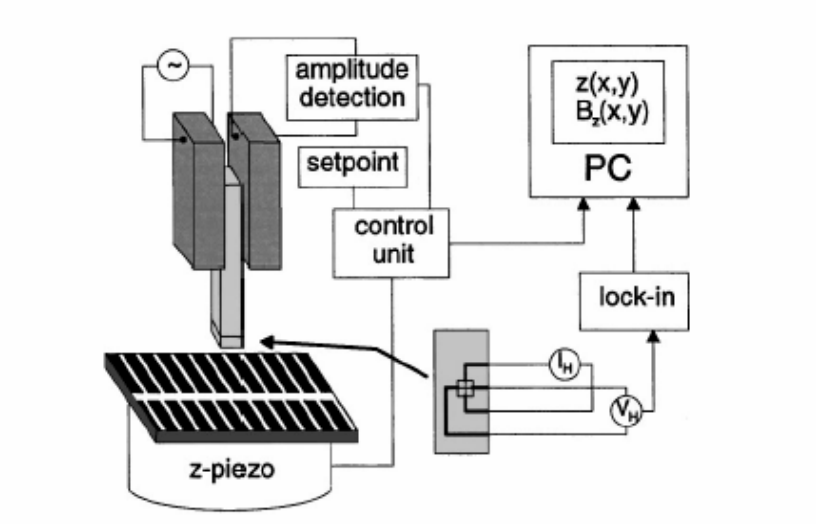

Figure 6.4: Piezoelectric feedback mechanism for SHPM with two piezo plates [32]

Figure 6.5: Quartz Tuning Fork AFM guided Scanning Hall Probe

In this thesis work, micro-fabricated P-HEMT Hall Probes are used for SHPM scanning. The fabrication of these hall probes is given in chapter 3, step by step.

The Hall Probes are fabricated without STM tip metallization for AFM feed-back. Because of Hall Probes big mass respect to the AFM tips, we examine firstly the feedback capability of big mass glued to the quartz tuning fork. For this purpose dummy chips are used which are has the same mass and shape with the Hall probes. The first experiment is performed in air condition by using RT-AFM system. Both prongs of the quartz tuning fork were let free to oscillate. In this first experiment the dummy chip is glued on quartz tuning fork with 8º tilt angle to use the corner of it as a sharp tip. A Standford Research Systems SR830 model lock-in amplifier is used to dither the dither and to measure amplitude & phase. A 6μm period gold coated square grating used as a sample. Although the Hall Probe with volume (2.5mm x 2.5 mm x 0.5mm) has a very big mass for quartz tuning fork, we have succeeded to protect the Q factor above 50 and the resonance frequency just above 20 kHz. The results are given in Figure 6.6. With this work we succeed to have clear error and feedback signals with very low resonance frequency and Q-factor. The images are also so clear although corner of the dummy chip is not very sharp as much as etched AFM tips. The cloudy image of feedback signal can also be explained with this non-sharp corner of the dummy probe. In this experiment it is thought that the signal is taken from the free prong instead of Hall probe glued one because of the high resonance frequency.

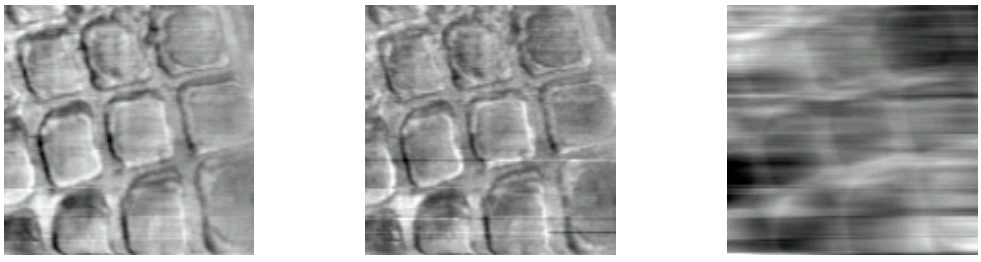

Error image (Forward) Error image (Forward) V_z (Forward)

Figure 6.6: Forward of 6μm period grating with the corner of a dummy Hall Probe chip

After feedback problem is solved for the big masses, a working Hall Probe is glued with super glue on 32 kHz, and the connections bonded with using silver epoxy 50 μm anti-magnetic wires. Both prongs of the quartz tuning fork were let free to oscillate. The floppy disk is used as a sample. RT-SHPM system is used as experimental setup. But because of the thick contacts and resonance shift stabilizing problem SHPM imaging could not succeed.

As a second step the bonding changed with 12μm Au wires and we used LT-SHPM system as experimental setup for this time. The Hall Probes are glued to quartz crystals with both super glue and Oxford Low Temperature Epoxy. LT-epoxy is used to avoid the effects of the deformations of superglue at low temperature. A high capacity zip disk was used as a magnetic sample without any gold coating. We align the probe with about 1º angle respect to the surface. The force stabilizing problem occurs again which is caused because of the compressed air between two flat surface. After the system is evacuated to ~ 2 x 10^{-5} mbar the input signal is stabilized. Again, in this step both of the prongs were let to oscillate freely. In this experiment we succeed to have a magnetic image in lift off mode. The results of this experiment are given in next section as liftoff mode SHPM imaging with AFM feed-back.

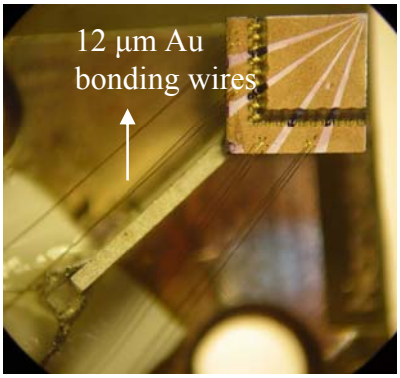

Figure 6.7: Quartz Tuning Fork AFM guided Scanning Hall Probe

In literature search, it is found that the big masses that fixed on the quartz tuning fork breaks the symmetry of the movement of the prongs respect to each

other. In this broken symmetry only slow scanning speeds are possible and the imaging signal is very difficult to interpret. Fixing one of the prongs to supporting structure overcomes this problem and allows using tuning forks in a similar manner as conventional cantilevers. [29] So one of the prongs is completely fixed to the PCB (Figure 6.9). Two kinds of quartz tuning forks with 32 kHz and 100 kHz resonance frequencies are used. The resonance shifts that caused by the masses are calculated. Calculation can be given as,

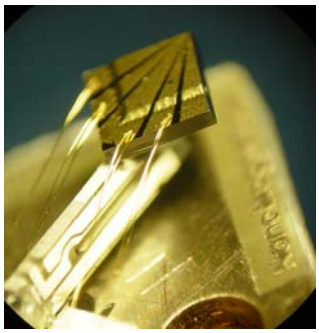

Figure 6.8: Quartz Tuning Fork AFM guided Scanning Hall Probe with two free prongs

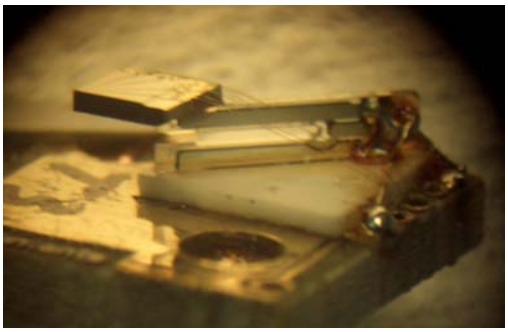

Figure 6.9: Getting glued one of the prongs of the quartz tuning fork to avoid the broken symmetry problem.

For 32 kHz quartz tuning fork,

Width of the prong (w)	Length of the prong (t)	Thickness of the prong (l)	Density of the quartz
0.34 mm	3.81 mm	0.62 mm	2.65 g/cm^3

Table 6.1: Sizes of one prong of 32 kHz quartz tuning fork and density of quartz

Width of the Hall probe	Length of the Hall probe	Thickness of the Hall probe	Density of the Hall probe
2.5 mm	2.5 mm	0.5 mm	5.315g/cm^3

Table 6.2: Sizes and density of Hall probe

$$m_{probe} = d \times V = 0.01661g \approx 17mg \tag{6.1}$$

The Young modulus of the quartz is,

$$E = 7.87 \times 10^{10}\ N/m^2 \tag{6.2}$$

Theoretical spring constant is,

$$k = \frac{Ewst^3}{4l^3} = 3\frac{EI_z}{l^3} \tag{6.3}$$

Moment of inertia of the quartz tuning fork can be found as,

$$I_z = \frac{wt^3}{12} = \frac{0.34 \times 10^{-3} \times (0.62 \times 10^{-3})^3}{12} = 6.76 \times 10^{-15} \tag{6.4}$$

Then we can calculate the spring constant of quartz tuning fork as,

$$k = 3\frac{EI}{l^3} = 3.\frac{7.87\times10^{10}\times6.76\times10^{-15}}{(3.81\times10^{-3})^3} = 2.89\times10^4\ N/m \tag{6.5}$$

The frequency change is,

$$\omega = \sqrt{\frac{k}{m_{eff}}} \tag{6.6}$$

Where m_{eff} is effective mass and can be calculate as,

$$m^* = \frac{m_1.m_2}{m_1 + m_2} \tag{6.7}$$

where,

$$m_T = 17mg + 0.68mg = 17.68mg \tag{6.8}$$

So,

$$m_{eff} = \frac{k}{\omega^2} = \frac{k}{4\pi^2 f_0^2} = 6.8\times10^{-7}\,kg \tag{6.9}$$

Finally one can find the new shifted resonance frequency f_0 by using the relation that given above as,

$$f = \frac{1}{2\pi}\sqrt{\frac{2.89\times10^4}{17.68\times10^{-6}}} = 6.434Hz \tag{6.10}$$

It can be easily seen that with decreasing Hall Probe mass to half, the resonance frequency will increase to $\sqrt{2}\ f_0$.

If we calculate the resonance frequency for the 100 kHz quartz tuning fork,

Width of the prong (w)	Length of the prong (t)	Thickness of the prong (l)	Density of the quartz
0.32 mm	1.72 mm	0.4 mm	2.65 g/cm^3

Table 6.3: Sizes of one prong of 100 kHz quartz tuning fork and density of quartz

$$I_z = \frac{wt^3}{12} = \frac{0.32\times10^{-3}\times(0.4\times10^{-3})^3}{12} = 4.26\times10^{-15} \tag{6.11}$$

$$k = 3\frac{EI}{l^3} = 3.\frac{7.87\times10^{10}\times4.26\times10^{-15}}{(1.72\times10^{-3})^3} = 19.768\times10^4\ N/m \tag{6.12}$$

$$m_T = 17mg + 0.5mg = 17.5mg \tag{6.13}$$

$$m_{eff} = \frac{k}{\omega^2} = \frac{k}{4\pi^2 f_0^2} = 5.1\times10^{-7}\,kg \tag{6.14}$$

And finally the new shifted resonance can be found for 100 kHz quartz tuning fork as,

$$f = \frac{1}{2\pi}\sqrt{\frac{19.768\times0^4}{17.5\times10^{-6}}} = 16.923Hz \tag{6.15}$$

We can summarize the calculated spring constants (k) and resonance frequencies with the sizes of forks for 32 kHz, 100 kHz and 153 kHz quartz tuning forks as,

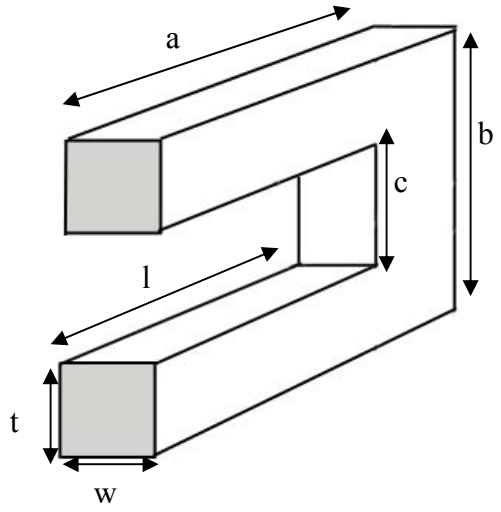

Figure 6.10: Quartz tuning fork, prong and crystal sizes

	32,768 Hz	100 kHz	153 kHz
Width (w)	0.34 mm	0.32 mm	0.25 mm
Length (l)	3.81 mm	1.72 mm	1.27 mm
Thickness (t)	0.62 mm	0.4 mm	0.445 mm
Total length (a)	5.842 mm	4.35 mm	3 mm
Total height (b)	1.524 mm	1 mm	0.9 mm
Calculated Spring constant (k)	$2.89\times10^4\ N/m$	$19.768\times10^4\ N/m$	$21.55\times10^4\ N/m$
Calculated f_{res}	$6.434Hz$	$16.923Hz$	$17.800Hz$

Table 6-4: Prong sizes, spring constants and calculated resonance frequencies of 32 kHz, 100 kHz and 153 kHz Quartz crystals

The experimental results of the resonance shift were found as,

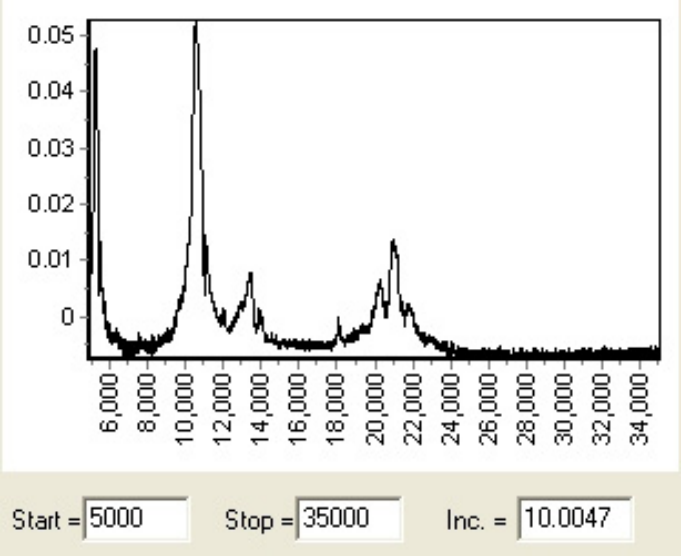

Figure 6.11: Measured resonance curve for a full Hall Probe attached 100 kHz quartz tuning fork between 5,000 Hz and 35,000 Hz

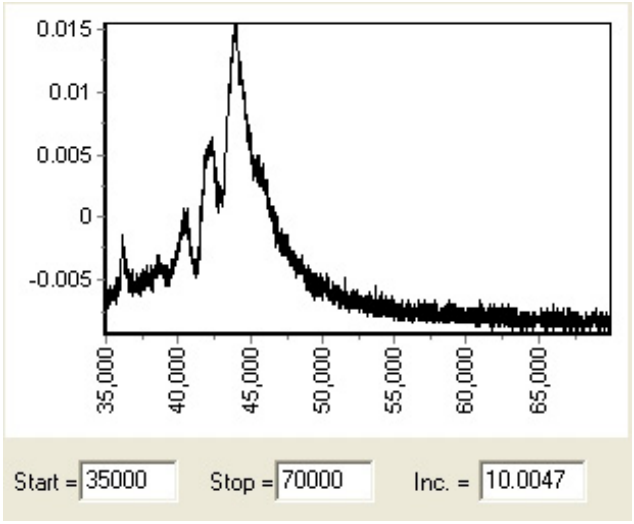

Figure 6.12: Measured resonance curve for a full Hall Probe attached 100 kHz quartz tuning fork between 35,000 Hz and 70,000 Hz

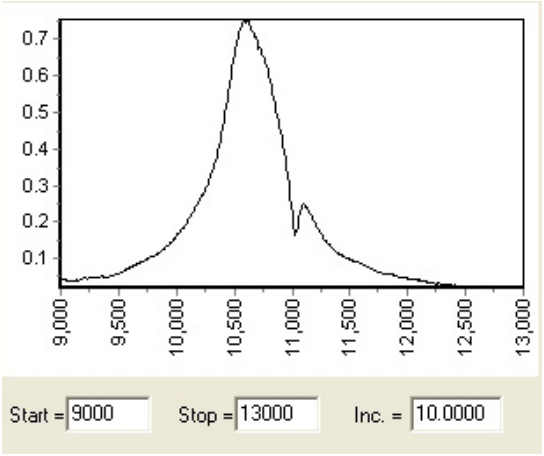

Figure 6.13: Measured resonance curve for a full Hall Probe attached 100 kHz quartz tuning fork between 9,000 Hz and 13,000 Hz with fixed prong.

In these experiments we saw that experimental results are lower than the theoretically calculated ones. This can be caused by the extra masses of used glue to fix the probe to the quartz. Another reason is probably the fixing point of the Hall Probe to the quartz tuning fork. Because Hall Probe is a heavy piece, it is nearly impossible to glue it exactly to the edge of the prong. So the fixing point will change the effective center of mass and then resonance frequency will be shifted to lower frequencies. This effect should occur much more for the 100 kHz quartz tuning fork instead of 32 kHz ones, because of the length of the prongs. The experimental result is also satisfying this condition.

We also had a surface topography data with using a dummy chip that has ¼ of the mass of normal Hall Probe. The dummy chip is cut at ODTU-MET laboratories to have a sharp corner and glued on a 32 kHz quartz tuning fork. 6 μm period, 100 nm deep gold coated grating is used as a sample for this experiment. The prong at the down side is fixed. System is vacuumed down to $4x10^{-4}$ mbar. The scan area of the images is 30 μm x30 μm and the scan speed that was used is 1 μm /sec. The Δf was set to 15 Hz for approach and feed-back

mechanism. The resonance curves and the results can be given in Figures 6.14 and 6.15.

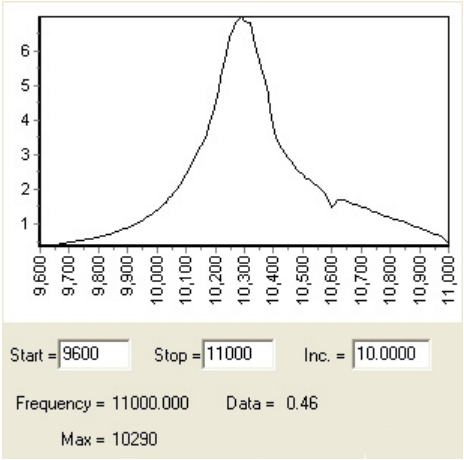

Figure 6.14: Resonance curve of the quartz tuning fork with ¼ sized Hall probe.

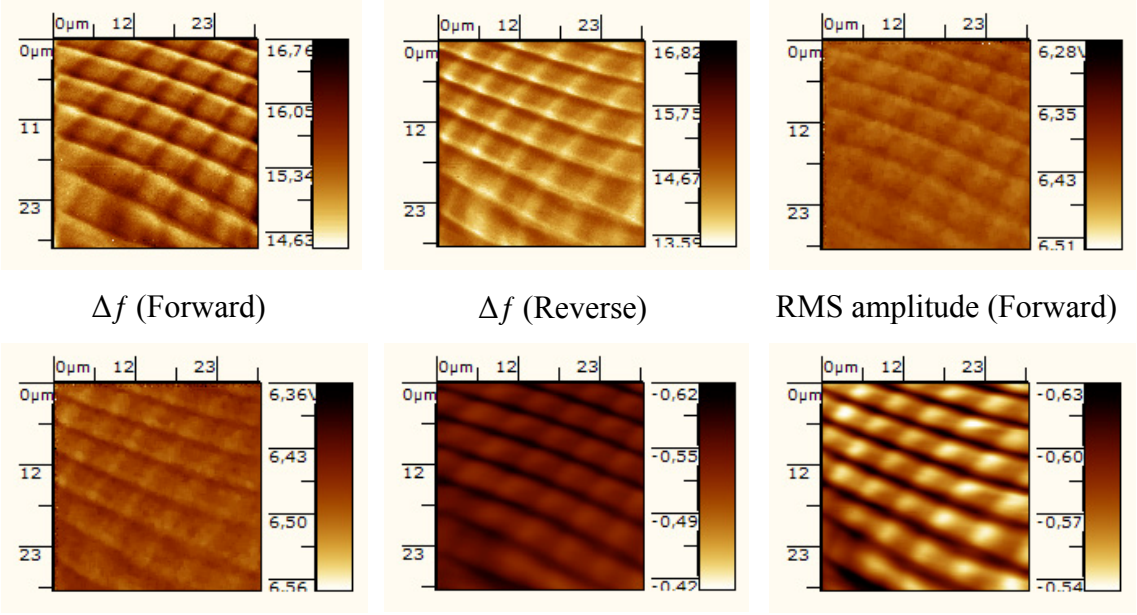

Δf (Forward) Δf (Reverse) RMS amplitude (Forward)

RMS amplitude (Reverse) V_z (Forward) V_z (Reverse)

Figure 6.15: AFM topography by using the corner of the dummy chip

All in these experiments, one of the sharp corners of a dummy chips were used. But for our main aim, SHPM imaging with quartz tuning fork AFM feed-

back, it is very important to have a good feed-back signal with using the mesa corner of the fabricated Hall Probe. For this purpose we glued a dummy Hall probe to the 100 kHz quartz tuning fork. We recorded photographs of the Hall Probe definition to examine the possible damage that can be caused by the scan. These photographs are given in Figures 6.16. Also resonance curves between 5,000 Hz and 100,000 Hz are examined as shown in Figures 6.17a, 6.17b, 6.17c. Two distinguishable resonance curves are found. One was found at 7,930 Hz with 60 mV rms, and the other was found at 58,825 Hz with 3mV rms. Because of higher amplitude and higher Q-factor, we preferred to use first resonance curve at 7,930 Hz. These resonance curves are given in Figure 6.18 in more details. The AFM tracking results are also given in Figures 6.19 – 6.22.

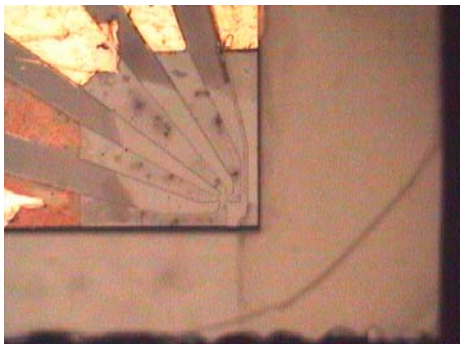

Before Experiment

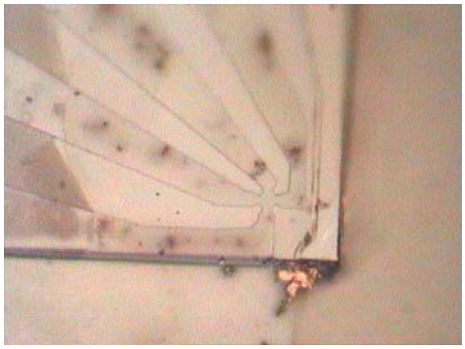

After Experiment

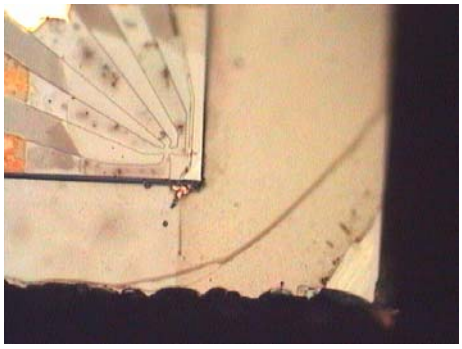

After Experiment

After Experiment

Figure 6.16: Photographs of Hall Probe definition and mesa corner of the used dummy Hall Probe for the feed-back tracking experiment

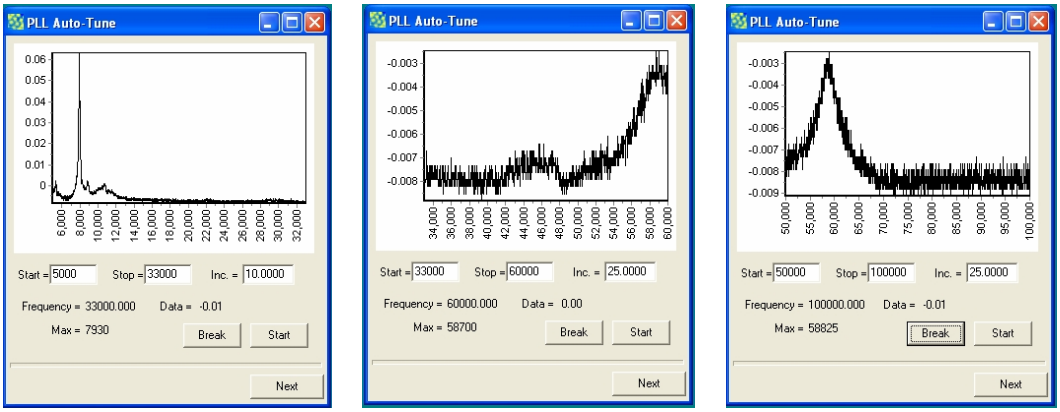

a b c

Figure 6.17: Resonance tune between 5,000 and 100,000 Hz of 100 kHz Quartz crystal with dummy Hall Probe

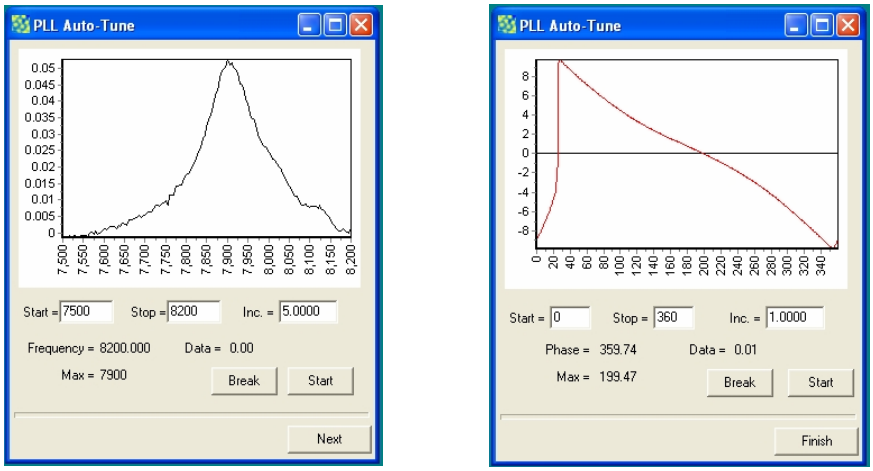

Figure 6.18: Resonance and the phase curve of 100 kHz Quartz crystal with dummy Hall Probe that is used for experiment

Results of this tracking by mesa corner experiment with using 100 kHz quartz tuning fork, can be given as for the parameters that listed below for 6 μm period grating sample,

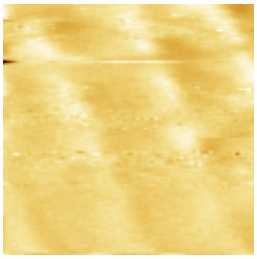
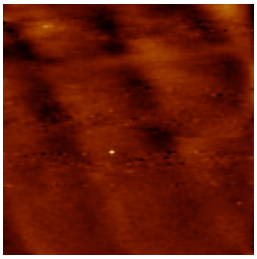
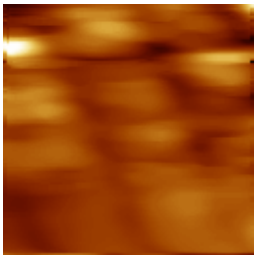


Δf (Forward) Δf (Reverse) V_z (Forward) V_z (Reverse)

Enhanced color :

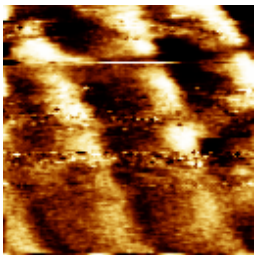
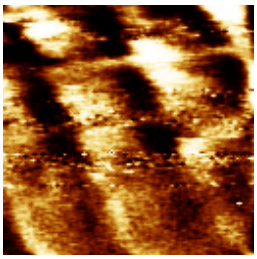

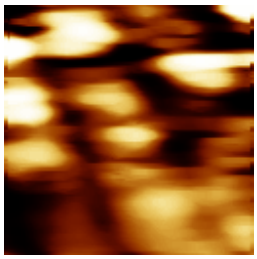

Δf (Forward) Δf (Reverse) V_z (Forward) V_z (Reverse)

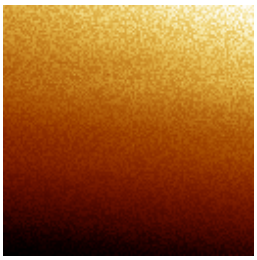
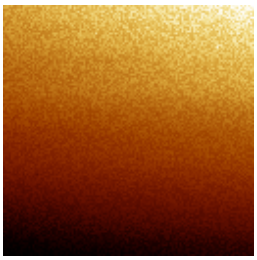

RMS (Forward) RMS (Reverse)

Figure 6.19: Results of AFM topography imaging by using corner of Mesa (1) over 20µm x 20µm area with Δf =15 Hz, 1µm/s

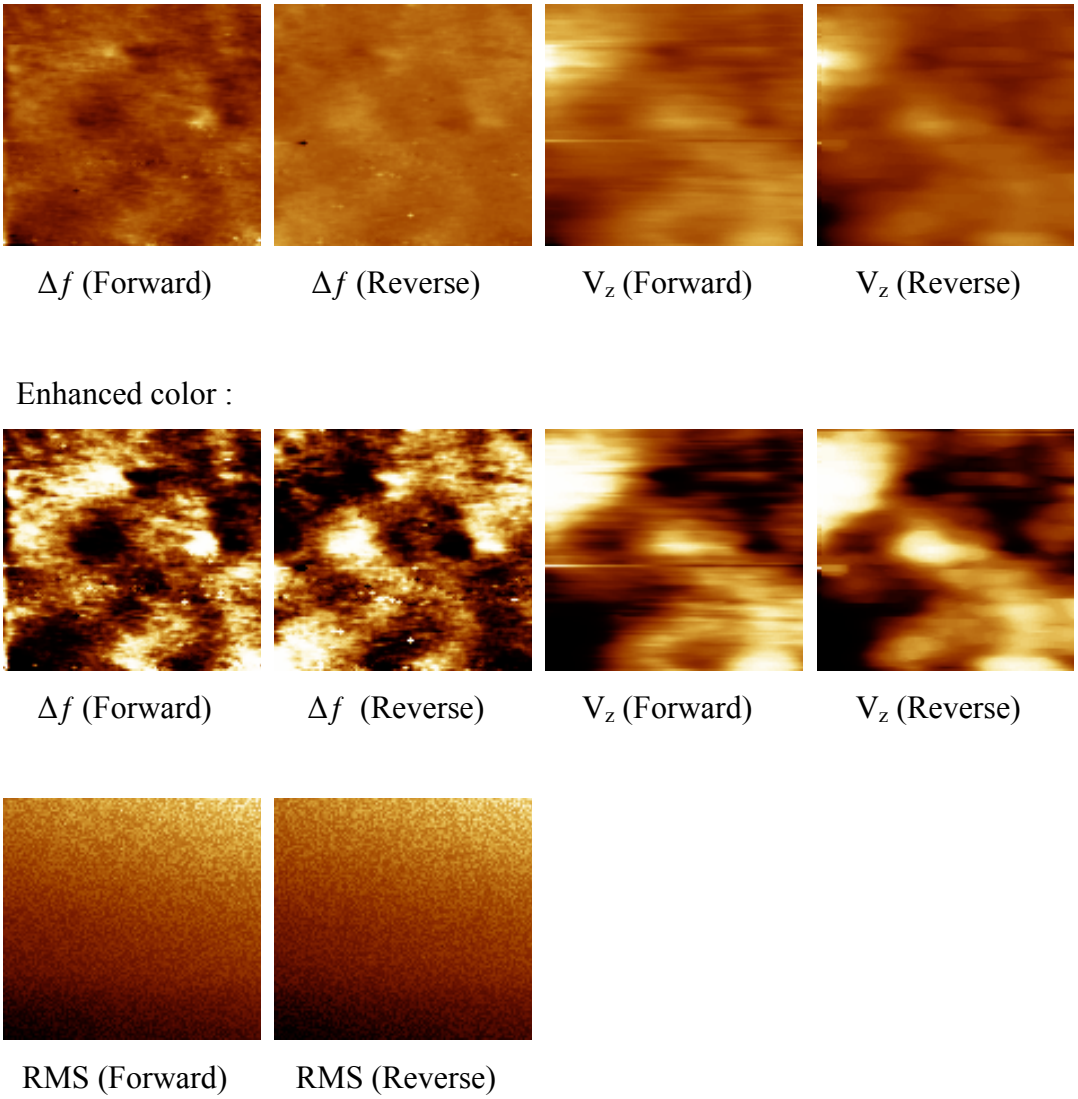

Figure 6.20: Results of AFM topography imaging by using corner of Mesa (2) over 15μm x 15μm area with Δf=8 Hz, 1μm/s

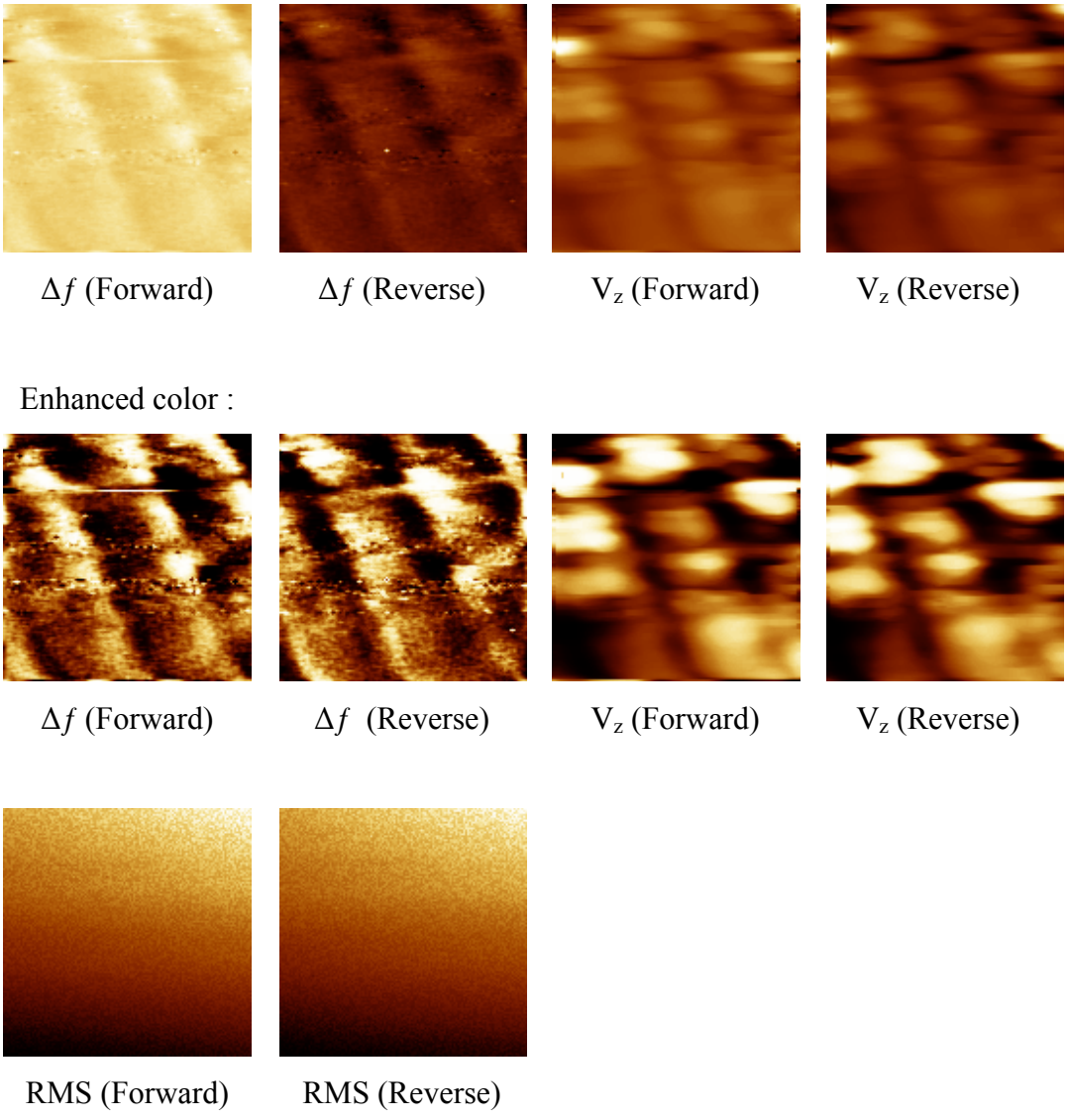

Figure 6.21: Results of AFM topography imaging by using corner of Mesa (1) over 20μm x 20μm area with Δf=15 Hz, 1μm/s

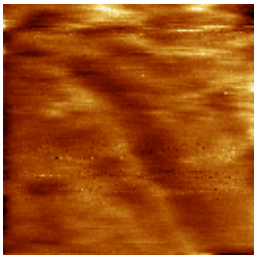
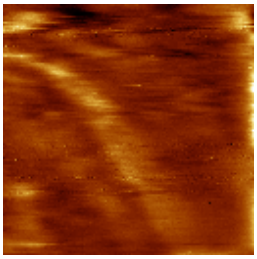
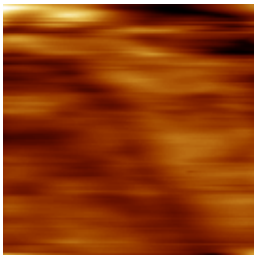
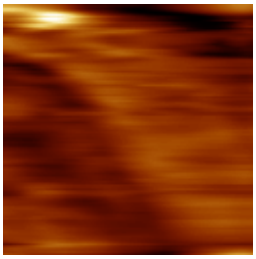

Δf (Forward) Δf (Reverse) V_z (Forward) V_z (Reverse)

Enhanced color:

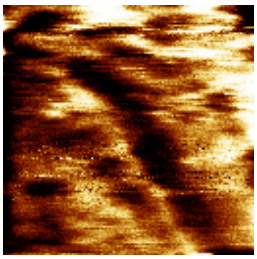
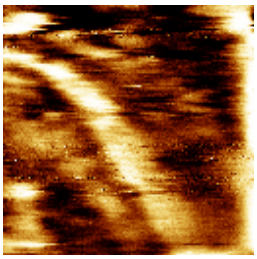
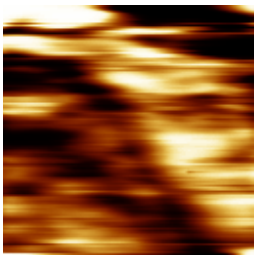
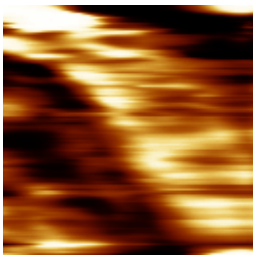

Δf (Forward) Δf (Reverse) V_z (Forward) V_z (Reverse)

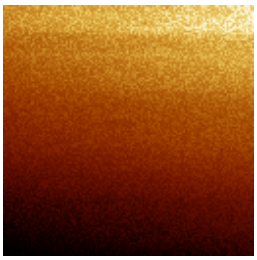
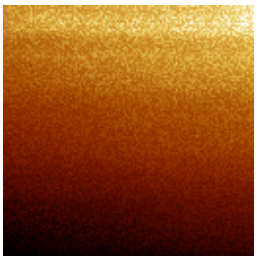

RMS (Forward) RMS (Reverse)

Figure 6.22: Results of AFM topography imaging by using Mesa corner (3), over 20µm x 20µm area with Δf =25 Hz, 2µm/s

In this last experiment we also proved that, it is possible to have a good feed-back tracking with mesa corner. Although we crashed to surface at the last imaging, only a gold piece is stick to the mesa corner. There is no important damage at the Hall Probe.

6.1 Lift-off mode SHPM imaging with AFM feed-back

We used lift-off mode scan as a first step for SHPM imaging with Quartz AFM feed-back, to save the Hall Probe. In this experiments we, aligned the Hall Probe respect to the sample surface, and we evacuated the insert shield to avoid from effect that caused by compressed air between sample and sensor. 5 x 10^{-4} mbar pressure is used for the experiments. The vacuum pumping system is shown in Figure 6.23.

Figure 6.23: Vacuuming pump for both insert shield and cryostat.

In first lift-off mode magnetic field imaging experiment a 100 MB zip disk is used as magnetic sample. We used a 2DEG GaAs Hall Probe with Hall coefficient 0.003 Ω/Gauss. The tilt angle set to 1º. The shield is pumped down ~ 4 x10^{-4} mbar. SR830 Lock-in amplifier was used for force measurement. After the interaction is

sensed, the Hall Probe is lifted by 10V (~2.69 μm). The gain parameter and bandwidth parameter of the Hall Probe was set to 10 and 1 respectively. There is a preamplifier with a gain of 1001. The magnetic image is taken at room temperature over 8 μm x 8 μm area with 256 x 256 pixels resolution, 50 μm/sec speeds and 100 μA Hall current. The result and cross section are given in Figures 6.24 and 6.25. Some of the tracks are clearly visible but the images are not as good as STM feedback SHPM as shown in Figure 4.7.

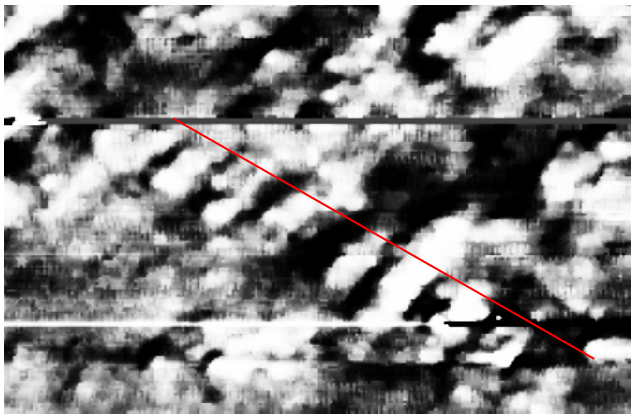

Figure 6.24: SHPM image of the data tracks on the 100 MB ZIP media obtained in the lift-off mode

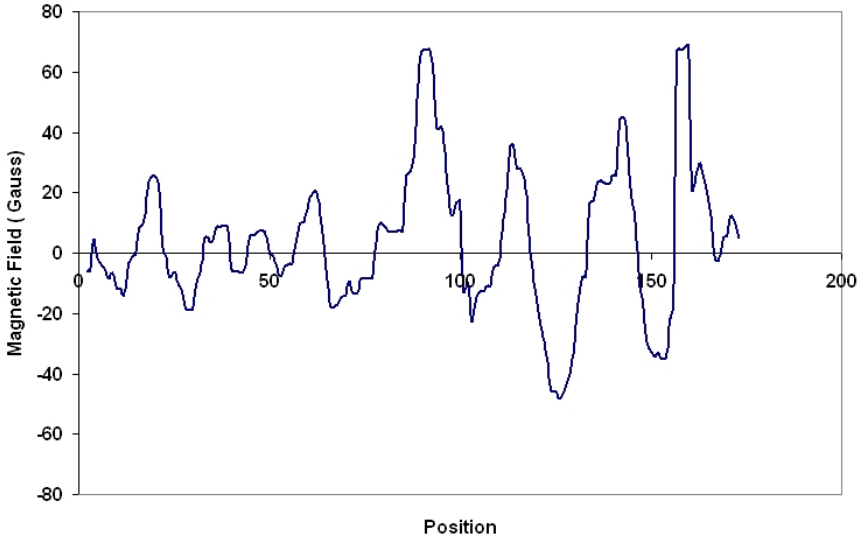

Figure 6.25: Cross section of the data tracks

In the second experiment we used NIST magnetic imaging reference sample. Again, ~ 1º tilt angle is given between sample and sensor. The shield is pumped down to ~ 4 x10^{-4} mbar. Then system was cooled with a controlled rate about 2K/min to run at 77K. The PLL system was used for force measurement. After the force interaction is sensed, the Hall Probe is lifted off to 5V (~0.43 µm). The gain parameter and bandwidth parameter of the Hall Probe was set to 10 and 1kHz respectively. The magnetic image is taken over 18.8 µm x 18.8 µm area with 512 x 512 pixels resolution, 100 µm/sec speeds and 500 µA Hall current. The result and cross section are given in Figures 6.26 and 6.27.

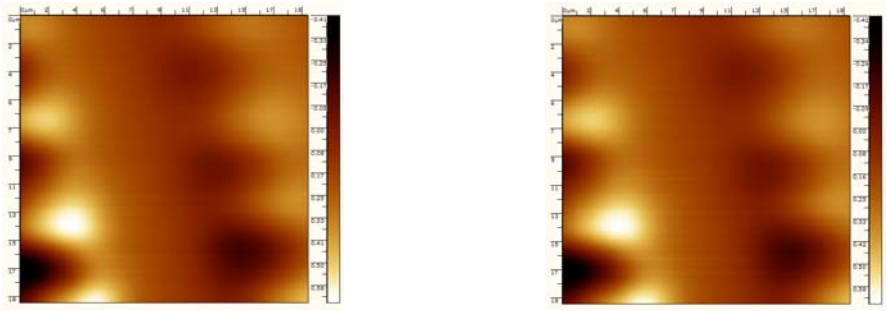

Hall Voltage (Forward) Hall Voltage (Reverse)

Figure 6.26: SHPM image with Quartz AFM feedback, at 77K by using 5V lift-off voltage

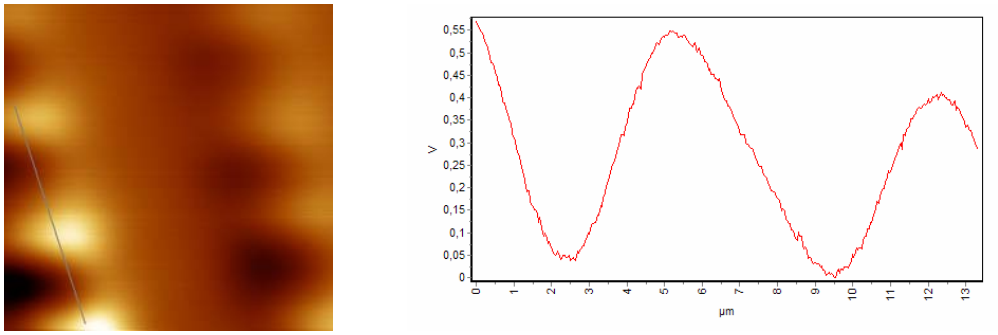

Figure 6.27: Cross section path on image and graph of cross section of the data tracks

LT-SHPM systems software is not supporting the Hall Voltage measurement directly at the moment for the AFM guided SHPM operation. The Hall Voltage was measured by using an extra channel of spare ADC card. The Hall voltage is not converted to the magnetic field strength by the software because of this reason. We calculated the strength of the magnetic field as,

$$V_H = I_H G B R_H \tag{6.16}$$

where G is Gain, I_H is Hall current, R_H is Hall constant and V_H is Hall voltage. For this experiment we applied 500 μA for I_H and we measured R_H as 0.003 Ω/Gauss with Hall Probe calibration. Other hand, gain includes two parts. The first one comes from pre-amplifier box and its value is 1,001, and the second one comes from the SPM electronic. In this experiment second gain was set at 10. Then,

$$B = \frac{V_H}{500\mu A \times 1001 \times 10 \times 0.003\Omega / Gauss} \tag{6.17}$$

The corresponding magnetic field per volt can be found as,

$$\frac{B}{V_H} = 66.6 Gauss / Volt \tag{6.18}$$

With using relation 6.22, cross section can be re-drown in Figure 6.27 as,

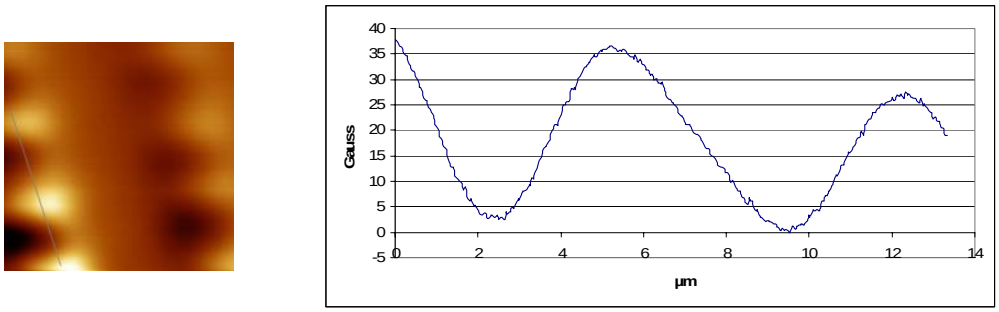

Figure 6.28: Cross section path on image and graph of cross section of the data tracks in Gauss scale

6.2 Tracking mode SHPM imaging with AFM feed-back

In last experiments we used AFM tracking mode. In this mode, the force interaction on the Hall Probe is kept fixed by feedback loop. Any lift-off distance is not used. So, the probe looses very little magnetic field strength because of the distance. To keep the feedback loop working properly, normal scan mode is preferred for tracking experiments. Although it gives high magnetic field resolution, it is hard to keep force interaction on probe because of low quality factor and the compressed air between the probe and surface. We succeed to run feed-back control without any problem and took several magnetic field images at different temperatures with AFM tracking mode.

In first tracking mode experiment we used an Iron garnet sample. Hall Probe is aligned ~ 1º with respect to the sample. The shield is pumped down to $4x10^{-4}$ mbar. The PLL system was used for force measurement. Resonance frequency is measured as 5,297 Hz and Q-factor is calculated as 230. When the force interaction is sensed we observed a signal problem for the normal dither voltages. The signal disturbed anomaly and noise with higher frequency then the resonance is observed. To decrease this problem, the dither voltage was decreased up to 16 mV peak to peak. We measured the corresponding amplitude of the signal

generated by the quartz crystal (input AC signal), as 40 mV_{pp}. With this lower dither voltage we managed to stabilize the force interaction measurement. The resonance shift, Δf was set to 15 Hz for feedback. The gain parameter and bandwidth parameter of the Hall Probe was set to 10 and 1kHz respectively. The magnetic image is taken over 40 µm x 40 µm area with 128 x 128 pixels resolution, 2 µm/sec speeds and 300 µA Hall current. The resonance curve of the quartz tuning fork result and cross section are given in Figures 6.29, 6.30 and 6.31.

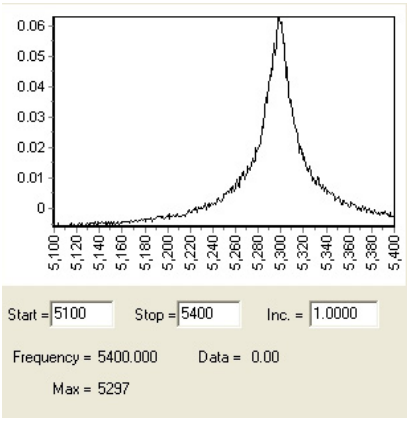

Figure 6.29: Resonance curve of the Hall Probe attached quartz tuning fork, at 300K.

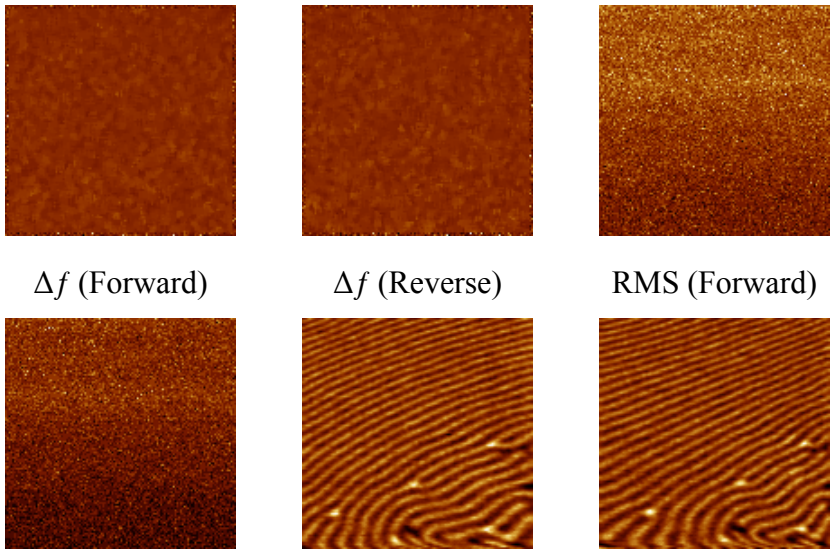

Δf (Forward) Δf (Reverse) RMS (Forward)

RMS (Reverse) V_{Hall} (Forward) V_{Hall} (Reverse)

Figure 6.30: Tracking mode SHPM image with Quartz AFM feedback, at 300K.

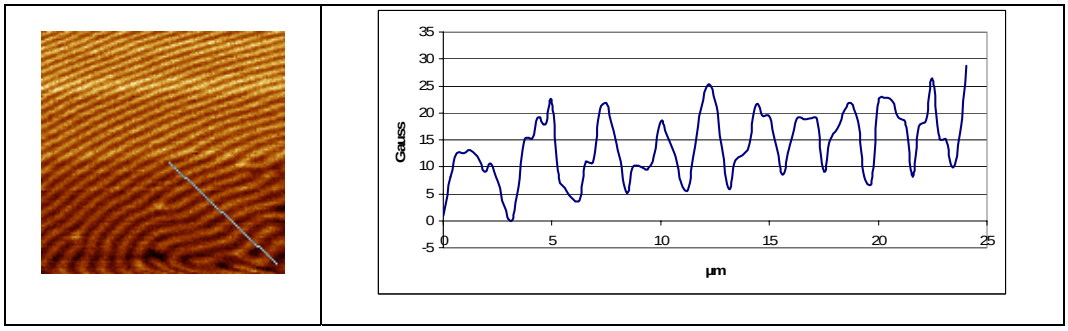

Figure 6.31: Cross section path on image and graph of cross section of domains

In second tracking mode experiment we used garnet sample again. Hall Probe is aligned to ~ 1º with respect to sample. The shield is evacuated to 1.8 x10^{-4} mbar. Then system was cooled with a controlled rate about 2K/min to 77K. The PLL system was used for force measurement. Resonance frequency is measured as 5,151 Hz and Q-factor is calculated as 103. To avoid force interaction stabilizing problem, the dither voltage was decreased up to 12 mV peak to peak and corresponding sensor signal was recorded as 24 mV peak to peak. The resonance shift, Δf was set to 5 Hz for feed-back. The gain parameter and bandwidth parameter of the Hall Probe was set to 10 and 1kHz respectively. The magnetic image is taken over 20 µm x 20 µm area with 128 x 128 pixels resolution, 1 µm/sec speeds and 300 µA Hall current. The resonance curve of the quartz tuning fork, images and cross section are given in Figures 6.32, 6.33, 6.34 and 6.35.

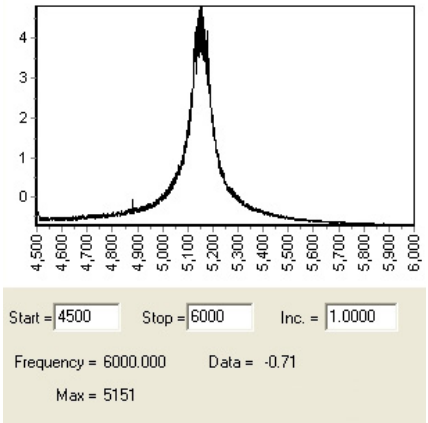

Figure 6.32: Resonance curve of the Hall Probe attached to quartz tuning fork, at 300K.

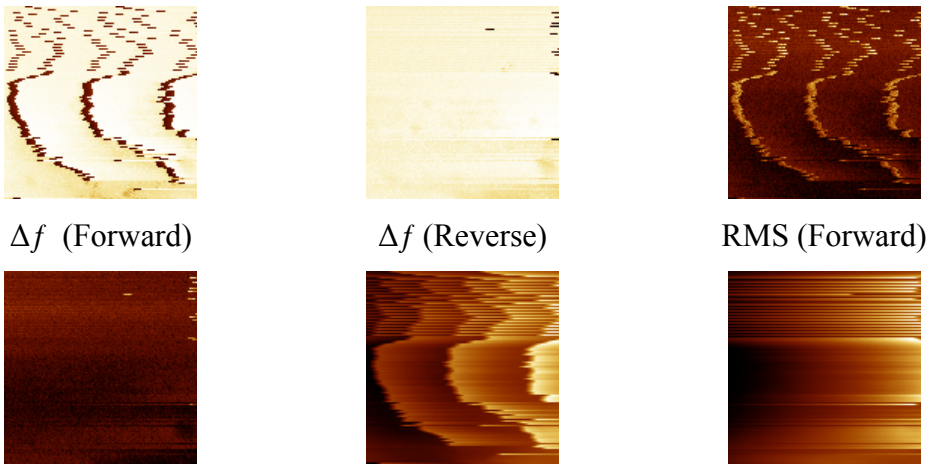

Δf (Forward) Δf (Reverse) RMS (Forward)

RMS (Reverse) V_z (Forward) V_z (Reverse)

Figure 6.33: Quartz AFM feedback tracking mode, force, phase and feedback data at 77K.

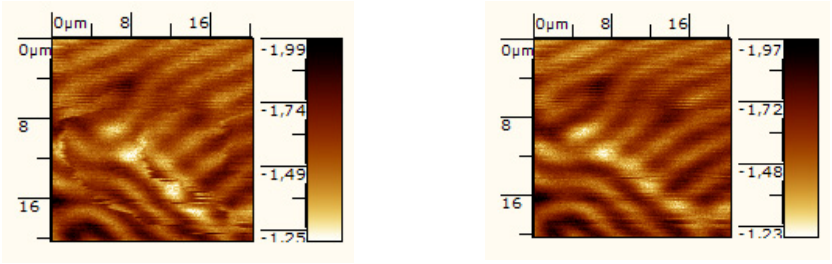

Hall Voltage (Forward) Hall Voltage (Reverse)

Figure 6.34: Quartz AFM feedback tracking mode SHPM image at 77K.

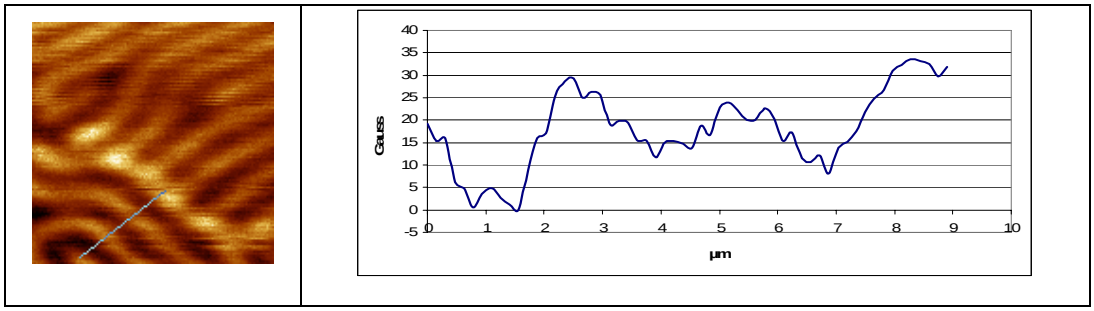

Figure 6.35: Cross section path on image and graph of cross section of domains

In third experiment, the probe moved on sample 50 steps to + y direction and 20 steps to – x direction with using coarse approach mechanism. The Hall current increased to 500 µA, scan speed is decreased to 0.4 µm/sec, scan area is decreased to 10 µm x 10 µm. The result and cross section are given in Figures 6.36, 6.37, 6.38 and 6.39.

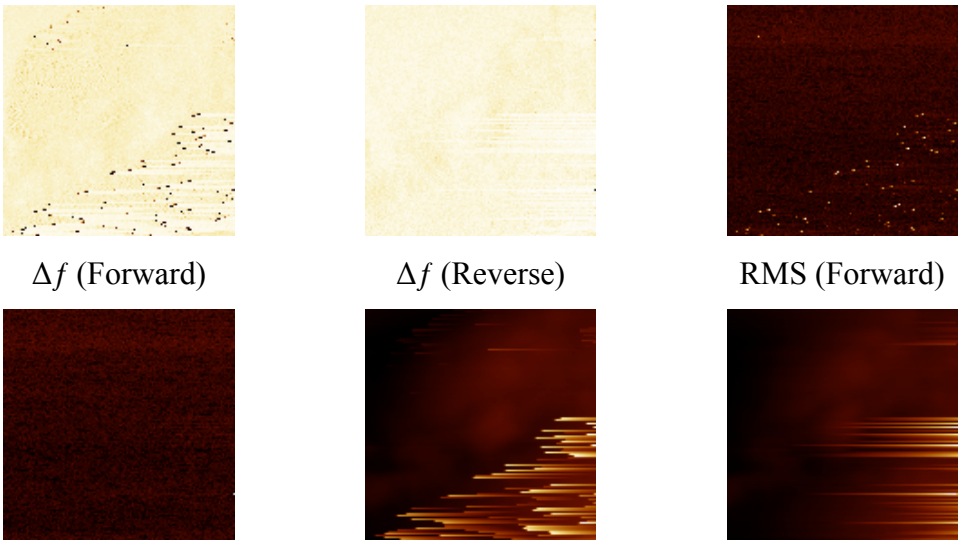

Δf (Forward) Δf (Reverse) RMS (Forward)

RMS (Reverse) V_z (Forward) V_z (Reverse)

Figure 6.36: Quartz AFM feedback tracking mode, force, and phase and feedback images at 77K.

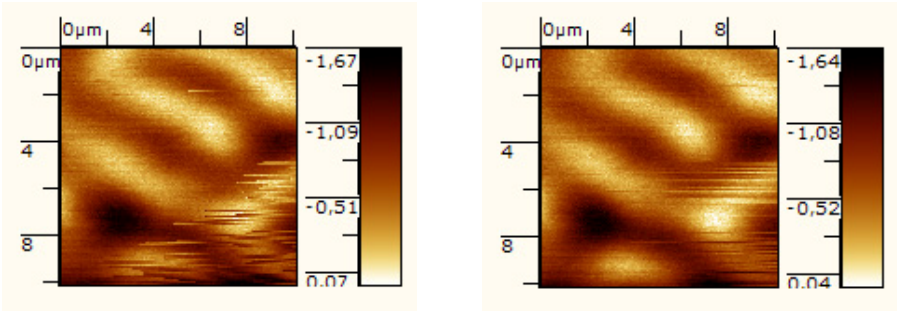

Hall Voltage (Forward) Hall Voltage (Reverse)

Figure 6.37: Tracking mode SHPM image with Q-AFM feedback, at 77K (2).

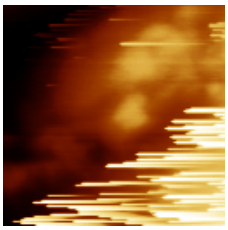

Filtered and enhanced V_z (Forward)

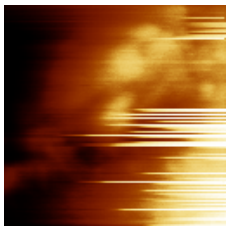

Filtered and enhanced V_z (Reverse)

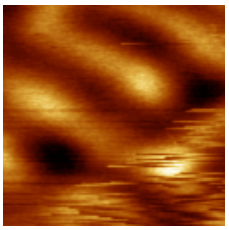

Filtered V_{Hall} (Forward)

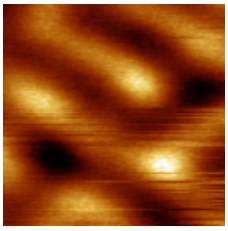

Filtered V_{Hall} (Reverse)

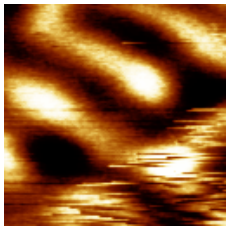

Filtered and enhanced V_{Hall} (Forward)

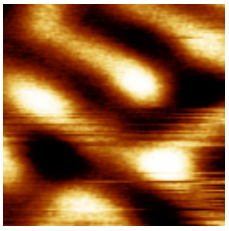

Filtered and enhanced V_{Hall} (Reverse)

Figure 6.38: Filtered and enhanced color tracking mode SHPM image with Q-AFM feedback, at 77K (2).

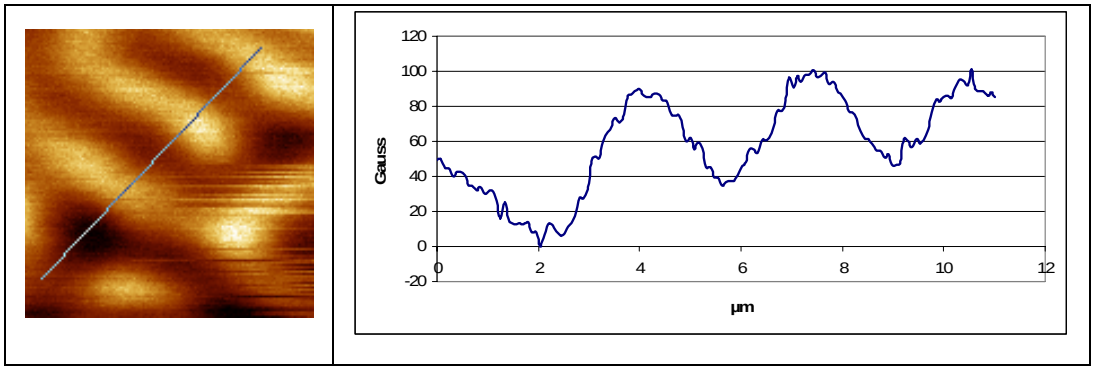

Figure 6.39: Cross section path on image and graph of cross section of the domains (2)

In last experiment, the Hall current increased to 300 µA, scan speed is reduced to 0.5 µm/s, and scan area is selected as 20 µm x 20 µm. The result and cross section are given in Figures 6.40, 6.41 and 6.42.

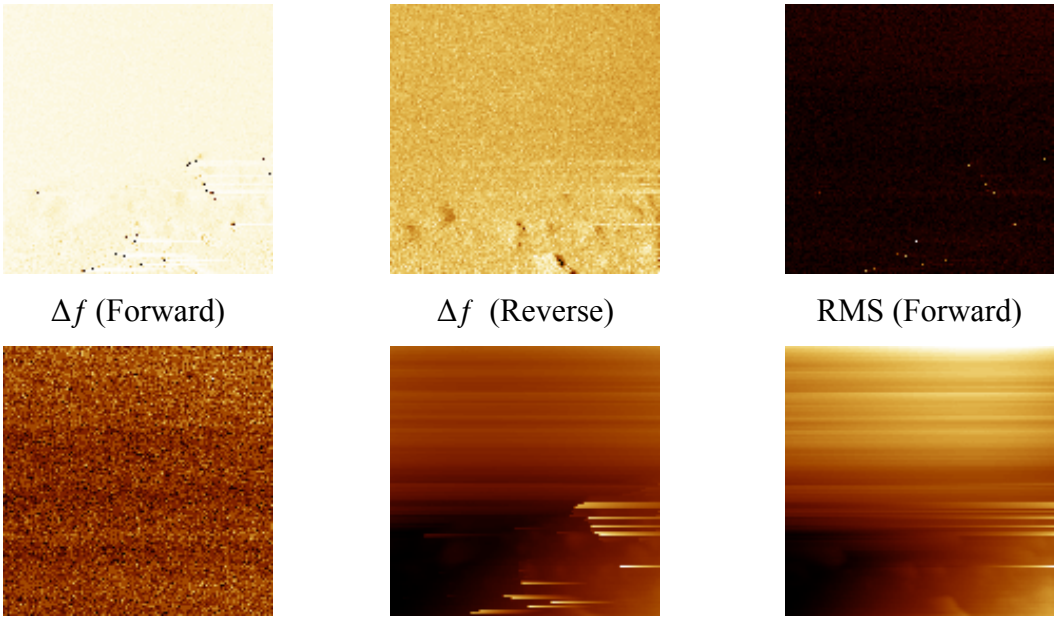

Δf (Forward) Δf (Reverse) RMS (Forward)

RMS (Reverse) V_z (Forward) V_z (Reverse)

Figure 6.40: Quartz AFM feedback tracking mode, force, phase and feedback data at 77K.

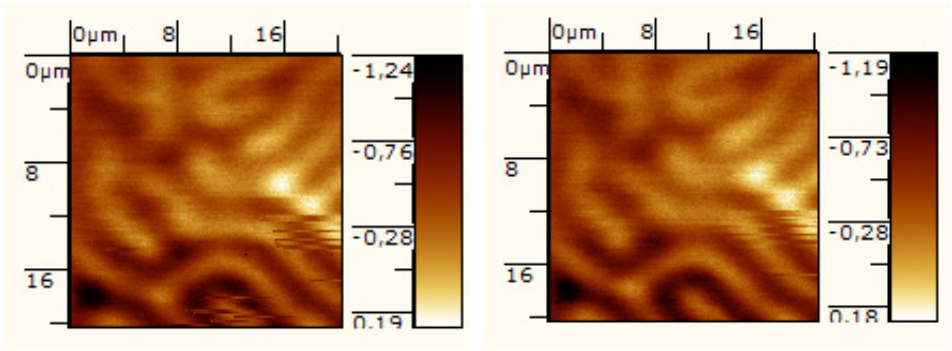

V_{Hall} (Forward) V_{Hall} (Reverse)

Figure 6.41: Tracking mode SHPM image with Quartz AFM feedback, at 77K.(3)

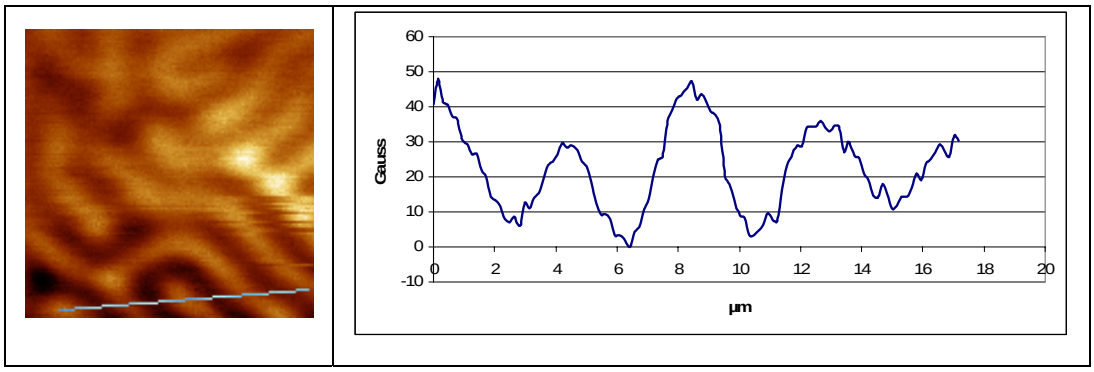

Figure 6.42: Cross section path on image and graph of cross section along the line (3)

Chapter 7

Conclusion

In this thesis, quartz tuning fork based AFM feed-back mechanism for SHPM is introduced. In the first step, capabilities and properties of quartz tuning forks were examined as a force sensor using tungsten tips and dummy Hall chips. The resonance frequency and Q-factor of the quartz tuning forks are measured as a function of temperature and attached mass towards Q-AFM tracking SHPM. Several images were taken at different temperatures and using different scanning modes to examine quartz tuning forks as a force sensor. Electrochemically etched AFM tips and dummy Hall probe chips with full and quarter sizes are used to perform these experiments. The experiments with the etched AFM tips gave us some insight about quartz tuning fork based AFM imaging mechanisms capabilities and limits. The experiments with dummy Hall chips proved that our feedback mechanism can work with low resonance frequency, low quality factor and non-sharp corners. After we managed to have good feedback images with very high mass and non-sharp corners of dummy chips, Quartz AFM guided SHPM system is developed. Quartz AFM guided SHPM experiments showed that feedback is working reasonably well for magnetic measurement at 300K. However, the performance is still not satisfactory at 77K. For some reason we can not establish a stable feedback.

In future work, Quartz AFM guided SHPM system will be developed to overcome this problem and to take 3D surface topography with using the mesa corner of the Hall Probe at low temperatures. With this development, the simultaneous 3D surface topography imaging will also be possible at the same time with magnetic field imaging across the full temperature range, 300-4.2K. We plan to fabricate smaller size Hall probe chips for this purpose. As it is observed during this thesis work, the smaller sized Hall probe chips will increase the resonance frequency and Q factor. Therefore, we believe that using smaller Hall Probes will give better results. We also plan to investigate vortex struc of superconducting materials with Quartz AFM guided SHPM.

Despite some stability problems, it is shown that quartz tuning fork guided AFM feedback can be used effectively for SHPM tracking mechanism as an easier and cheaper method.

Bibliography

[1] E. Meyer, H. J. Hug, R. Bennewitz, "Scanning Probe Microscopy", Springer, ISBN 3-540-43180-2674, (2004)

[2] J. Tersoff and D.R. Hamann, "Theory and Application of the Scanning Tunneling Microscope", Physical Review Letters, **50**, Number:25,1998-2001, (1983)

[3] J. Bardeen, Phys. Rev. Lett. , **6** (57), (1961)

[4] A.Oral, "Investigation of $Si_{1-x}Ge_x$ Alloy Formation by Using STM", Phd. Thesis, Bilkent University, (1994)

[5] J. H. Coombs and J. B. Pethica, J. Res. Develop., **30**, 559, (1986)

[6] D. A. Bonnel, "Scanning Tunneling Microscopy and Spectroscopy",VCH publishers, 1993

[7] G. Neubauer, S. R. Cohen, G. M. McClelland, D. Horne and C. Mate; "Force microscopy with bidirectional capacitance sensor", Rev. Sci. Inst., **61**, 2296

[8] G. Meyer, N. M. Amer; "Novel optical approach to atomic force microscopy", Applied Physics Letters; **53**, 1045, (1988)

[9] F. J. Giessibl; "Advances in atomic force microscopy", Review of Modern Physics; **75**, (2003)

[10] M. Tortonese, H. Yamada, R.C. Barrett and C.F. Quate, Proc. Transducers **91** (IEEE), 448, (1991)

[11] J. Ferrante and J. R. Smith, Phys. Rev. B, **19**, 3911; (1979)

[12] T. R. Albrectht, P. Grütter, D. Horne, D. Rugar; "Frequency modulation detection using high Q-cantilevers for enhanced force microscope sensitivity"; Journal of Applied Physics; **69**, 668, (1991)

[13] A. Sandhu, K. Kurosawa, M. Dede and A. Oral, "50nm Hall Sensors for Room Temperature Scanning Hall Probe Microscopy", Japanese Journal of Applied PhysicsVol. **43**, No. 2, pp. 777–778, (2004)

[14] L.A. Nagahara, T. Thundat and S.M. Lindsay, "Preparation and characterization of STM tips for electrochemical studies", Review of Scientific Instruments, **60** (10), (1999)

[15] A. H. Sørensen, U. Hvid, M.W. Mortensen, and K.A. Mørch, "Preparation of platinum/iridium scanning probe tips, Review of Scientific Instruments", **70** (7), (1999)

[16] Muharrem Demir, Nanomagnetics Instruments, (2005)

[17] "Piezoelectric Quartz Tuning Forks for Scanning Probe Microscopy", Nanonis GmbH, Switzerland, 2005

[18] K. Karrai, R. D. Grober, "Piezoelectric tip–sample distance control for near field optical microscopes, Applied Physics Letter", **66** (14), (1995)

[19] W. H. J. Rensen, N. F. van Hulst, A. G. T. Ruiter and P. E. West; "Atomic steps with tunning fork based noncontact atomic force microscopy"; Applied Physics Letters, Volume **75**, Number 11, (1999)

[20] F. J. Giessbl; "Atomic resolution on Si (111)-(7x7) by noncontact atomic force microscopy with a force sensor based on a quartz tuning fork"; Applied Physics Letters; **76** (11); (2000)

[21] M. Todorovic and S. Schultz; "Magnetic force microscopy with nonoptical piezoelectric quartz tunning fork detection design with applications to magnetic recording studies"; Journal of Applied Physics, **83** (11), (1998)

[22] M. Kageshima, H. Jensenius, M. Dienwiebel, Y. Nakayama, H. Tokumoto, S. P. Jarvis, T. H. Oosterkamp; "Noncontact atomic force microscopy in liquid environment with quartz tuning fork and carbon nanotube probe"; Applied Surface Science, **188**, 440-444, (2002)

[23] A.G.T. Ruiter, J.A.Veerman, K.O van der Werf, and N.F. van Hulst; "Dynamic behavior of tuning fork shear-force feedback", Applied Physics Letter, **71** (1), (1997)

[24] J.Rychen,T. Ihn, P.Studerus, A. Herrmann, and K. Ensslin; "A low temperature dynamic scanning force microscope operating in high magnetic fields", Review of Scientific Instruments, **70** (6), (1999)

[25] J.Rychen,T. Ihn, P.Studerus, A. Herrmann, K. Ensslin, H.J. Hug, P.J.A. van Schendel and H. J. Güntherodt; "Operation characteristics of piezoelectric quartz tunning forks in high magnetic fields at liquid Helium temperatures", Rev. Sci. Instr. **71**, 1695 (2000)

[26] K. R. Brown, L. Sun, and B. E. Kane; "Milikelvin scanned probe for measurement of nanostructures", Review of Scientific Instruments, **75** (6), (2004)

[27] A. J. Brook, S. J. Bending, J. Pinto, A. Oral, D. Ritchie, H. Beere, M. Henini, A. Springthorpe; "Integrated piezoresistive sensors for atomic force-guided scanning Hall Probe microscopy", Applied Physics Letters, **82** (20), (2003)

[28] A. J. Brook, S. J. Bending, J. Pinto, A. Oral, D Ritchie, H Beere,A Springthorpe and M Henini; "Micromachined III–V cantilevers for AFM-tracking scanning Hall probe microscopy",J. Micromech. Microeng. **13** (2003) 124–128

[29] F. J. Giessibl; "High speed force sensor for force microscopy and profilometry using a quartz tuning fork"; Applied Physics Letters; **73** (26); (1998)

[30] D. Rugar, H. J. Mamin, R, Erlandsson, J. E. Stern and B. D. Terris; "Force microscope using a fiber-optic displacement sensor.", Rev. Sci. Instr.; **59** 2337, (1988)

[31] Nanomagnetics Instruments; Suite 290, 266 Banbury Road, Oxford OX2 7DL, UK; www.nanomagnetics-inst.com

[32] T. Schweinböck, D. Weiss, M. Lipinski and K. Eberl, "Scanning Hall probe microscopy with shear force distance control, Journal of Applied Physics", **87** (9), (2000)